NASA Technical Paper 2818

June 1988

Sensitivity of F-106B Leading-Edge-Vortex Images to Flight and Vapor-Screen Parameters

John E. Lamar and
Thomas D. Johnson, Jr.

NASA

NASA Technical Paper 2818

1988

Sensitivity of F-106B Leading-Edge-Vortex Images to Flight and Vapor-Screen Parameters

John E. Lamar
Langley Research Center
Hampton, Virginia

Thomas D. Johnson, Jr.
Planning Research Corporation
Hampton, Virginia

National Aeronautics
and Space Administration

**Scientific and Technical
Information Division**

Summary

A flight research program was undertaken at NASA Langley Research Center in which vapor-screen and image-enhancement techniques were used to obtain qualitative and quantitative information about near-field vortex flows above the wings of fighter aircraft. In particular, the effects of Reynolds number and Mach number on the vortex system over an angle-of-attack range were sought. The relevance of these flows stems from their present and future use at many points in the flight envelope, especially during transonic maneuvers. The aircraft used in this flight program was the F-106B because it was available and had sufficient wing sweep (60°) to generate a significant leading-edge-vortex system.

Two kinds of results were obtained, those which are primarily related to vapor-screen hardware and those which are related to flow. For the hardware results, it was determined that the probe-tip location is critical to seeding the vortex system for illumination and visual recording, and the influence of its location is discernible from the measured values for vortex envelope extent and core lateral position; a slit-width opening of 0.012 in. is sufficient for the light sheet to illuminate the vortex system details; and data repeatability is fairly good for visual results obtained at a constant altitude when the light sheet is used in an intermittent operational mode. With respect to the flow-related results, it has been determined that the combinations of increasing Reynolds number and decreasing lift coefficient can significantly reduce the amount of vapor entrained in the leading-edge vortex below an angle of attack of 20°; during the transonic maneuver, increasing Mach number and load factor produces a well-defined vortex system which is larger and more inboard than that for the constant-altitude $1g$ flight; dual corotating primary vortices exist at higher Reynolds numbers; in general, the inner extent of the vortex-system envelope and lateral core locations are more inboard at lower Reynolds numbers and higher lift coefficients, whereas the core elevation is insensitive to Reynolds number change; and vortex breakdown does not occur at the light-sheet station for the tested combinations of angle of attack (up to 23°) and Reynolds number.

Introduction

Since vortex flows play such an important role in the design and operation of aerospace vehicles, there continues to be an active interest in visualizing these flows. This is especially important for aircraft that use the vortex systems shed from either their own forebody, strake, wing-leading-edge, or horizontal control surfaces to achieve high maneuverability. Combinations of these off-surface flows can be either beneficial or adverse, depending on the sense of rotation and location of the systems. Accurate information of this type needs to be known early in the aircraft design cycle so that unpredictable results will not occur in flight.

Vortex systems are routinely observed in wind tunnels to the extent that the shape of the feeding sheet, the location of the core, and the accompanying effect of its breakdown on the aerodynamic forces and moments are often noted. In the wind tunnel a variety of techniques are used to either identify the core and its diameter or infer its position over the wing. These techniques are distinguishable by whether they are used off or on the surface. Among the off-the-surface techniques are vapor screen, smoke, helium bubble, total pressure survey (ref. 1), schlieren (ref. 2), and tuft grid (ref. 3). The on-the-surface techniques include oil flow, tufting (ref. 1), and pressure measurement (ref. 4). In flight many of these same techniques have also been applied, including smoke (refs. 5 and 6), oil flow (ref. 7), pressure measurement (ref. 4), and tufting (ref. 8). Moreover, due to condensation of atmospheric water vapor, vortex cores have been made visible without additional seeding both in wind tunnels and in flight, as shown in figures 1 to 3. The cores are the dark regions (void of seeding particles) surrounded by the white bands (concentration of particles). Actual knowledge of the vortex-system location is important when one intends for it, particularly the core, to be in a certain aerodynamically beneficial location, as in the case of vortex-flow-management devices. There is much interest in several of these devices for flight application, including the leading-edge-vortex flap (ref. 9), because future fighters will have to operate efficiently at multiple design points, where the flow can range from attached to vortical. These devices, when properly deflected, can work well with either flow type. Hence, the flight testing of such devices would benefit from the verification of the flow type present and its extent.

The vapor-screen technique is a logical way to examine the leading-edge-vortex flow on aircraft with or without vortex-flow devices, since only a thin cross section of the flow is illuminated. Furthermore, only three basic systems are involved—seeding, light-sheet generation, and image recording. In the late 1970's, the Soviets applied this technique successfully in flight to an ogee-winged aircraft and published the work in 1982 (ref. 10). They used atmospheric water vapor for seeding, a ruby laser for light-sheet generation, and a camera (presumably a film camera) for image recording. The latter two are illustrated in figure 3 in a sketch of

the research aircraft. This figure also shows two vapor-screen photographs taken at the higher angles of attack, in which the free vortex off the forward part of the wing has been illuminated by the laser sheet over the aft part (ref. 10). These photographs show a coherent and well-organized vortex, typical of the expected results from a flight vapor-screen study.

In 1984, when the work reported herein began, the capability for doing flight vapor-screen studies was not available in the United States. Therefore, in order to begin a flight study of the effects of Reynolds number and Mach number on the leading-edge-vortex system, two items had to be accomplished. The first was to have available a suitable aircraft for the vortex-system generation, and the second was to have developed the necessary hardware to visualize the vortices. The aircraft chosen for this flight program was the F-106B because of its availability and because its wing sweep (60°) was sufficiently high to generate a significant leading-edge-vortex system (ref. 8). Hardware development, its operational performance, and details of the flight operations are discussed in reference 11. Because of the restricted time available for this project, certain constraints were imposed to assure that delays associated with the weather and hardware developments would be minimized. The consequences of these constraints led to the following hardware decisions: for seeding, propylene glycol vapor was generated, rather than relying on atmospheric moisture; for light-sheet generation, a mercury-arc lamp with appropriate optics was used; and for image recording, a low-light-level video camera with a videocassette recorder (VCR) was employed. Figure 4 shows a photograph of the aircraft with the various systems and their locations depicted.

This report provides the basic visual data, already summarized in references 12 and 13, in order to explore more extensively the effects on the vortex system of changing Reynolds number and Mach number over an angle-of-attack range. The vortex core characteristics of diameter and location are of particular interest since the vortex system generated by this round-edged and cambered wing is likely to be more diffuse than for a sharp-edged wing. Image-enhancement technology was applied to the visual data in order to assist in determining these and other vortex-system internal details and boundaries. Furthermore, selected time-history plots (from ref. 11) of pertinent flight-test parameters, associated with significant data segments, are provided for completeness.

Symbols

BL	butt line on aircraft, in. (see fig. 5)
C_r	root chord, ft
$\bar{c}$	reference wing chord, 23.75 ft
d	distance along leading edge to probe tip from wing-fuselage juncture, in.
FS	fuselage station on aircraft, in. (see fig. 5)
g	load factor normal to longitudinal axis of aircraft
LE	leading edge
l	inboard distance to vortex core from leading edge along light-sheet footprint, in. (see fig. 30)
M	Mach number
m	inboard distance to inner edge of vortex-system envelope from leading edge along light-sheet footprint, in. (see fig. 30)
p	static pressure of free stream, lb/ft^2
R_n	Reynolds number, $1.232\ \bar{c}pM[(T + 216)/T^2]10^6$ (ref. 14, eq. (23))
r	perpendicular distance from leading edge to probe tip, in.
s	distance from center of probe tip to wing surface, in.
T	absolute temperature, °R
TE	trailing edge
WL	waterline on aircraft, in. (see fig. 5)
z	vertical distance to vortex core above upper surface, in. (see fig. 30)
α	angle of attack, deg

Description of Aircraft and Flight-Test Program

Aircraft

The F-106B aircraft is a two-place supersonic all-weather interceptor. It has an area-ruled fuselage, has a 60° delta-like wing of aspect ratio 2.20 (based on a theoretical span of 39.16 ft), and uses elevons instead of a conventional aileron-elevator arrangement, as shown in figure 5. The aircraft wing is based on a modified NACA 0004-65 airfoil (streamwise) coupled with conic-like camber from the leading edge to 80 percent of the local semispan. Actual thickness-to-chord ratios specified for this wing section are

3.89 percent at the aircraft centerline and 3.47 percent at 82 percent of the semispan, with the corresponding streamwise leading-edge radii of 0.717 in. and 0.113 in. These radii correspond to radius-to-chord ratios of 0.17 and 0.13 percent. (Values of the thickness-to-chord and leading-edge radius-to-chord ratios at other spanwise locations are not documented; hence these precise spanwise variations are not available.) The aircraft used in this experiment was highly instrumented to measure and record onboard parameters associated with the vapor-screen system, the aircraft motion, and the surrounding environment.

It should be noted that the aluminum-skinned wing of the F-106B remained unpainted during this flight program because the initial emphasis was on the development of the various systems. The consequence of having unwanted reflected light (glare) off the wing was considered to be insignificant with respect to the visual data to be obtained. This assumption is examined subsequently.

Flight-Test Program

The aim of the flight-test program was to examine the effects on vortex systems of Reynolds number and Mach number over an angle-of-attack range. Variations of Reynolds number with angle of attack were accomplished by flying a $1g$ deceleration maneuver, mostly near $M = 0.4$, at altitudes decreasing from 35 000 to 15 000 ft in 5000-ft increments. However, the Mach numbers associated with transonic maneuvering (at load factors between $4g$ and $5g$) at a constant altitude were impossible to sustain because this aircraft is thrust limited. Thus, these transonic maneuvering tests had to be made during a spiral descent with the afterburner on. The Mach number generally reached was between 0.7 and 0.8 for $\alpha \approx 19°$. For all maneuvers, the best vapor-screen contrast was obtained by flying at night with the Moon down. Operational procedures led to an angle-of-attack variation of $\pm 0.5°$ during data taking.

During the flight test several parameters associated with the vapor-screen system were varied from flight to flight to determine their effect on the visual data. These test parameters include the probe-tip location and light-sheet width. The former appears in the data figures directly, whereas the latter is given in terms of the light-sheet box slit-width opening. There were six probe-tip locations, as shown in figure 6, and three light-sheet widths. At the wing leading edge the widths were 0.18, 0.75, and 1.50 in., corresponding to light-sheet slit widths of 0.003, 0.012, and 0.041 in., respectively. (The height of the light sheet at the wing leading edge was a constant 34 in. measured perpendicular to the upper surface.) A more complete discussion of the flight-test program is given in reference 11.

Basic Video-Image Results

General

Video Orientation

Because almost all published vapor-screen photographs are taken from either the rear or the side, figure 7 has been prepared to help orient the reader to the basic visual record generated by the front-mounted, aft-looking video camera used in this flight test. The left-hand portion of figure 7 shows the arrangement of the light sheet, video camera, and seeding probe on a plan-view sketch of the aircraft. This figure also shows the camera field of view, which is highlighted on the right-hand portion in terms of the monitor image. Towards the top is the wing trailing edge, intersecting the right side is the wing leading edge, and across the lower left corner is a portion of the fuselage. In the middle of the image, parallel to the trailing edge, is a line depicting the light-sheet footprint. Note that it does not extend to the leading edge because of wing camber. The wing outline was not visible at night (except with afterburner on); nevertheless, the vortex system could be seen above the wing upper surface since the concentrated, condensed vapor scattered or reflected the light provided by the sheet.

This figure also shows the plane of the light sheet to be 11.2° ahead of perpendicular to the aircraft longitudinal axis and to cross the leading edge ahead of the wing slot. This location was chosen in order to study the classical delta-wing vortex system. The light for the sheet is generated in the light-sheet box (see fig. 4) and projected downward onto a 45° mirror to produce a sheet oriented perpendicular to the upper surface of the wing.

Video Data Development

The video data were recorded in black and white from which the original set of photographed images was generated. Each image had associated with it a set of vapor-screen and aircraft test conditions, including angle of attack, altitude, Mach number, and Reynolds number. However, since the images were recorded with a VCR at a rate of 30 frames/sec and each data point was held for about 10 sec, there was a group of images with little difference in picture content (i.e., stable flow) at essentially the same test conditions. Therefore, it was decided to select one of these images off the monitor with the "brightest reflection" for photographing. It is these images

which form the basic (i.e., qualitative) video data from the flight test.

The phrase "brightest reflection" refers to the consequence of the light-sheet operation. The intended mode of operation was to be continuous but it was determined, because of the occurrence of an electrical fault, that an intermittent operation produced a brighter reflection. Furthermore, a brief illumination of the light sheet was sufficient for image viewing, since the video data were being recorded. Thus, it was decided to operate the sheet in an intermittent mode.

To obtain quantitative information about the vortex system, a grid composed of 6-in. squares, laid out on a 4- by 8-ft plywood sheet, was recorded in daylight with the camera in its flight position. This took place with the grid positioned along the light-sheet footprint, perpendicular to the wing upper surface and extending to the leading edge. The grid was then traced onto plastic off the monitor face in order to establish a scale to measure details about the leading-edge-vortex system. Though data have been developed in this manner and reported in references 12 and 13, the accuracy of the results is much better for the external extent of the envelope than for the internal details, particularly the core location.

Core Location Defined

The process of quantifying the vortex-system envelope from the video flight records is straightforward if a VCR with freeze-frame capability, a monitor, and a grid is used. What was not straightforward was the determination of the core location, since this round-edged, cambered wing seemed to develop a more diffuse vortex system devoid of a "classical" core. The reason to support the existence of a core for this vortex system is based on the hypothesis that if no core were present, the distribution of reflective particles would be nearly uniform throughout. Since there was a variation in the distribution of reflective particles within the vortex system, a core is said to have existed.

The core location is defined (for both black-and-white and enhanced images) as occurring within the vortex envelope where a spot existed about which both the light scattering or reflection was the brightest (i.e., highest concentration of reflective particles) and the system rotated. This is different than what happens when seeding with water particles. There the identification process for the core uses thermodynamics, in particular vaporization within the core (if the pressure is low enough or temperature high enough) and condensation on the boundary. However, this does not work nearly as well for the condensed propylene-glycol-vapor particles since they are much slower in vaporizing than water due to glycol having a much lower vapor pressure at the temperatures of interest. Furthermore, these glycol particles are about 6 μm in diameter, have a density approximately that of air, and diffuse slowly. These factors result in the particles being involved in the simple process of following the local flow, which in turn leads to a particle concentration in the core region (because of inflow) and, upon illumination, a bright reflection (private communication from Robert A. Bruce, NASA Langley Research Center).

One unexpected result from this flight test was the occurrence of multiple large-scale corotating vortices on the left wing panel ahead of the leading-edge slot. This consistently occurred when seeding was from probe-tip location 1. Since the vortex system at the leading edge was of fundamental interest—it being the only one which grew in size with increasing angle of attack—then the spot within its envelope was chosen to be *the* core location. Thus, the documented results presented herein focus on the outermost vortex system—the leading-edge one—and its core.

The present results showing multiple vortices are recognized to be in contrast with the abundance of published vapor-screen photographs of sharp-edged wings, regardless of scale, which show the wings to have a single primary vortex system and a classical core. However, it should be remembered that the photographic results presented herein may be considered as a first opportunity to observe the effects of full-scale Reynolds number on the vortex system generated by a round-edged, cambered, swept wing.

Discussion of Images

The sensitivity of the recorded vortex-system images to variations in the vapor-screen and flight parameters is discussed in this section.

Vapor-Screen Parameters

Effect of probe-tip location. The location of the seeding probe tip is critical to the entrainment of vapor into the vortex system, as shown by the recorded images in figure 8(a) at $\alpha = 19°$. (Slit-width opening is 0.041 in.) The locations of the four probe tips cited in this figure are given in figure 6 in terms of distance perpendicular to the leading edge and distance along it from the wing-inlet juncture. Upon an examination of these photographs, it is evident that only a small part of the vapor dispensed from probe locations 4 and 5 was entrained into the leading-edge vortex system. Moreover, that vapor which was entrained revealed the faint image of multiple vortices (see fig. 8(b)), similar to the more distinct

dual vortices of probe 1. Since one of the main focuses of this investigation was the vortex core region, a higher level of vapor entrainment than that provided by probes 4 and 5 is needed in order to supply more flow details. This can be accomplished by using probe location 1, but location 6 is also a viable possibility. (The vortices to be discussed are those outboard since those inboard, near the fuselage, are not completely defined by this vapor-screen system.)

Just entraining more vapor was no guarantee that what was seen faintly would be made more visible, as evidenced by the single leading-edge vortex in the photograph associated with probe 6. Thus, although it is not surprising that the probe-tip location could cause the vapor to be entrained in different parts of the upper-surface flow, it is surprising that a different leading-edge vortex system would be shown in figure 8 once sufficient entrainment occurred. Furthermore, the difference was not trivial, since one image (for probe 6) shows the anticipated single vortex while the other (for probe 1) shows two vortices. Therefore, an understanding is sought as to the cause of the difference.

One key factor must be the seed-particle trajectory, which is dependent on the aircraft local flow in the probe region—principally associated with whether the probe tip is ahead of or behind the attachment line—and on the probe orientation. However, even if these details are unknown, the major issue concerning the number of vortices can be settled because, at a high enough value of α, all videotape data show only a single primary leading-edge vortex present. Based on this knowledge and a reexamination of the videotape data for probe 6 at $\alpha = 17°$ and 18°, the difference can be resolved in that these data showed multiple vortices to exist at $\alpha = 17°$ and 18° but only a single vortex existed at $\alpha = 19°$. Hence, this probe location did not behave fundamentally different than the others; it only caused the merging of multiple vortices into a single vortex at a slightly lower value of α than did probe 1.

The conclusion, then, is that this wing develops both multiple and single leading-edge-vortex systems, and the probe location affects the angle of attack at which the multiple vortices merge into a single one. Furthermore, from figure 8 it is learned that the probe should be located on the lower surface, about 7 to 8 in. inboard and perpendicular to the leading edge, and not too far forward or else little entrainment will occur and, hence, marginal information will be generated about the vortex system. However, moving the probe tip to a forward location gives the most vortex-system detail for both the $1g$ level deceleration and the high-g spiral descent. Probe-tip location 6 was the best compromise for both maneuvers; hence, black-and-white photographs associated with this location were the ones studied to determine the effects of the various test parameters.

Effect of slit-width opening. This study centered on establishing a balance between two conflicting aspects of the mercury-arc lamp light-sheet system, which are light-sheet illumination and thickness. The first is associated with the generation of sufficient lumens in the light sheet and requires a large slit opening, and the second is to be minimized in order to create a sheet thin enough to reveal the system details and requires a small opening.

Figures 9(a) to 9(h) show the vortex system images over the angle-of-attack range from 16° to 23° at nominal altitudes of 25 000 and 35 000 for slit widths of 0.041 and 0.012 in. with probe-tip location 6 during a $1g$ maneuver. The associated time-history plots of pertinent flight parameters are presented in figures 10 and 11 for the larger slit opening and in figures 12 and 13 for the smaller slit opening. (See ref. 11 for a description of how the time-history plots were developed.) No results are reported for the third slit width, which was the smallest at 0.003 in., because its uncentered mounting in the optical train (see ref. 11) produced insufficient light in the sheet during flight. With respect to the visual-data figures, it should be noted that since the probe location was the same for both openings, any image change—other than that due to the expected illumination intensity change—is attributed to small but measurable differences in the nominal test conditions, primarily angle of attack. (Refer to the *Video Data Development* section for an explanation as to how the images presented herein were acquired.)

Figure 9 shows, in general, that at both altitudes the same global features were identified. However, there were specific differences which are discernible; for example, at $\alpha = 18°$ and an altitude of 25 000 ft the smaller opening better illuminated the other vortex shown in the middle of the picture. Furthermore, it is clear that for $\alpha > 18°$ the wider opening did provide more lumens for vapor particle reflection in the vortex, as indicated by the larger area of white. In this same angle-of-attack range at 25 000 ft, other image differences are noted in that for the smaller opening the outboard vortex was slightly smaller and a larger amount of vapor was illuminated inboard. The outboard feature was dependent on angle of attack and leads to the tentative conclusion that the actual values of aircraft angle of attack, associated with the video frames from which these photographs were made, were greater for the larger opening than for the smaller one. This is reexamined subsequently with the enhanced images.

The effect of slit width was also examined for flights during high-g maneuvers, as shown in figure 14. Therein the details of the vortex systems are compared at $\alpha \approx 19°$ for the $1g$ and high-g maneuvers, which occurred at Mach numbers of roughly 0.4 and 0.7, respectively; and figures 15, 16, and 17 provide the time-history plots for $M \approx 0.7$. The photographs in figure 14 were taken for the same two slit widths, and the high-g maneuvers were done both to the left and to the right to help determine if the results were biased due to centrifugal force effects. The basic conclusions from figure 14 are that with either slit width the vortex system appears similar under the same maneuver conditions and there were no appreciable centrifugal force effects. This is obvious at $1g$ but not so for the high-g maneuver. The images recorded for the latter show a "classical" core or void region to be visible only with the 0.012-in. opening. However, the location of that void region compares favorably with the core for the 0.041-in. slit width, obtained by application of the core location process described previously. Hence, a tentative confirmation of the location process exists. Since there was only one image which displayed a classical core for the entire flight program, no other comparisons of this type are possible.

Based on the preceding, it is clear that follow-on flight tests can use the 0.012-in. slit width to obtain acceptable visual data, even though most of the visual data taken during this test were with a slit-width opening of 0.041 in. (There were only three flights with the smaller openings, one at 0.012 in. and two at 0.003 in.)

Effect of light-sheet reflection from the wing. Vapor-screen models tested in wind tunnels are painted flat black to minimize the consequence of having reflected light illuminate the vortex at an undesirable location or produce a glare in the camera. For the present study the wing was not painted, and this is shown in figures 8, 9, and 14 to have had no significant consequences. Furthermore, just as assumed, the unpainted wing did not interfere with the recording of the vortex-system details for this flight program. However, an initial inspection of one image in figure 14, associated with the 0.012-in. slit width at the high-g maneuver, indicates it has a reflection or glare problem at the lower left side which might be attributed to the unpainted aircraft. Yet a closer inspection shows the glare did not come from a wing reflection but instead from the light reflecting off the condensed vapor. Regardless, painting the wing upper surface flat black may be desirable in future flight tests, so it is recommended that it be done to help prevent any unwanted light capture.

Flight Parameters

It needs to be understood that in a flight program the effects of Mach number, Reynolds number, angle of attack, lift coefficient, and load factor are difficult to isolate exactly without an extensive test matrix. The flight test reported herein was based on a limited test matrix which resulted in the effects of certain parameters being masked individually because they appeared in combination with others. Therefore, all succeeding sections reporting on the effects of flight parameters need to be read from this perspective.

Effects of Reynolds number and lift coefficient. Figures 18(a) to 18(h) display the vapor-screen images obtained with probe-tip location 6 and a slit-width opening of 0.041 in. for subsonic speeds over a Reynolds number range (associated with altitudes of 20 000, 25 000, 30 000, and 35 000 ft) and an angle-of-attack range. The affiliated time-history plots for these altitudes are given in figures 19, 10, 20, and 11. Unfortunately, the Reynolds number could not be maintained at a constant value for any of these altitudes, in part because the altitude could not be held constant for the $1g$ maneuver; hence, these altitudes only serve as nominal values. The $1g$ maneuver started near the nominal altitude at a moderate angle of attack for trimmed flight. Then, as angle of attack was increased, the thrust was adjusted to maintain altitude until the military power setting was reached after which, with angle of attack and drag still increasing and thrust not, a gradual descent commenced. This caused the altitude and Mach number to decrease, and since the speed was falling faster than the atmospheric density was increasing, the Reynolds number also decreased. However, this does not prevent the effect of Reynolds number from being examined for these images; it only means that the range of Reynolds numbers to be considered is relative to the images at a particular angle of attack.

An examination of figure 18 shows the primary Reynolds number effect was associated with the flow around the round leading edge. For example, at $\alpha = 18°$, figure 18(c) shows that at $R_n = 28 \times 10^6$, which corresponds to the highest altitude, the leading-edge vortex was well established, but it was not discernible at $R_n = 32 \times 10^6$. Between these extremes, progressively smaller leading-edge vortices were observed with increasing Reynolds number. These photographs indicate that the leading-edge vortex was first clearly visible at $\alpha = 19°$ for the

highest Reynolds number. This delay in vortex visualization has been attributed in reference 12 to the lack of leading-edge separation at the higher Reynolds number, as would be expected for round-edged wings. However, a reexamination of the lower-altitude videotape data for the smaller values of α can lead to an alternate conclusion, one in which the effects previously associated only with increasing Reynolds number may involve other parameters. This is possible because it is extremely difficult in a flight program, even a research one, to have only a single parameter change at a time. In particular, the issue centers on what parameter(s), besides Reynolds number, could change sufficiently at a fixed angle of attack and decreasing altitude to cause a decrease in the vapor entrained in the vortex and a reduction in its size.

Both of these effects make the leading-edge vortex difficult to see and are associated with the location of the lower-surface attachment line. Since this line is generally not very sensitive to Reynolds number, its primary dependence is sought. The obvious answer is angle of attack, but that value is being held essentially constant for each figure. A related answer is lift coefficient, since it is dependent on angle of attack as well as Mach number and controls the vortex strength, which affects both vortex size and vapor entrainment. Though lift coefficient is not calculable because the instantaneous total weight value is not available during or after flight, what is known is that the $1g$ maneuvers were done in the order of decreasing nominal altitude. Hence, the associated beginning fuel weight decreased as the nominal altitudes declined from 35 000 to 20 000 ft, and the average value of Mach number required to maintain $1g$ during a maneuver was reduced from 0.43 to 0.31. The associated lift-coefficient reduction was not great; however, it may have been enough at the lower values of α and altitudes to be a major contributor to the generation of a slightly weaker vortex—one having a smaller size and developing less entrainment. So what had been initially identified only as a Reynolds number effect has been expanded to include the effect of lift coefficient. For $\alpha > 19°$, the leading-edge vortices are shown in figure 18 to have been of appropriate strength (and size) to entrain adequate vapor for visualization at all Reynolds numbers and associated lift coefficients.

As an aside, a reexamination of the videotape data for lower angles of attack showed there existed three to four weak vortices for both $\alpha = 17°$ at 25 000 ft, $R_n = 31 \times 10^6$, and $M = 0.37$ (see fig. 18(b)) and $\alpha = 18°$ at 20 000 ft, $R_n = 32 \times 10^6$, and $M = 0.32$ (see fig. 18(c)). This is interesting and gives added credence to the importance of lift coefficient in the generation of vortex systems in that one can estimate the two effects of increasing angle of attack and decreasing Mach number to yield a similar value of lift coefficient and, hence, a similar flow situation. However, it should also be noted that the Reynolds numbers for these two situations were almost the same, and this too could have contributed to the flow similarity.

The occurrence of more than one vortex of the same rotational sense on the same wing panel (based on the video visual cues) is an unexpected vortex flow feature which is Reynolds number dependent and is somewhat discernible in figure 18(b). This is more clearly shown after image-enhancement techniques are applied to the photographs associated with probe-tip location 1; therefore, a discussion of this feature is delayed until that section.

Effect of Mach number. The effect of Mach number cannot be totally isolated from the change in load factor in figure 21, since both increased for the transonic maneuver. However, based on wind-tunnel tests, an expected change would be for the vortex core to move to a more inboard location with a Mach number increase (ref. 15). This figure is obtained by tracing the vortex envelopes, single or dual, off of black-and-white photographs (fig. 14 bottom center and fig. 9(c), respectively) and estimating the core locations, as described previously. Figure 21 shows that at $\alpha \approx 18°$, for the two maneuvers flown, doubling the Reynolds number by increasing the Mach number did not delay the formation of the leading-edge vortex, as might be anticipated. Hence, the more inboard extents of the envelope and core are attributed to the Mach number doubling and the load factor difference. The latter will be manifested as aeroelastic effects.

Enhanced-Video-Image Results

General

Image-enhancement techniques were applied to the videotape images to help quantify some of the global properties of the vortex system, particularly the core location. This was needed because of two major deficiencies associated with use of the previously described video data development for black-and-white images. The first deficiency deals with the wrong comparative answer being obtained when a group of photographs is examined. This can occur if the setting for monitor brightness is changed significantly during the photographic session, thereby resulting in a "ballooning" effect produced for the white part of some images but not others. The second deficiency is due to the subjective nature of establishing details within the vortex envelope when

one relies on visual cues from the monitor, rather than on a more objective procedure associated with using a still image. Both deficiencies were overcome through image enhancement.

The image processing laboratory (TIPL) at the NASA Langley Research Center, described in reference 16, was the system utilized to obtain enhanced images. The steps employed in going from the video data to enhanced images are as follows:

1. Digitize the videotape frames in real time (30 frames/sec), converting the visual information into a matrix of integer gray-level values (ranging from 0 to 255) representing the brightness of the image at each picture element (pixel); this brightness can be processed by the computer. This digital image (512 × 512 pixels) is then stored onto the real-time disk.
2. Select the image having the brightest reflection from the images at a given test point stored on the disk.
3. Save that image as a named file.
4. Use a lookup table to apply pseudocolor to the black-and-white image, making subtle changes in particle concentration more evident.
5. Convolve (with a low-pass filter) each saved image to smooth out the graininess induced by digitizing low-contrast images.
6. Use the lookup table to black out pixels in the image with gray-level values within a range selected by the use of a trackball, thereby establishing contour lines of constant particle concentration.
7. Save the lookup table for each image.
8. Transmit both the lookup table and the image to a film recorder to convert the enhanced digital image back into a photographic medium (Polaroid photographs or negatives).

For images in which quantitative information was desired, such as core location and inner extent of the vortex envelope, a grid was added to the previously developed image so that when the photographic negative was made it contained its own scale. This grid was obtained by correlating the image of the physical grid, described previously, with the enhanced image through the use of a warping board. (See ref. 17.) Then step 8 above was implemented to obtain a permanent record.

Discussion of Enhanced Images

Effects of Multiple Vortices and Reynolds Number

During the flight test at $1g$ and subsonic speeds, large-scale multiple vortices were recorded via the black-and-white video camera. Their appearance was indicated by the concentration of reflective vapor at more than one location, the assumption being that one vortex exists per concentration. This phenomenon was also noted to occur at many test points rather than just as an isolated example, especially for probe-tip location 1. However, it was not until image-enhancement techniques were applied that the internal details of these concentrations became discernible.

Figure 22 shows clear evidence of the enhanced images at $\alpha = 17°$ and $20°$ having three and two vortex core regions, respectively. It is also clear that at $\alpha = 20°$ the vortices had the same rotational sense (i.e., corotating) above the left-wing panel (as viewed from the front) since they are both *leaning* in the same direction. It should be further noted that no large-scale multiple vortices have been previously reported from other flight tests or observations, though reference 18 reports a dual-vortex result for a round-edged 65° cropped delta wing at $\alpha = 20°$ and $M = 0.85$ from an Euler code. This is the only known computational fluid dynamics (CFD) multiple-vortex solution for wings with swept leading edges. Furthermore, the dual-vortex result at $\alpha = 20°$ differs from the result obtained in the Langley 30- by 60-Foot Tunnel (ref. 12) in that in the wind-tunnel test of the F-106B half-aircraft model only a single vortex was found to exist, as shown by the photograph in figure 23. The region photographed was above the left wing (as viewed from an aft-mounted video camera) in a test setup which had the probe tip in essentially the same location as that for probe 1 in the flight test.

In flight, single leading-edge vortices were found to occur at the higher test angles of attack at all altitudes. However, the angle of attack required for the single-vortex occurrence was a function of altitude (or Reynolds number), in that at the higher altitudes (lower Reynolds numbers) the vortex was formed at a lower angle of attack. In retrospect, it is understood that the wind-tunnel result was consistent with the flight result, because the wind-tunnel Reynolds number (12×10^6) was about half of the lowest flight value.

Effects of Test Conditions on Vortex System at an Altitude of 25 000 Ft

Figures 24 to 27 contain enhanced images obtained for a nominal altitude of 25 000 ft at a variety of test conditions relating to probe-tip location, slit-width opening, and intermittent or continuous light-sheet operation. The associated flight-parameter time histories are presented in figures 28, 29, 10, and 12. Figure 30 summarizes the vortex features of envelope inboard extent m, core lateral

location l, and core height above the wing z, for the outboard vortex for these four flight serials. (A flight serial is one particular maneuver during a flight and is denoted herein by the integers yy in 85-xxx/yy, where the flight number is 85-xxx; however, in this paper the term "flight serial," or just "serial," will refer to the entire number.)

Figure 30 shows each feature to have a generally increasing trend with α, though z is only a weak function of α, for all serials. Furthermore, this figure shows there exists considerable data scatter for each feature between serials at a fixed value of α. The maximum values of the scatter are 16, 10, and 5 in. for m, l, and z, respectively, with an accuracy of ± 1 in. The individual results for serials 85-011/05 and 85-012/06 provide an opportunity to reexamine a previous conclusion made in the discussion of the effect of slit width on the black-and-white images of figure 9. The conclusion was that the actual angles of attack for the images with the larger slit width (0.041 in. on 85-011/05) must have been greater than those for the images with the smaller opening (0.012 in. on 85-012/06), since the envelope was larger and since envelope size, in general, varied directly with α. Figure 30 lends some credence to the conclusion for the envelope feature principally at $\alpha = 18°$ and 19°; however, the remainder of the data lie nearly within the accuracy band. Further support comes from an examination of the data for the core lateral location at $\alpha = 19°$ and 20°. Beyond these values of α the rest of these data generally lie within the accuracy band. However, the core height data suggest that the higher values of α occurred during the test with the smaller opening rather than with the larger one. In summary, then, the previous conclusion about the angles of attack associated with the images for the 0.041-in. slit width being greater than those associated with the images for the 0.012-in. slit width opening cannot be conclusively confirmed through use of the enhanced images, though at $\alpha = 19°$ the conclusion seems to be correct.

For serials 85-009/06a and 85-009/09 (from fig. 30), in which the only difference was the light-sheet operation, it appears possible, upon examination of m, l, and z, that the actual angles of attack associated with the intermittent operation may be higher than those associated with the continuous operation by about 0.5°. This may not be surprising when one considers the discussion in the *Video Data Development* section. However, the preceding is not necessarily conclusive because it is more difficult to obtain accurate values for the vortex-system features, especially the core location, with the continuous light-sheet operation because of the reduced amount of light emitted, and subsequently scattered, in that mode. Nevertheless, there appears to be enough consistent evidence to support the conclusion that there existed a difference in actual angles of attack between the two sets of results. This difference indicates a probable accuracy of 0.5° in the reported values of α for the vortex-system features.

With this in mind a reexamination of figure 30, in which only the intermittent light-sheet data are considered, is in order. The maximum values of the scatter for this condition are 8, 8, and 3 in. for m, l, and z, respectively, which is a great improvement in m but only a slight improvement in l and z when the data accuracy of ± 1 in. is considered. However, it is apparent from this figure that below $\alpha = 22°$ the data are in even closer agreement, with the maximum scatter for m and l being limited to 6 and 5 in., respectively. Hence, the intermittent results compare fairly well, even when some are determined from the outer vortex of a dual system rather than from a single-vortex system. Furthermore, a general conclusion from all the intermittent results is that they only agree completely at $\alpha = 21°$.

With regard to the variation of the vortex-system features with angle of attack for the same slit-width opening but for different probe-tip locations, figure 30 shows both m and l to behave similarly. In particular, probe-tip location 6 results (serial 85-011/05) are generally more inboard for $\alpha < 22°$, while those for probe-tip location 1 (serial 85-009/06a) are more inboard for $\alpha > 22°$. In general, the more inboard results for probe location 6 are likely due to the probe location 1 measurements being made on the outer vortex of the dual-vortex set, which finally does merge around 21°. Another factor to consider for $\alpha > 21°$ is that the actual angles of attack for serial 85-009/06a may be slightly higher in this range. A comparison of figures 28 and 10 shows this to be possible.

Effects of Lift Coefficient and Reynolds Number on Vortex Systems

Lift coefficient has been identified as an important parameter, along with Reynolds number, in the previous section on black-and-white visual images; however, the coefficient values are not known. This limits their usefulness in the following discussion to only a global implication. That is, a higher lift coefficient will most likely be generated at 35 000 ft than at 25 000 ft at the same value of α because of the higher fuel weight present and higher Mach number required for the $1g$ maneuver. Notwithstanding the preceding, this section examines enhanced images to look for Reynolds number effects on the vortex envelope and core over an angle-of-attack range from

17° to 23°. The data used are from figures 31 and 32 for a nominal altitude of 35 000 ft and from figures 26 and 27 for a nominal altitude of 25 000 ft. Angles of attack and Mach numbers are similar for all four figures. The data have been summarized in figure 33. (The associated time-history plots are given in figs. 10 to 13.) In figure 33 it is shown that, in general, the inner extent of the vortex-system envelope and the lateral core location are more inboard at the lower Reynolds number (i.e., higher altitudes). Also, at the lower altitude, the envelope and core tend to be more monotonic in their growth with angle of attack. It is interesting to note that at 20° and 21° the results seem to coalesce, after which the measurements corresponding to the higher Reynolds number (i.e., lower altitudes) have a significant slope change, indicating the occurrence of a vortex-sensitive event by $\alpha = 22°$. Figure 33 shows the core elevation to be insensitive to changing Reynolds number.

For comparison, reference 12 reports that during the F-106B half-aircraft test at $\alpha = 20°$, $M = 0.1$, and $R_n = 12 \times 10^6$ a similar flight-sized vortex envelope and lateral core location were developed. However, the core elevation was about 4 in. higher in the Langley 30- by 60-Foot Tunnel test.

In summary, the combinations of increasing lift coefficient and decreasing Reynolds numbers at a fixed angle of attack yield vortex systems which have their core lateral locations and inner extent of the envelope more inboard.

Vortex Breakdown

Vortex breakdown is often stated to occur when there occurs a sudden "trumpeting" or "ballooning" of the vortex core at a fixed longitudinal location with only a small change in a test variable, usually angle of attack. From an examination of all enhanced images contained in figures 24 to 27 and 31 to 32—with special emphasis on the results for higher angles of attack—the prevalent conclusion is that core vortex breakdown has *not* occurred at the light-sheet station over the test angle-of-attack range. This conclusion is based on the supposition that breakdown would be manifested in these images as a large inner region with the same color, associated with the pixels having the same gray-level values, representative of a uniform distribution of reflective particles. The preceding is not shown in these figures. Instead what is observed is a small region of the brighter colors at the higher test angles of attack, an indication of particle concentration in or around a *coherent* vortex core.

If vortex core size is regarded as a function of angle of attack, it should be realized that the large core observed at the lower values of α is not associated with vortex breakdown, but instead is the product of the diffuse vorticity produced by this round-edged wing. Therefore, a concentrated core could reasonably be expected to be delayed in forming until the higher values of α.

Conclusions

The vortex flow above an F-106B aircraft wing has been examined through use of the vapor-screen and image-enhancement techniques. With these techniques the following conclusions have been determined:

1. The seeding probe-tip location is critical to seeding the vortex system for illumination and visual recording. Moreover, most probe-tip locations used in this investigation entrain particles in multiple vortices at and below angles of attack of 19°. An exception is the forward, lower surface probe-tip location, (probe location 6) for which the multiple vortices have already merged into a single vortex at this test condition.

2. A slit-width opening of 0.012 in. is sufficient for the light sheet to illuminate the vortex-system details.

3. Painting the wing upper surface flat black for future flight tests may help to minimize the already small amount of light-sheet reflection (glare) off the aircraft wing.

4. Increasing the Reynolds number and decreasing the lift coefficient can reduce significantly the amount of vapor entrained in the leading-edge vortex below an angle of attack of 20°.

5. During the transonic maneuver, increasing the Mach number and the load factor produces a well-defined vortex system which is larger and more inboard than that for the constant-altitude $1g$ flight.

6. Dual large-scale corotating primary vortices have been found to exist at the higher flight Reynolds numbers.

7. A tentative conclusion, based on the black-and-white images, which states that the actual angle of attack associated with the 0.041-in. slit width is larger than that for the 0.012-in. opening cannot be conclusively confirmed from the enhanced images.

8. It appears to be possible that the actual angles of attack for the intermittent light-sheet operation may be higher than those for the continuous operation by about 0.5°.

9. All results for intermittent light-sheet operation compare fairly well, even when some are determined from the outer vortex of a dual system rather than from a single-vortex system.

10. The effect of the seeding probe-tip location on the vortex envelope and the core lateral location is that for an angle of attack less than 22°, the probe 6

results are generally more inboard than those for an aft probe location (probe location 1), while for higher angles of attack the results for probe 1 are more inboard. In large part the more inboard results for probe 6 are likely because the probe 1 measurements are made on the outer vortex of the dual-vortex set, which finally merges into a single vortex at an angle of attack around 21°.

11. In general, the inner extent of the vortex system envelope and the lateral core location are more inboard at the lower Reynolds number and higher lift coefficients (higher altitudes). Also, at the lower Reynolds number, the envelope and core tend to be more monotonic in their growth with angle of attack. The core elevation is insensitive to Reynolds number change.

12. Vortex breakdown does not occur at the light-sheet station for the tested combinations of angle of attack (up to 23°) and Reynolds number.

NASA Langley Research Center
Hampton, VA 23665-5225
April 11, 1988

References

1. Settles, Gary S.: Flow Visualization Techniques for Practical Aerodynamic Testing. *Flow Visualization III*, W. J. Yang, ed., Hemisphere Publ. Corp., c.1985, pp. 306–315.
2. Wentz, William H., Jr.; and Kohlman, David L.: *Wind Tunnel Investigations of Vortex Breakdown on Slender Sharp-Edged Wings.* Rep. FRL 68-013 (Grant NGR-17-002-043), Univ. of Kansas Center for Research, Inc., Nov. 27, 1969. (Available as NASA CR-98737.)
3. Bird, John D.: *Tuft-Grid Surveys at Low Speeds for Delta Wings.* NASA TN D-5045, 1969.
4. Pelagatti, C.; Pilon, J. C.; and Bardaud, J.: Analyse Critique des Comparaisons des Resultats de Vol aux Previsions de Soufflerie Pour des Avions de Transport Subsonique et Supersonique. *Flight/Ground Testing Facilities Correlation*, AGARD-CP-187, Apr. 1976, pp. 23-1–23-24.
5. Fennell, L. J.: *Vortex Breakdown—Some Observations in Flight on the HP 115 Aircraft.* R. & M. No. 3805, British Aeronautical Research Council, 1977.
6. Perry, D. H.; Port, W. G. A.; and Morrall, J. C.: *Low Speed Flight Tests on a Tailless Delta Wing Aircraft (AVRO 707B), Part 4—Wing Flow.* C.P. No. 1107, British Aeronautical Research Council, 1970.
7. Curry, Robert E.; Meyer, Robert R., Jr.; and O'Connor, Maureen: *The Use of Oil for In-Flight Flow Visualization.* NASA TM-84915, 1983. (Revis. 1984.)
8. Chamberlin, Roger: *Flight Investigation of 24° Boattail Nozzle Drag at Varying Subsonic Flight Conditions.* NASA TM X-2626, 1972.
9. Lamar, John E.; and Campbell, James F.: Vortex Flaps—Advanced Control Devices for Supercruise Fighters. *Aerosp. America*, vol. 22, no. 1, Jan. 1984, pp. 95–99.
10. Burdin, I. Yu.; Zhirnov, A. V.; Kulesh, V. P.; Orlov, A. A.; Pesetskiy, V. A.; and Fonov, S. D. (Foreign Technol. Div., Wright-Patterson Air Force Base, transl.): *Use of Laser Methods for the Study of Detached Flows in a Wind Tunnel and in Flight.* FTD-ID(RS)T-1053-82, U.S. Air Force, Oct. 20, 1982, pp. 2–19. (Available from DTIC as AD B069 459.)
11. Lamar, John E.; Brown, Philip W.; Bruce, Robert A.; Pride, Joseph D., Jr.; Smith, Ronald H.; and Johnson, Thomas D., Jr.: *Operational Performance of Vapor-Screen Systems for In-Flight Visualization of Leading-Edge Vortices on the F-106B Aircraft.* NASA TM-4004, 1987.
12. Lamar, John E.: In-Flight and Wind Tunnel Leading-Edge Vortex Study on the F-106B Airplane. *Vortex Flow Aerodynamics, Volume I*, James F. Campbell, Russell F. Osborn, and Jerome T. Foughner, Jr., eds., NASA CP-2416, 1986, pp. 187–201.
13. Lamar, J. E.; Bruce, R. A.; Pride, J. D., Jr.; Smith, R. H.; Brown, P. W.; and Johnson, T. D., Jr.: In-Flight Flow Visualization of F-106B Leading-Edge Vortex Using the Vapor-Screen Technique. AIAA-86-9785, Apr. 1986.
14. Aiken, William S., Jr.: *Standard Nomenclature for Airspeeds With Tables and Charts for Use in Calculation of Airspeed.* NACA Rep. 837, 1946. (Supersedes NACA TN 1120.)
15. Erickson, Gary E.; and Rogers, Lawrence W.: Experimental Study of the Vortex Flow Behavior on a Generic Fighter Wing at Subsonic and Transonic Speeds. AIAA-87-1262, June 1987.
16. Kudlinski, Robert A.; and Park, Stephen K.: *Digital Enhancement of Flow Field Images.* NASA TP-2770, 1988.
17. Rosenfeld, Azriel; and Kak, Avinash C.: *Digital Picture Processing, Second ed., Volume 1.* Academic Press, Inc., 1982.
18. Rizzi, Arthur; Drougge, Georg; and Purcell, Charles J.: Euler Simulation of Shed Vortex Flows Over the 65 Degree Delta Wings. *International Vortex Flow Experiment on Euler Code Validation*, A. Elsenaar and G. Eriksson, eds., FFA, Flygtekniska Försöksanstalten (Sweden), 1986, pp. 289–343.

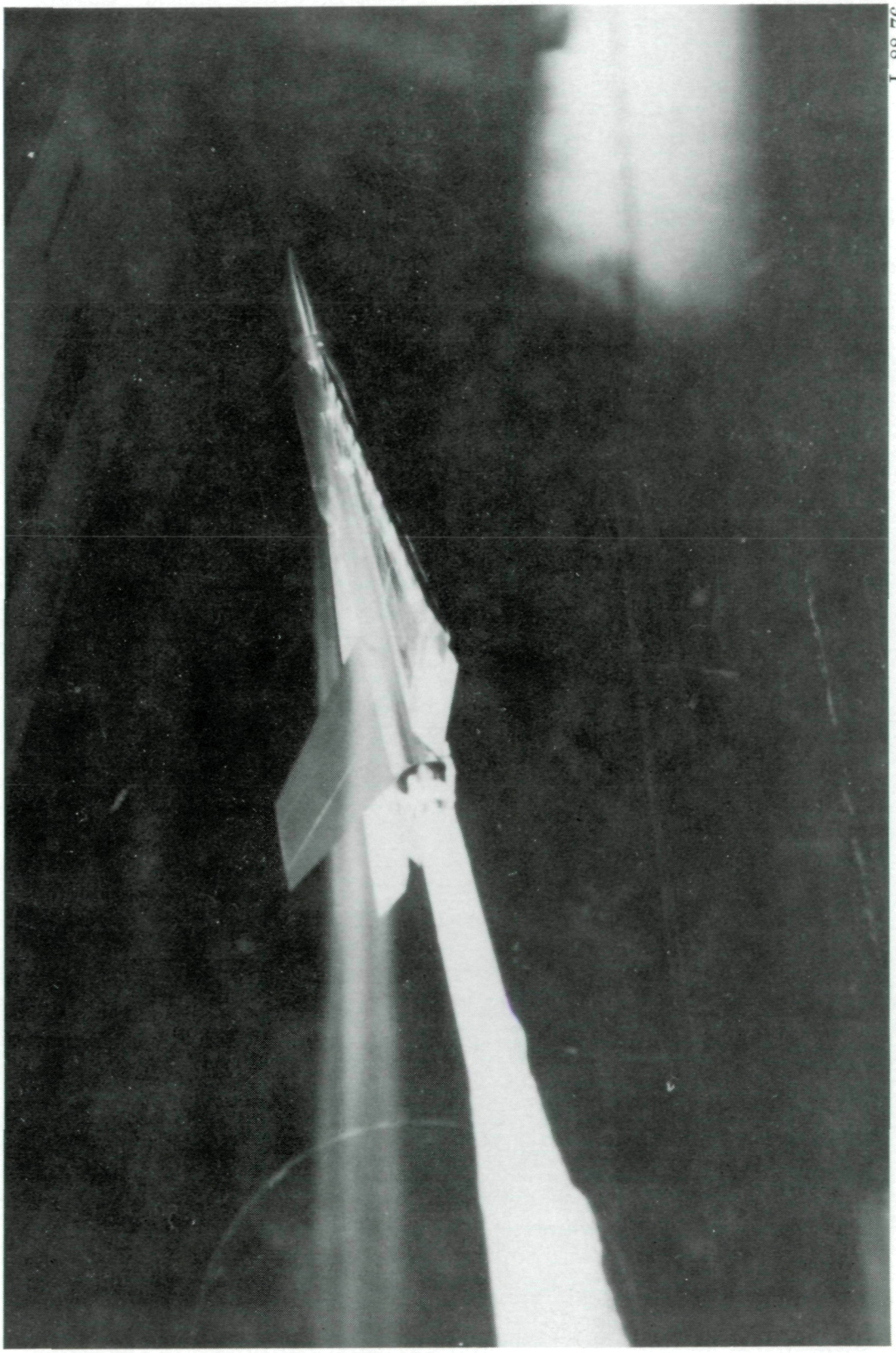

L-88-76

Figure 1. Visualization of leading-edge vortex core on 74° delta wing with upward-deflected vortex flap at subsonic speed.

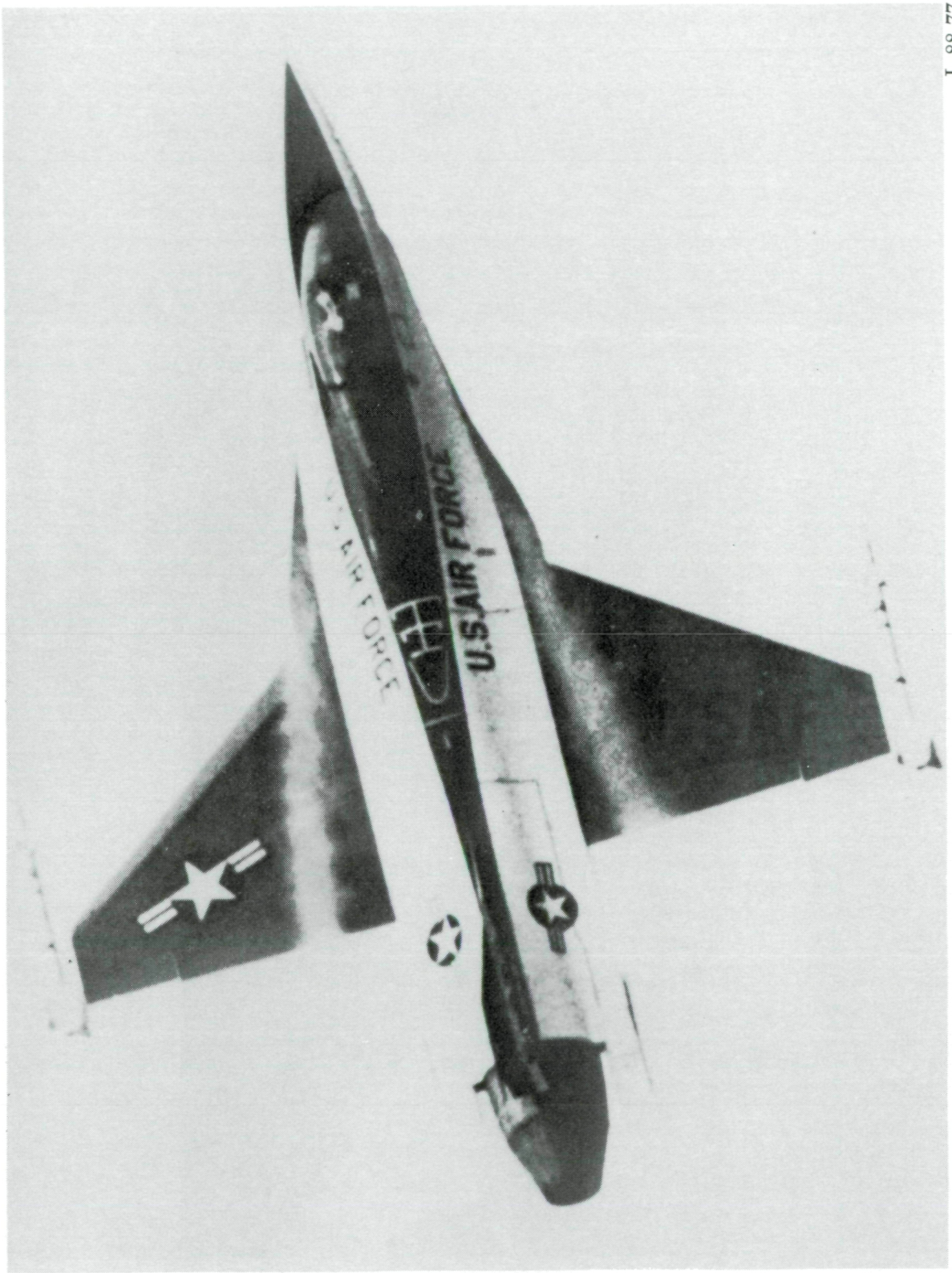

L-88-77

Figure 2. Strake vortex core visible on F-16 during low-speed maneuver.

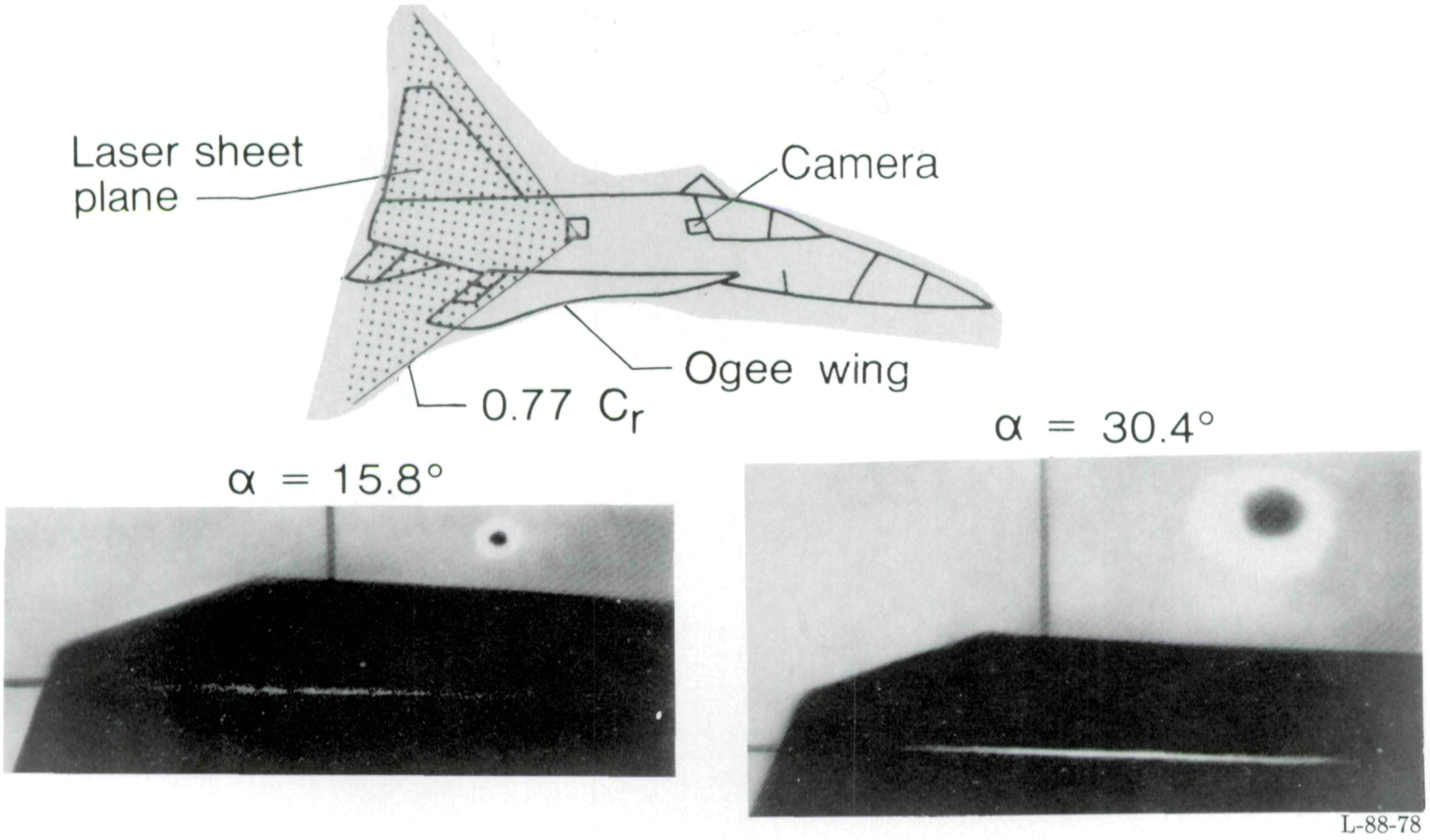

Figure 3. Vapor-screen technique applied to Soviet research aircraft. (From ref. 10.)

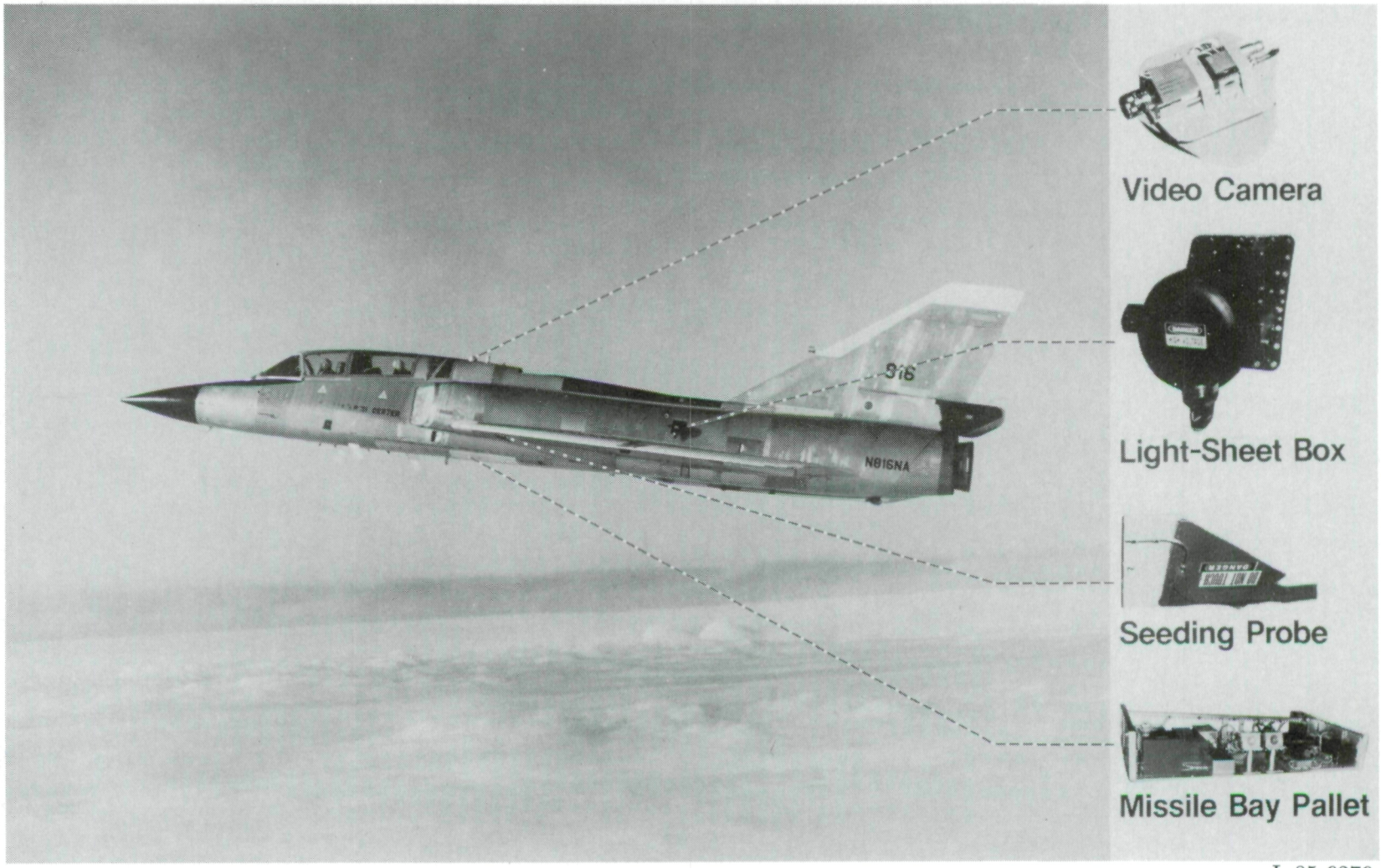

L-85-6276

Figure 4. F-106B flow-visualization elements.

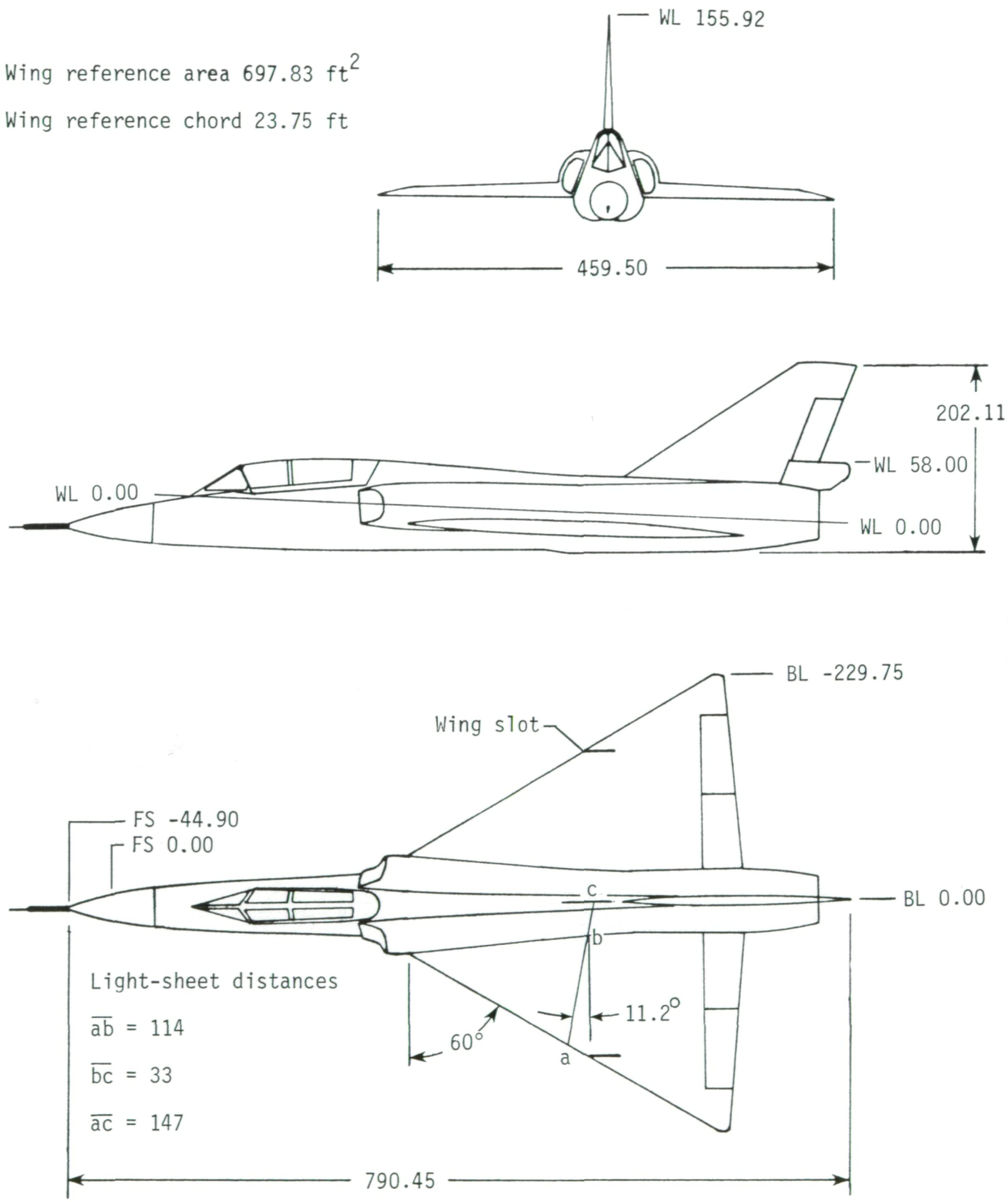

Figure 5. Three-view sketch of the F-106B aircraft. Dimensions are in inches.

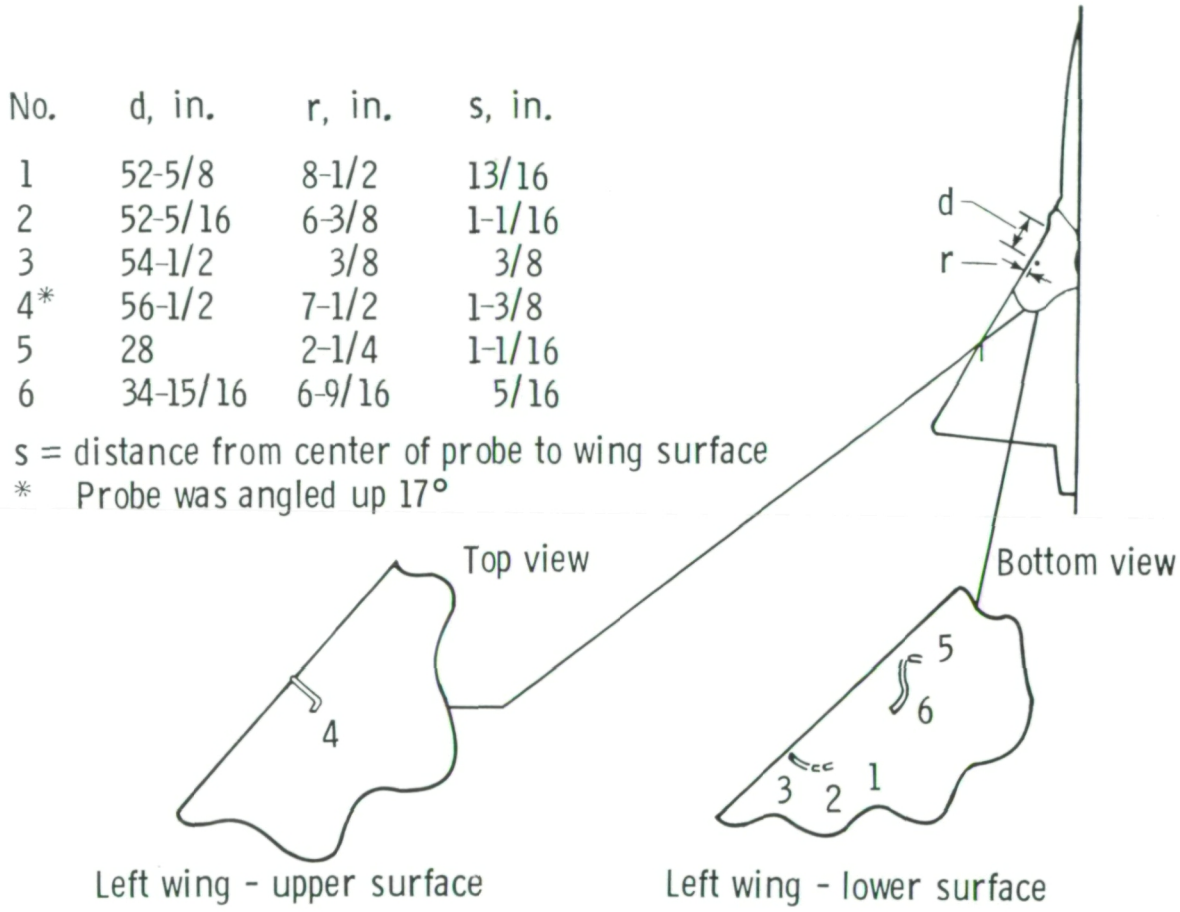

(a) Probe tips.

Figure 6. Seeding system probe-tip locations and probe external housings.

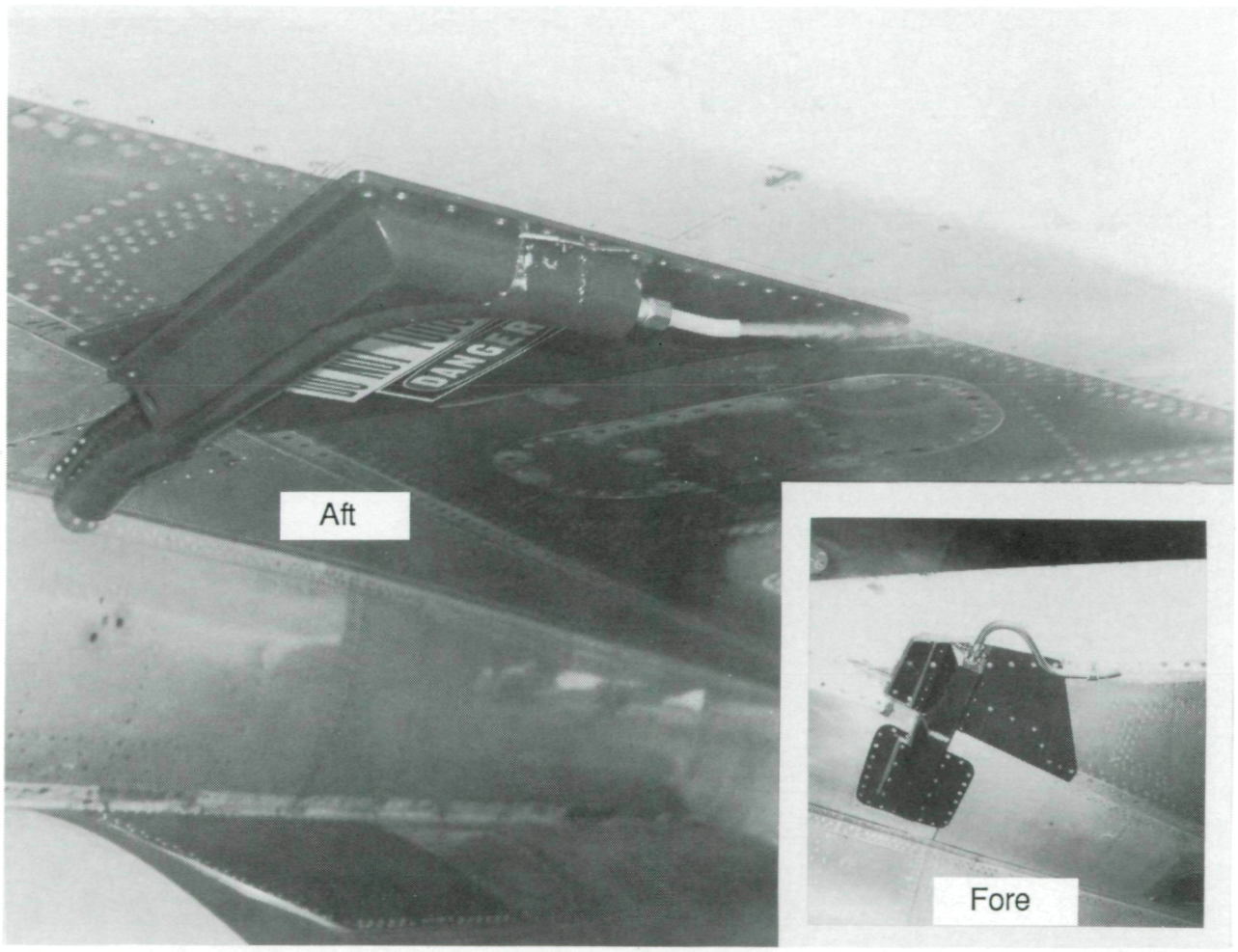

L-87-586

(b) External housings.

Figure 6. Concluded.

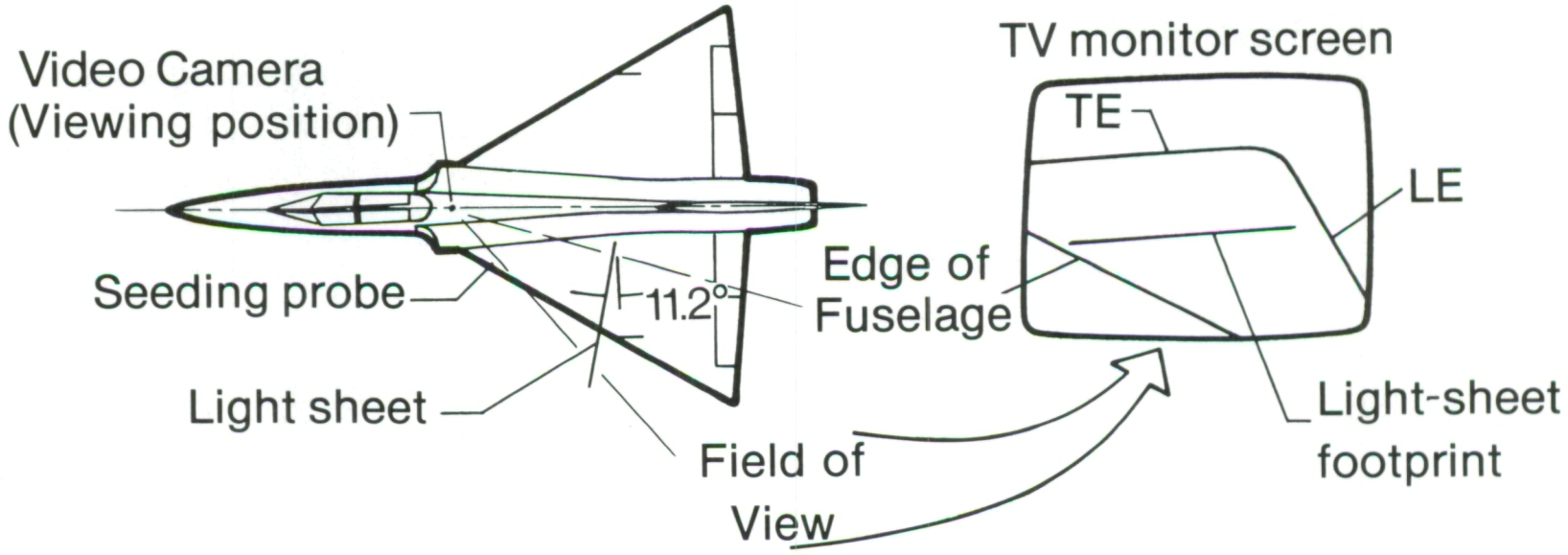

Figure 7. In-flight leading-edge-vortex flow visualization on F-106B.

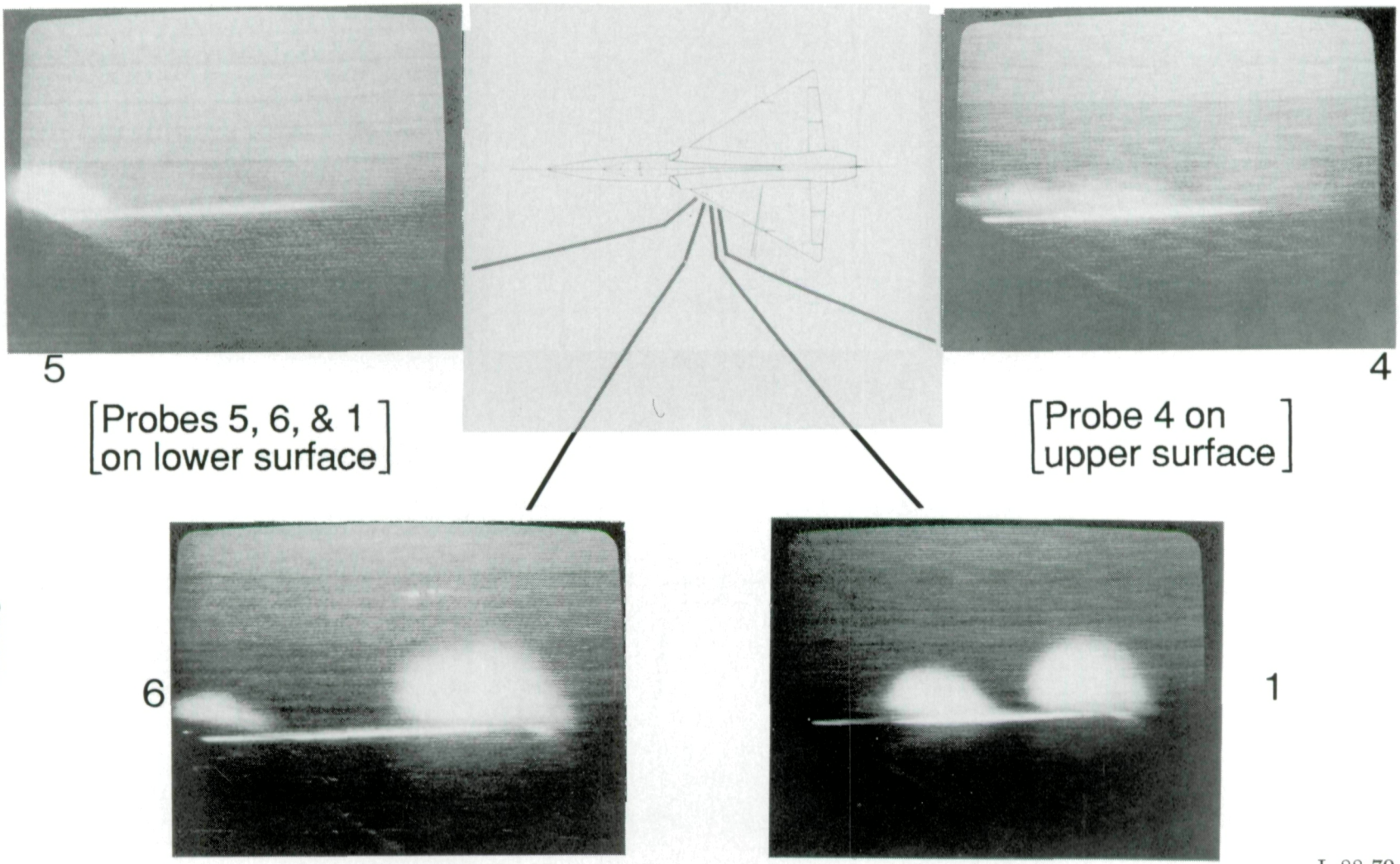

(a) Images.

Figure 8. Effect of probe-tip locations on vortex-system images and tracings. $1g$ maneuver; $M = 0.4°$; altitude, 25 000 ft; $\alpha = 19°$; intermittent light-sheet operation; slit width, 0.041 in.

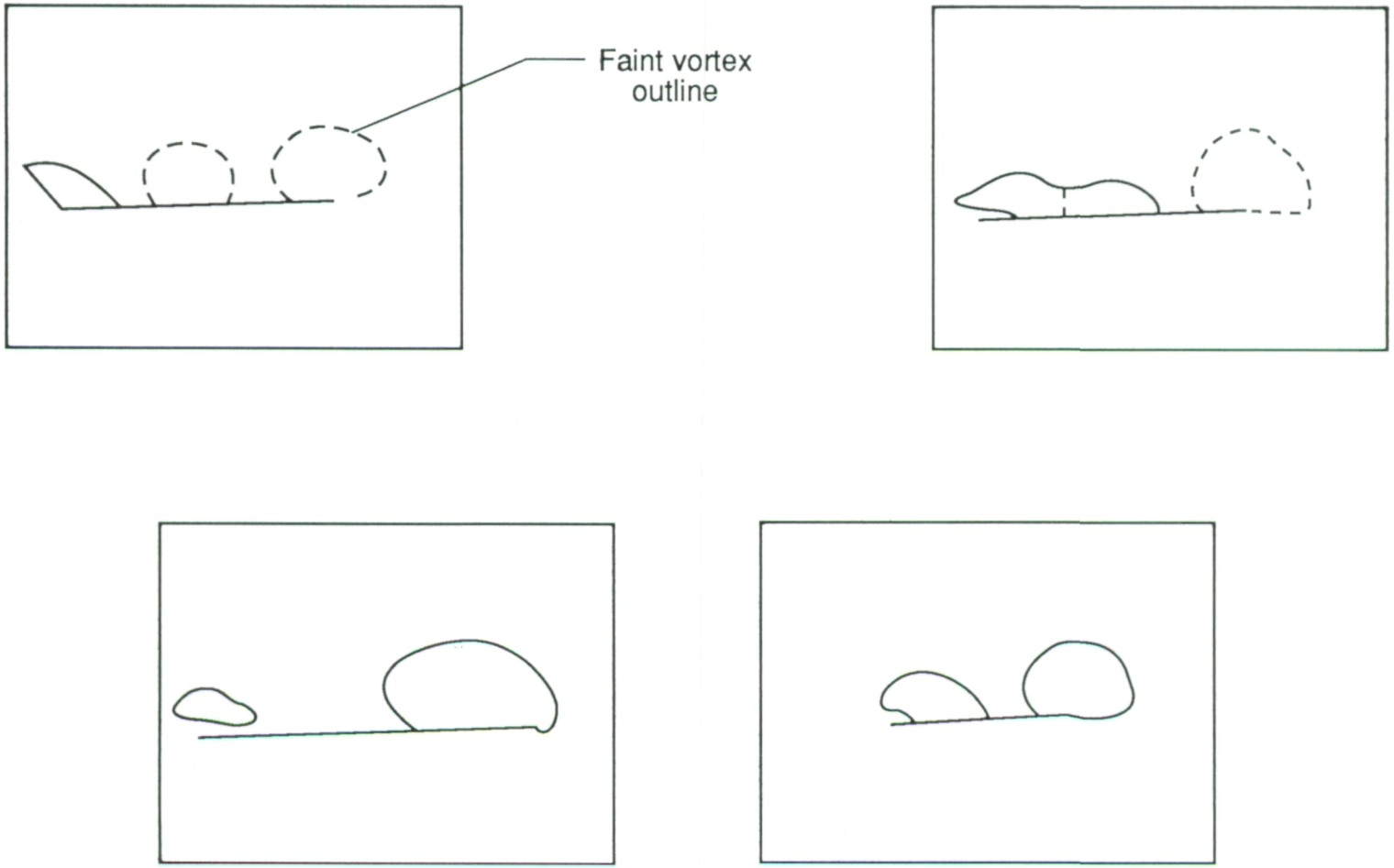

(b) Tracings.

Figure 8. Concluded.

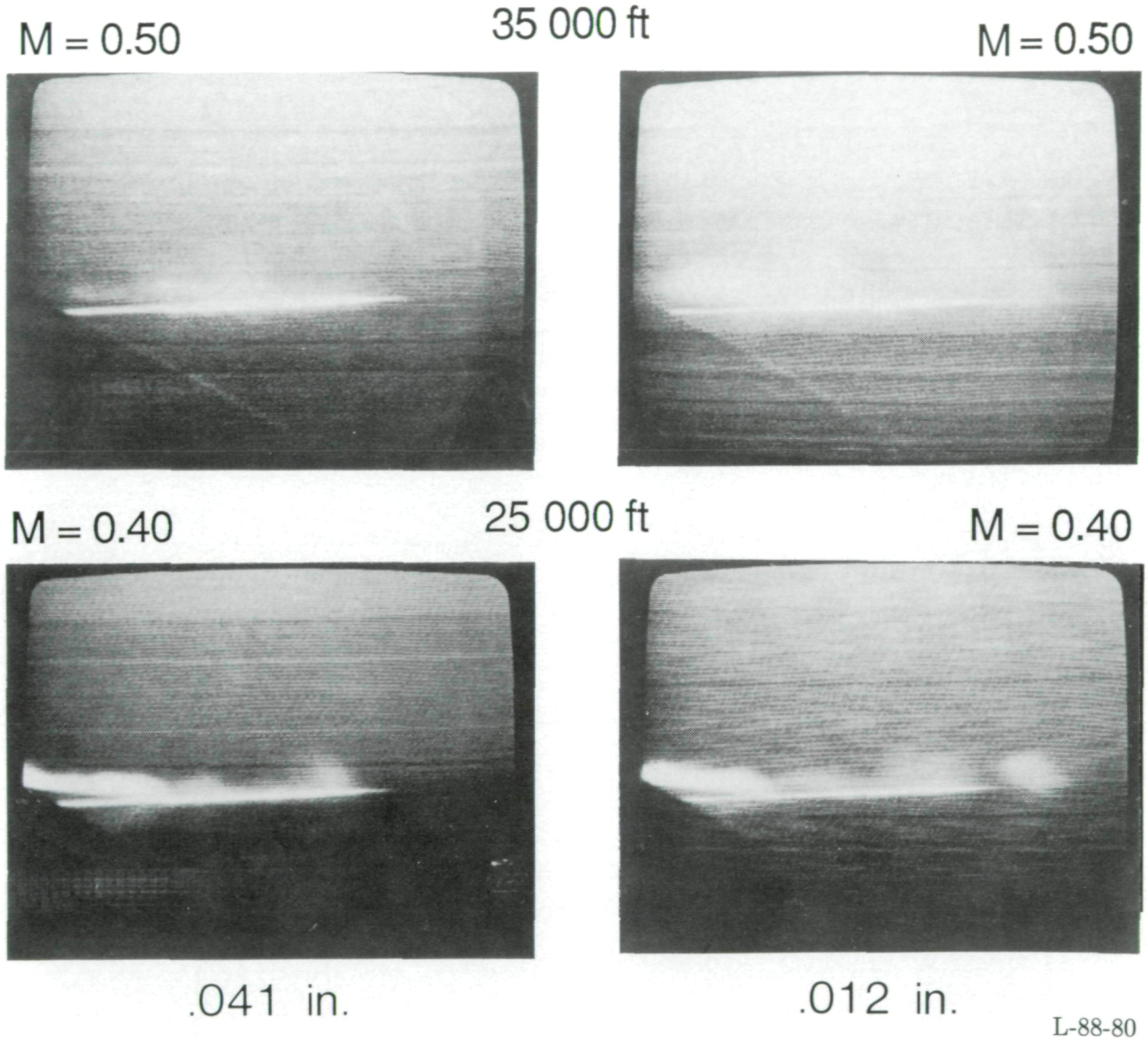

(a) $\alpha = 16°$.

Figure 9. Vortex-system images at two slit widths. $1g$ maneuver; probe-tip location 6; intermittent light-sheet operation.

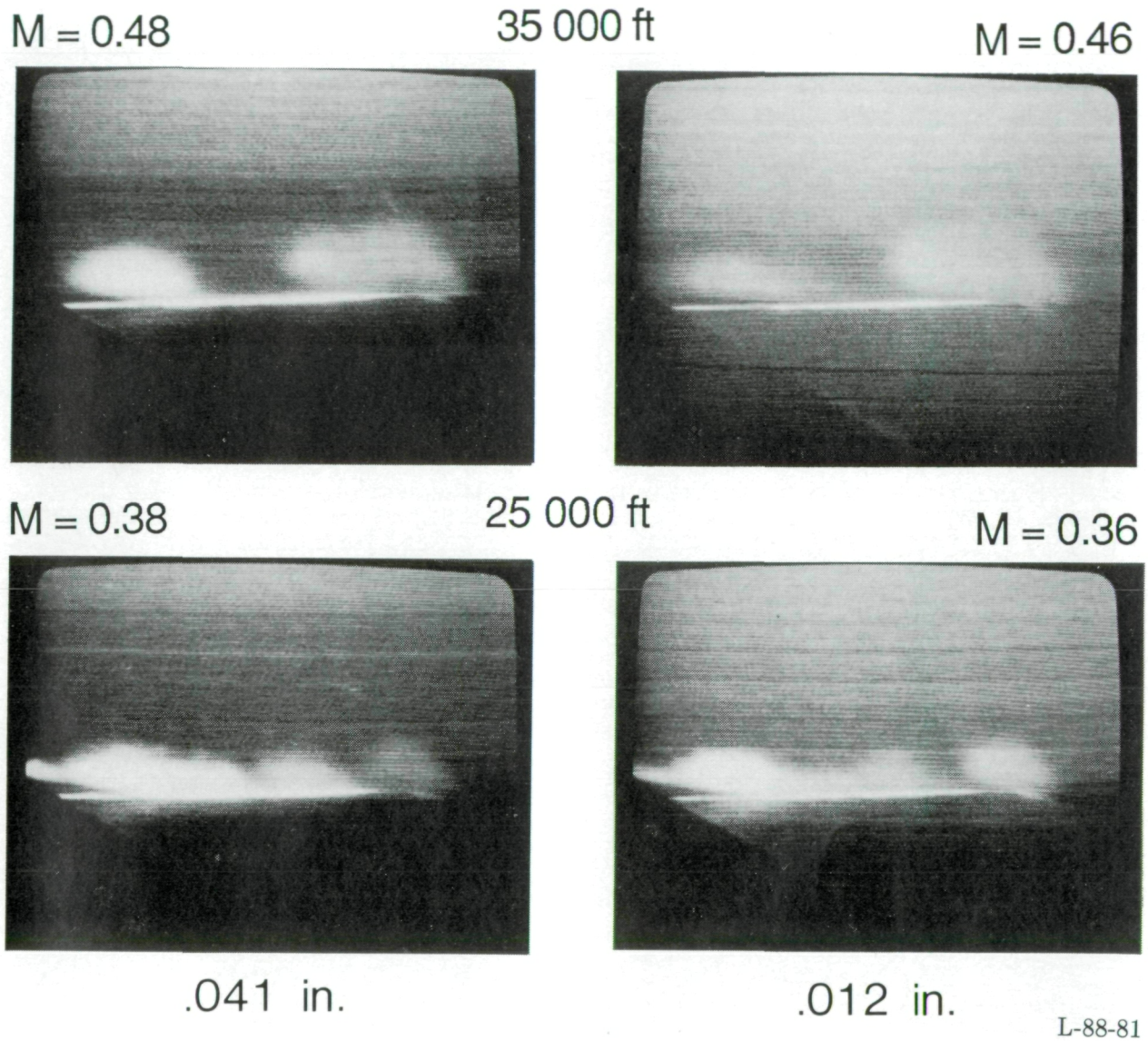

(b) $\alpha = 17°$.

Figure 9. Continued.

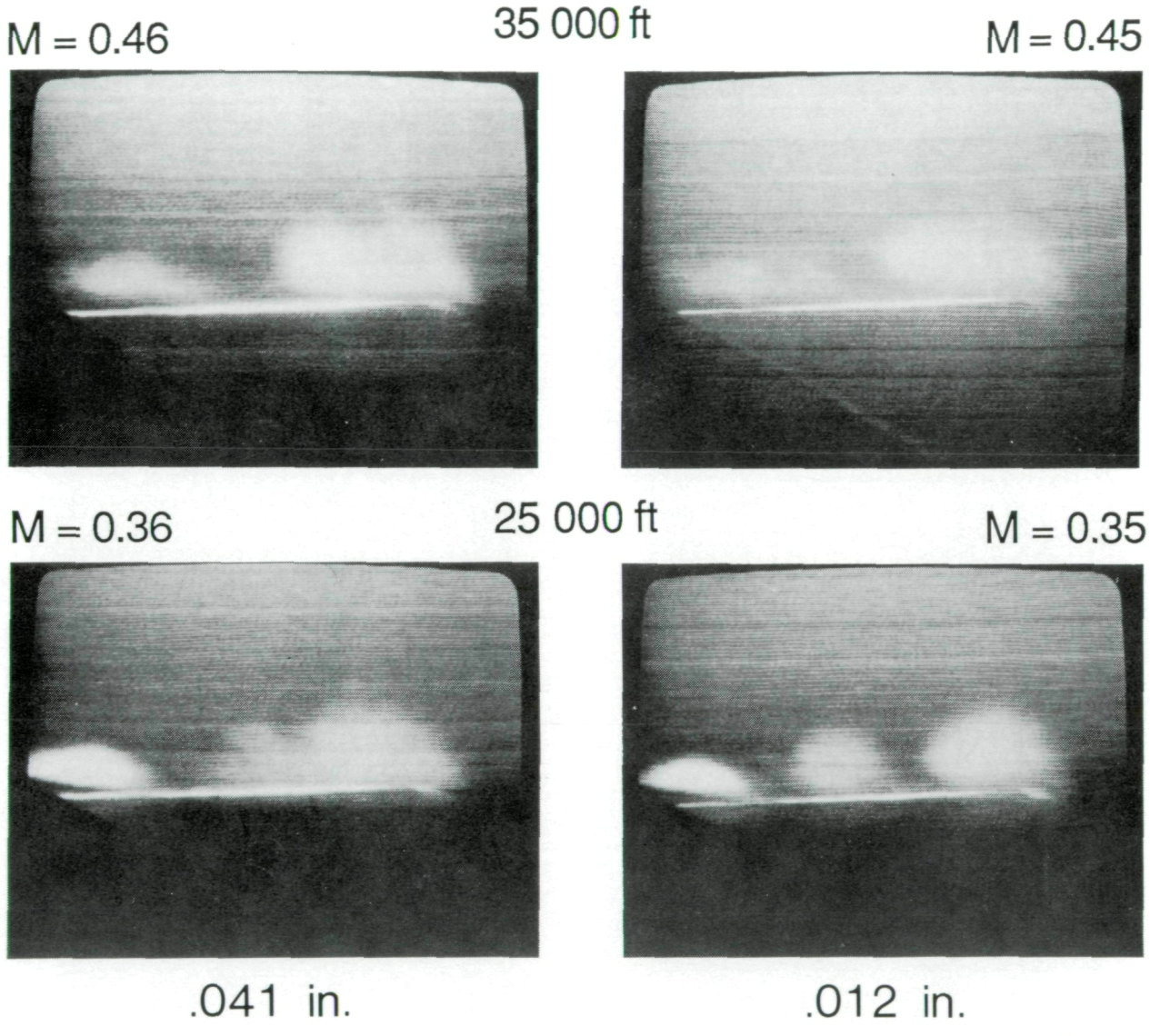

(c) $\alpha = 18°$.

Figure 9. Continued.

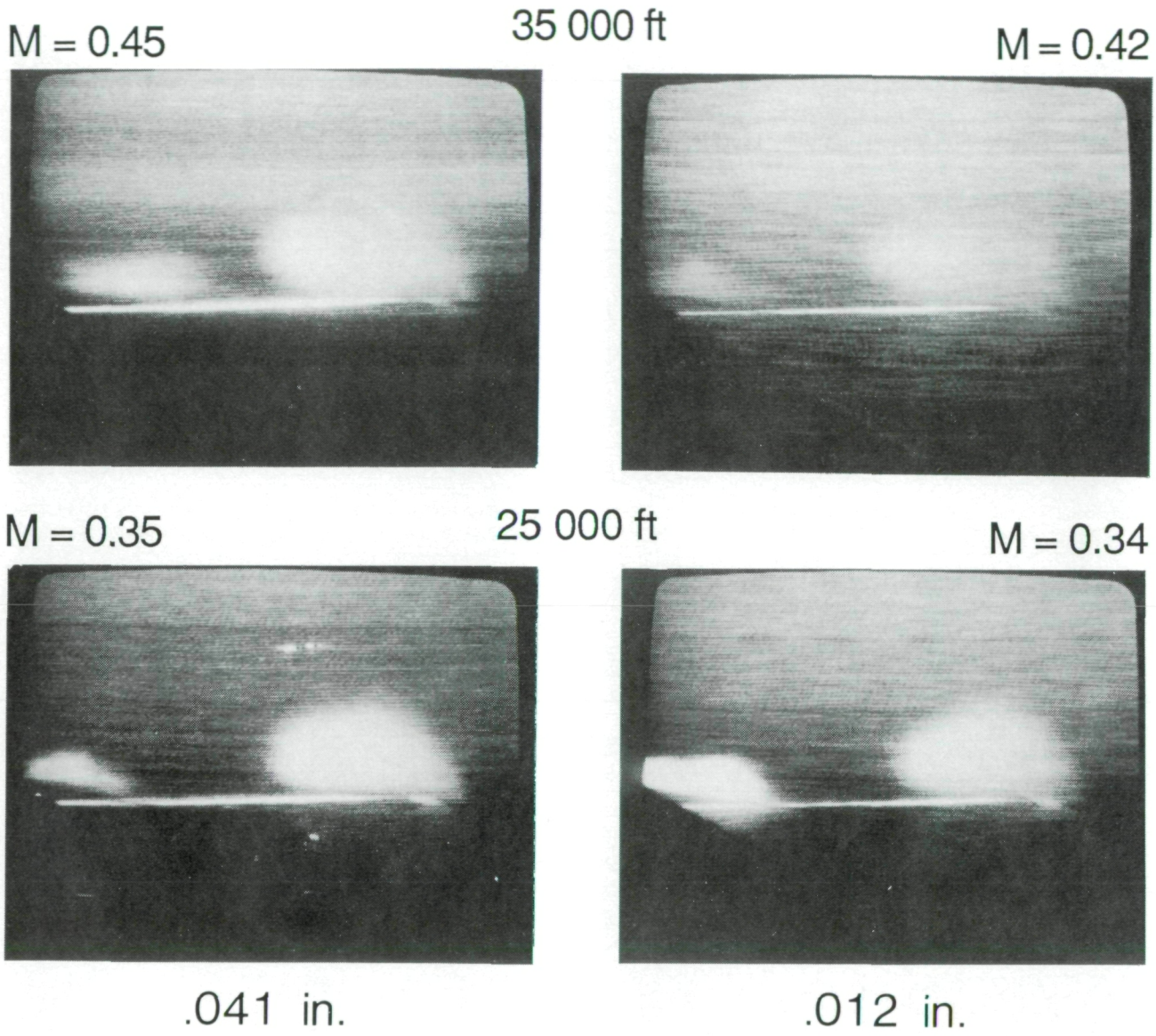

(d) $\alpha = 19°$.

Figure 9. Continued.

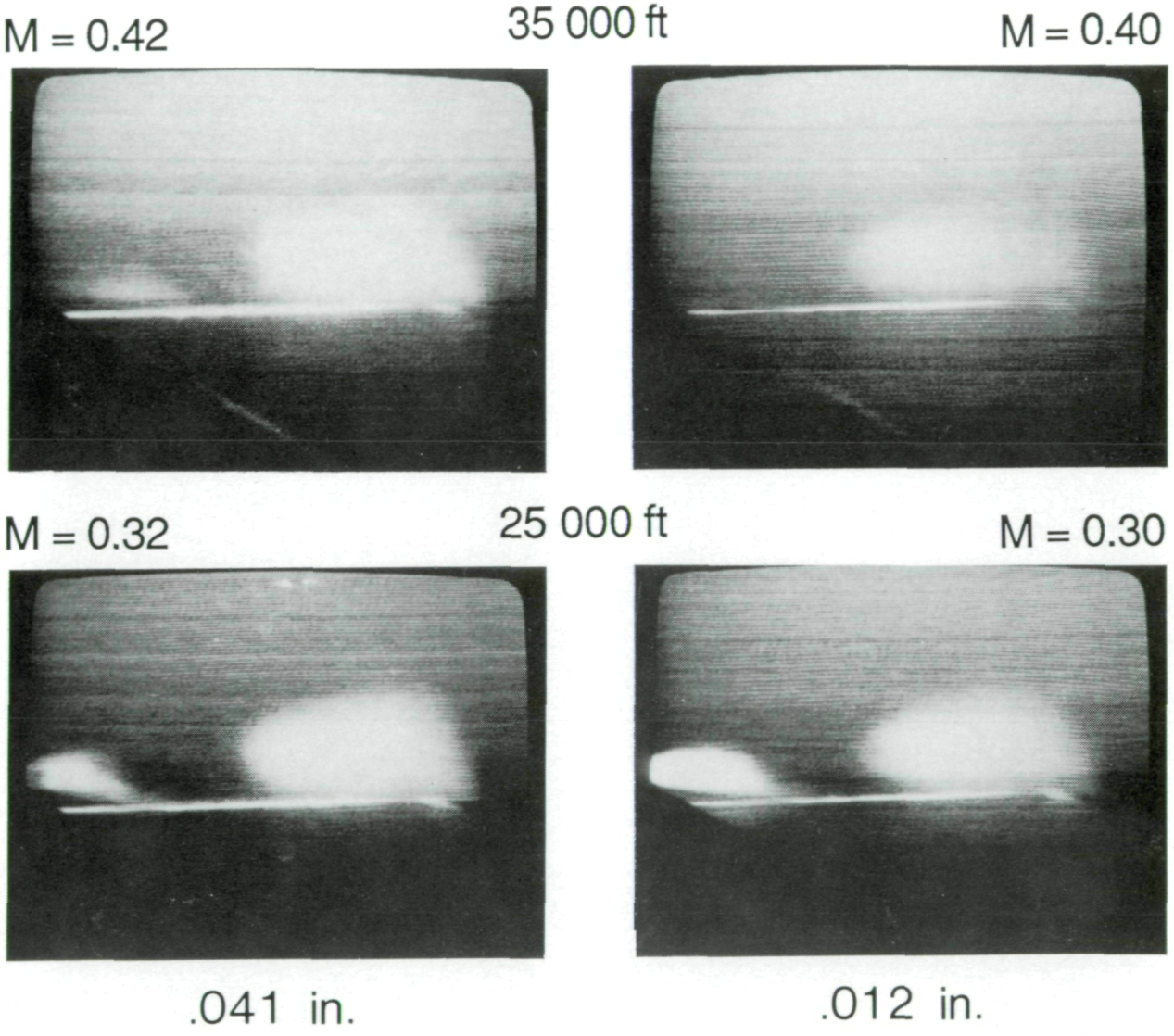

(e) $\alpha = 20°$.

Figure 9. Continued.

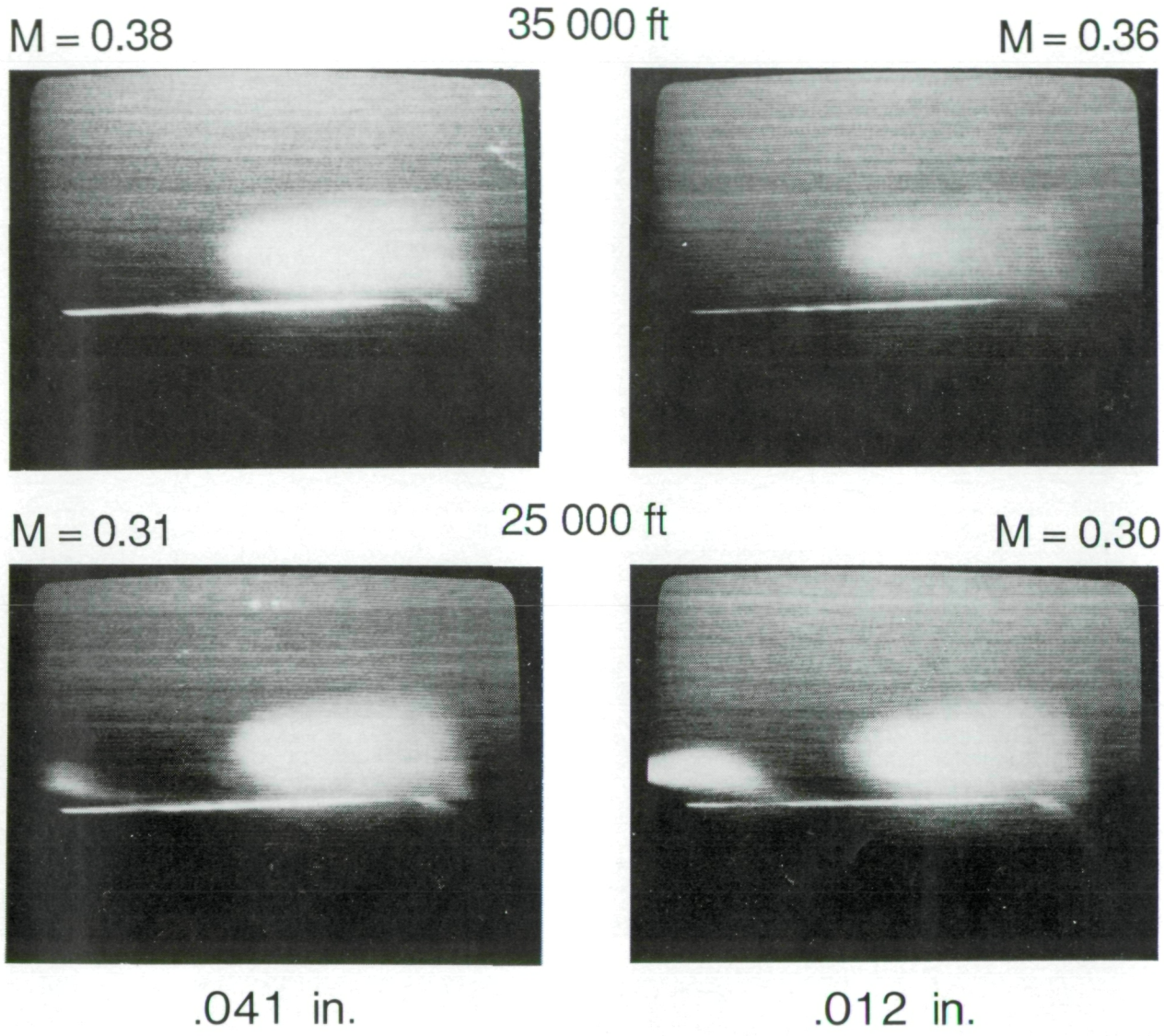

(f) $\alpha = 21°$.

Figure 9. Continued.

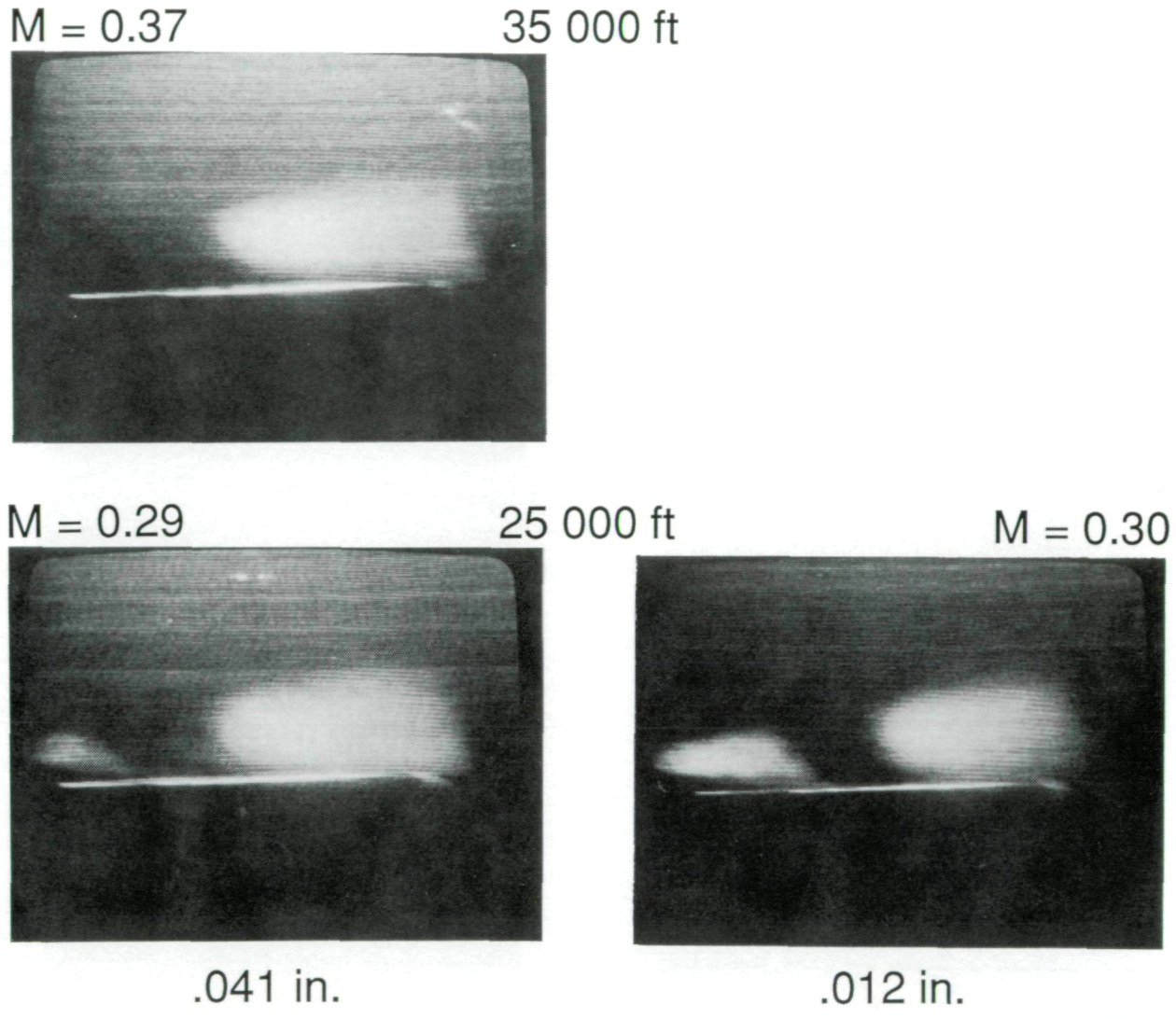

(g) $\alpha = 22°$.

Figure 9. Continued.

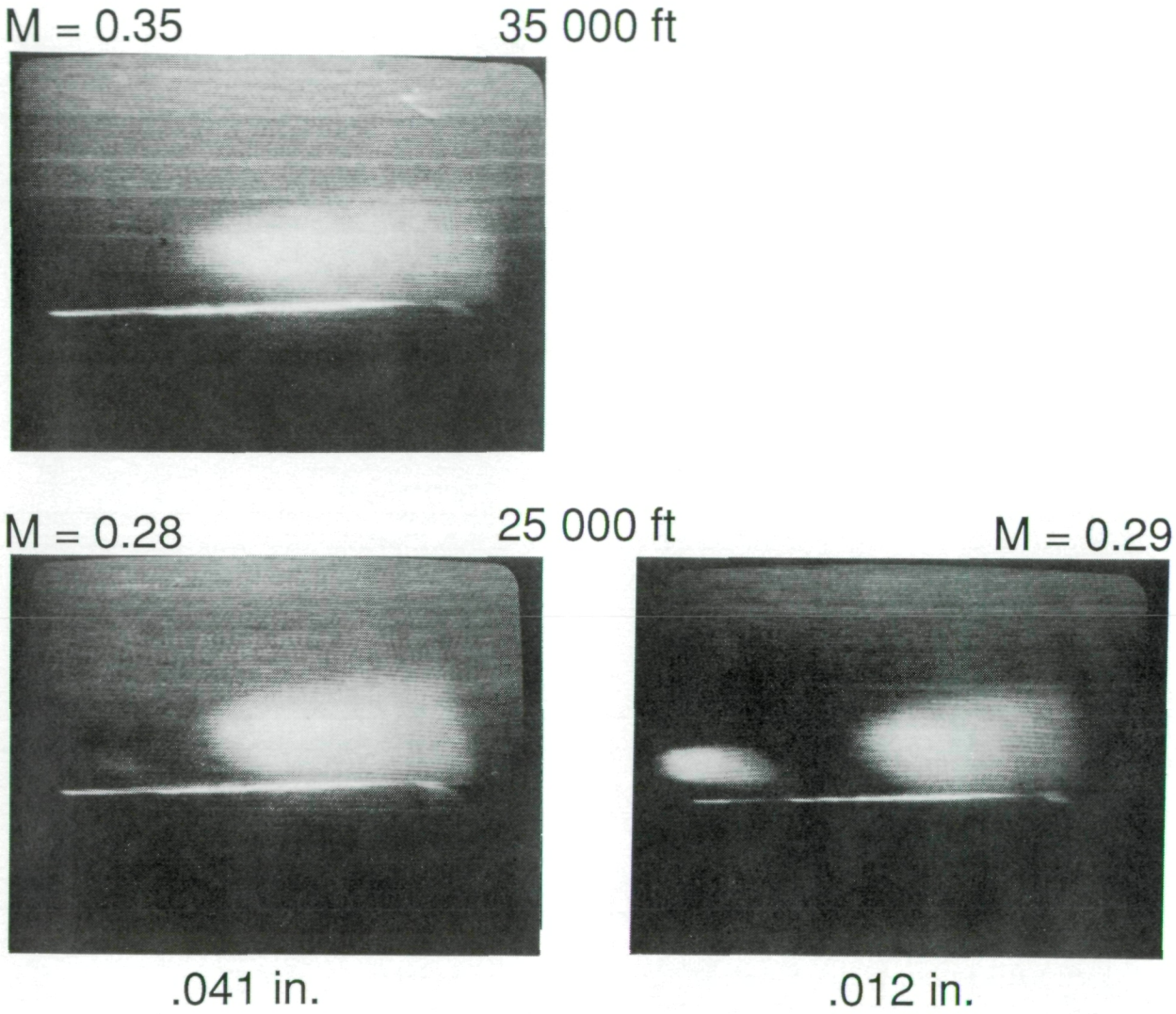

(h) $\alpha = 23°$.

Figure 9. Concluded.

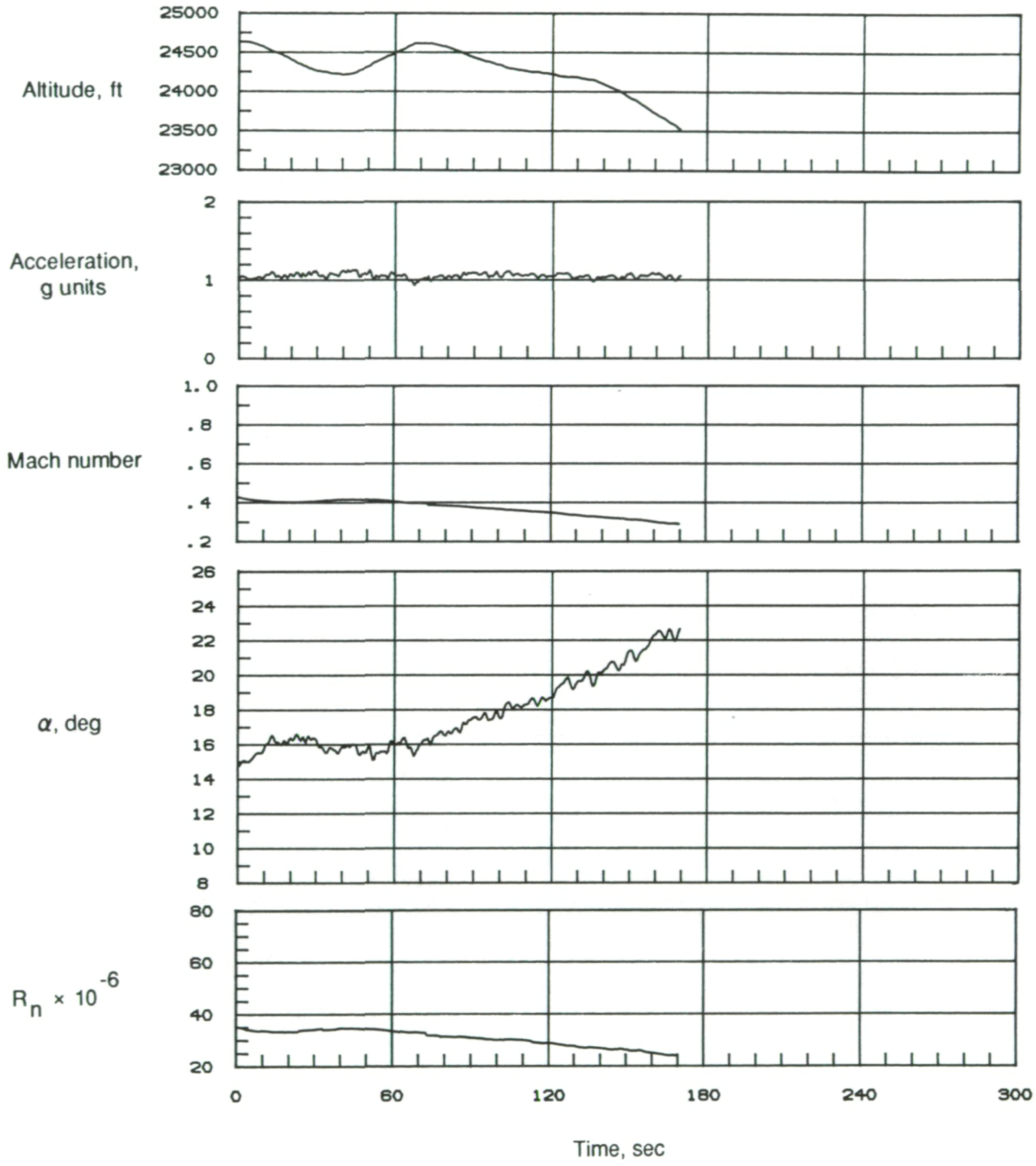

Figure 10. Time history of selected flight parameters for 1g maneuver at 25 000 ft (85-011/05). Probe-tip location 6; slit width, 0.041 in.

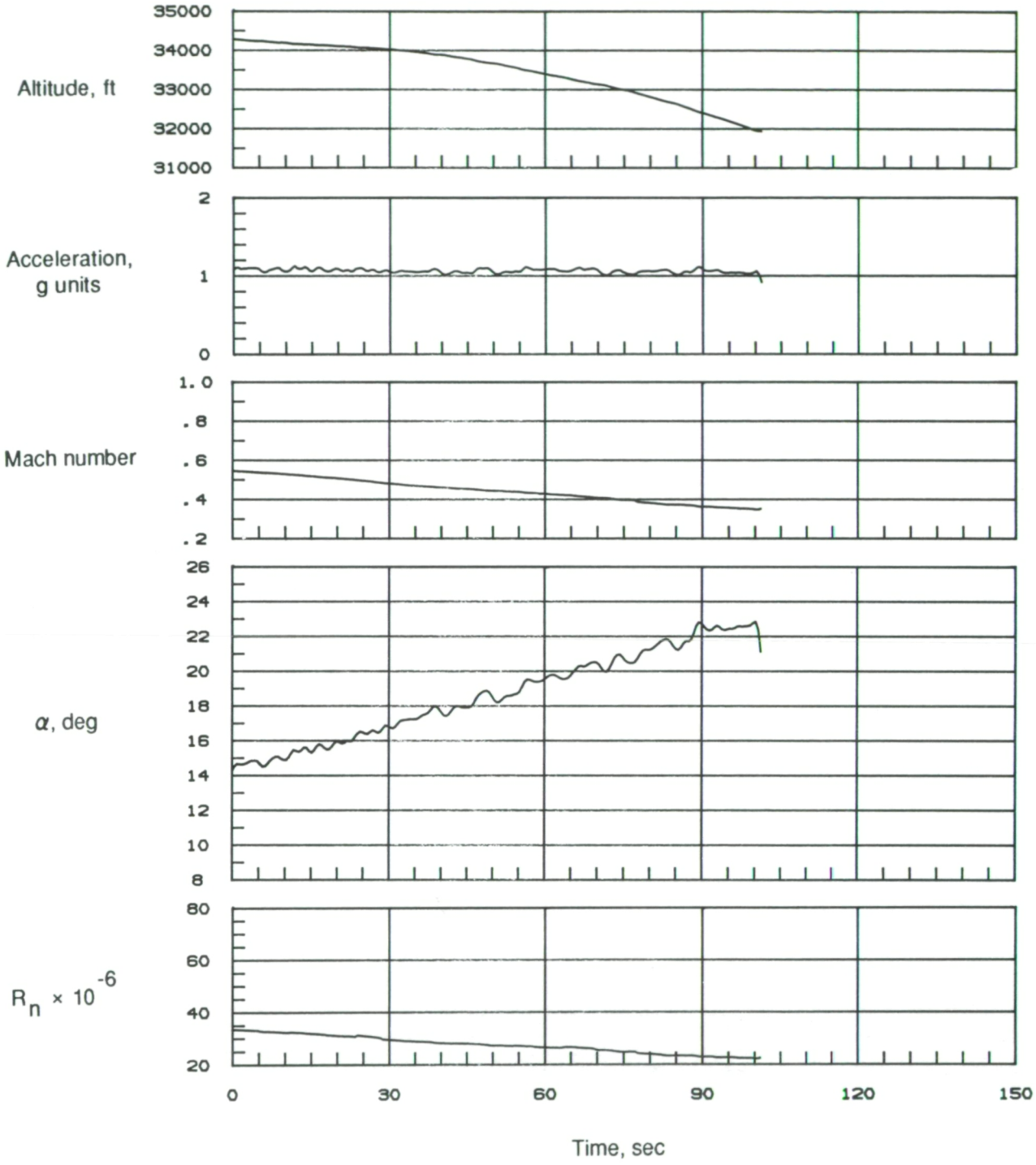

Figure 11. Time history of selected flight parameters for 1g maneuver at 35 000 ft (85-011/03). Probe-tip location 6; slit width, 0.041 in.

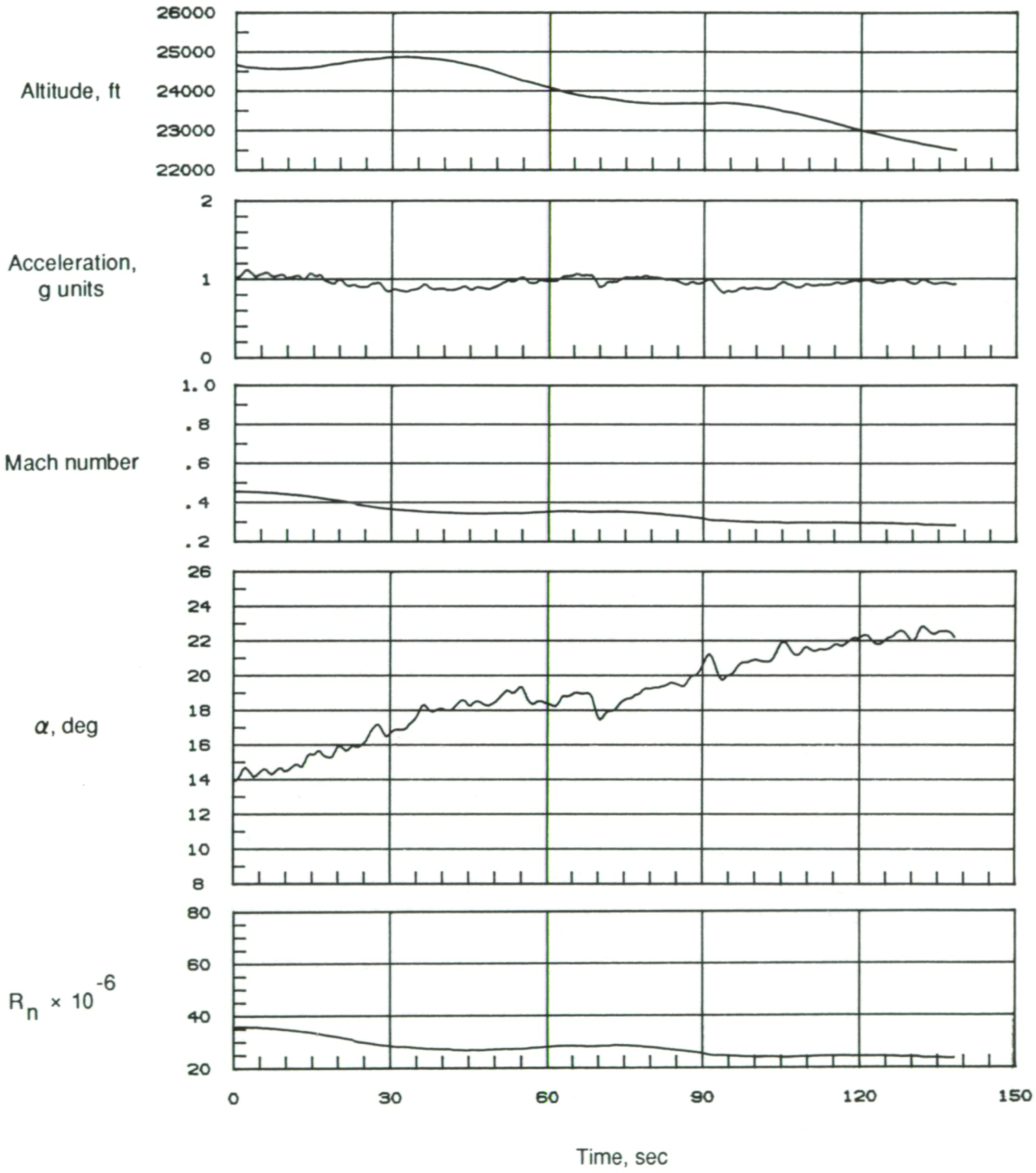

Figure 12. Time history of selected flight parameters for 1g maneuver at 25 000 ft (85-012/06). Probe-tip location 6; slit width, 0.012 in.

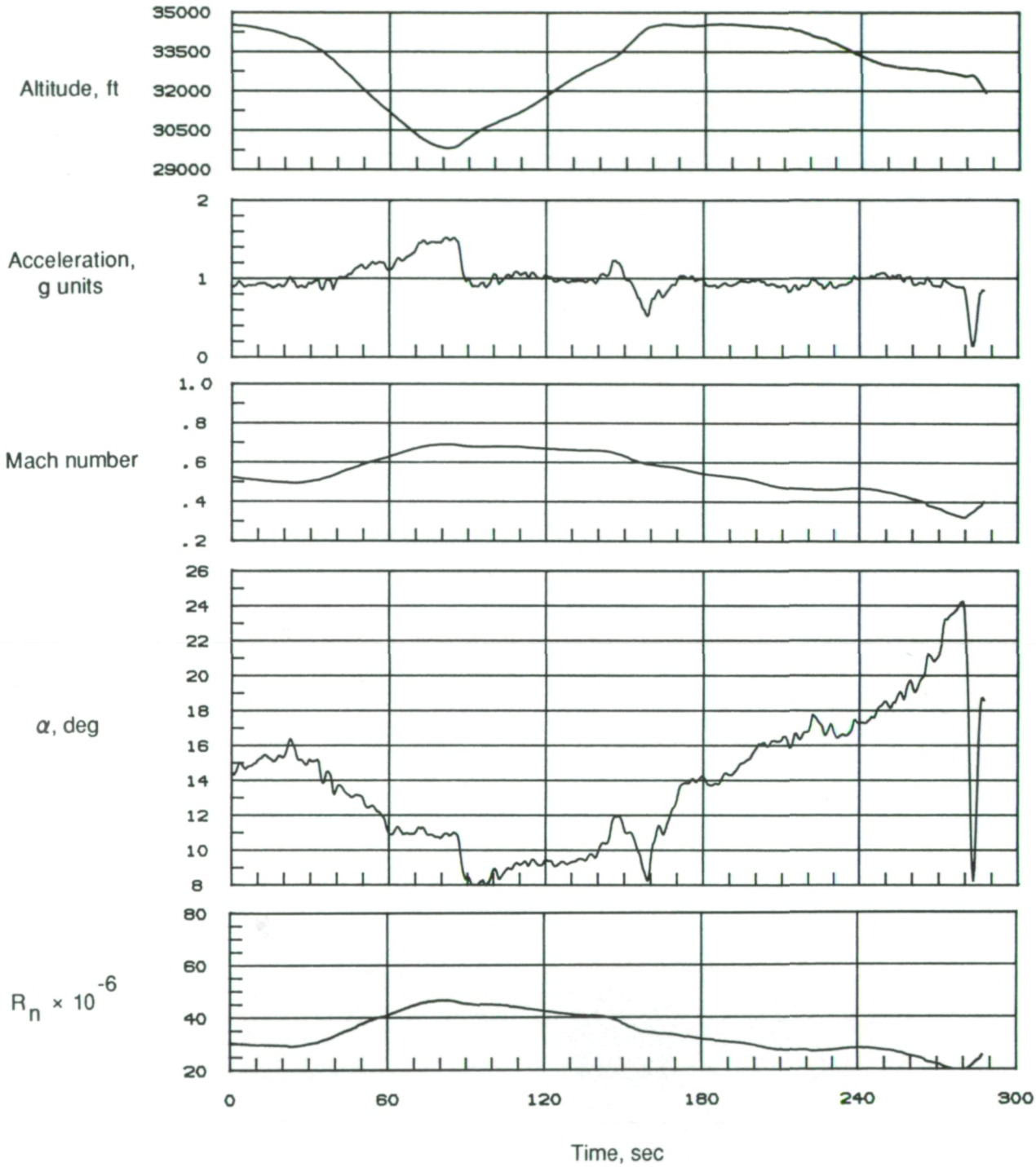

Figure 13. Time history of selected flight parameters for 1g maneuver at 35 000 ft (85-012/04). Probe-tip location 6; slit width, 0.012 in.

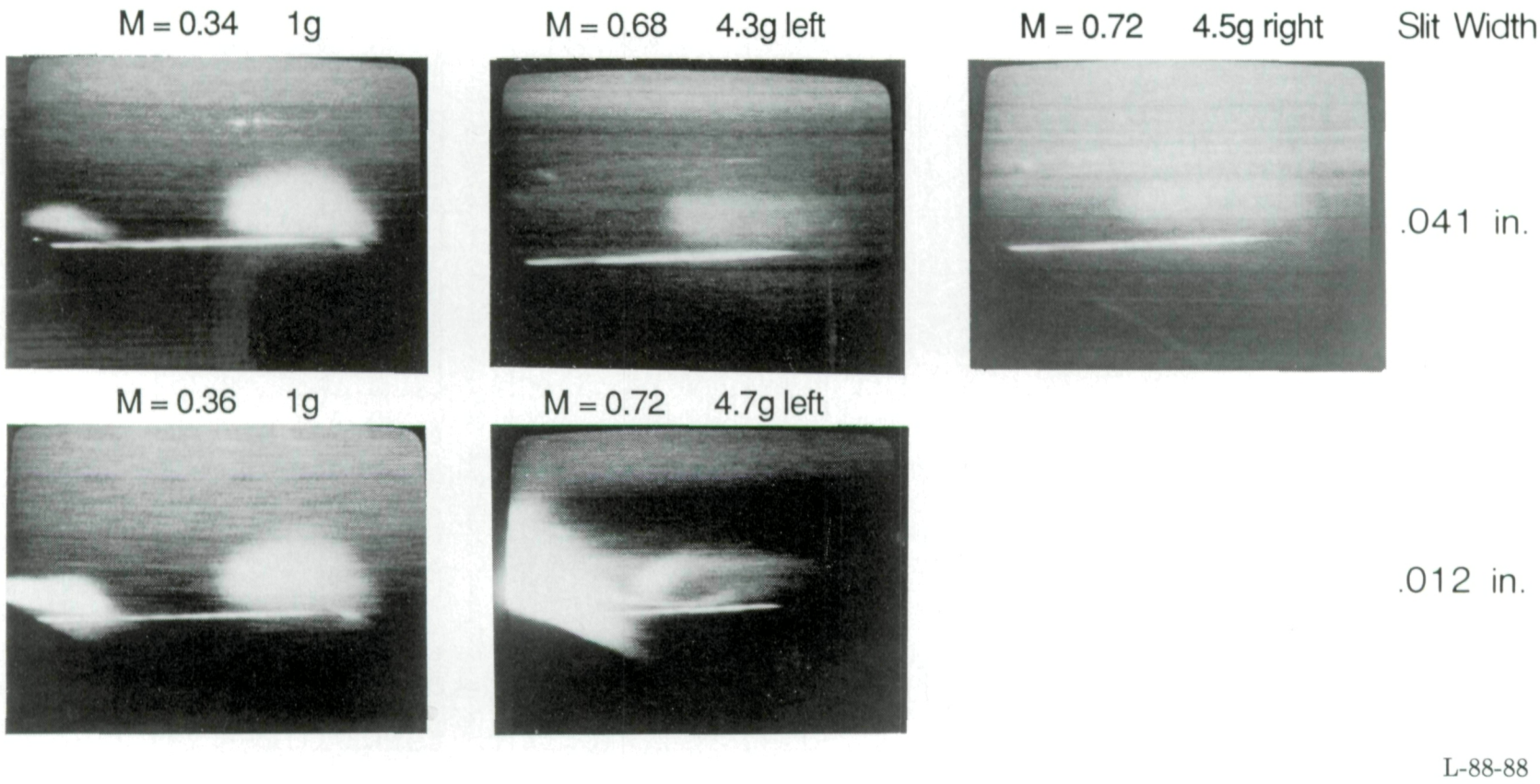

Figure 14. Vortex system details for two maneuvers and slit widths. $\alpha \approx 19°$; altitude, 25 000 ft; probe-tip location 6; intermittent light-sheet operation.

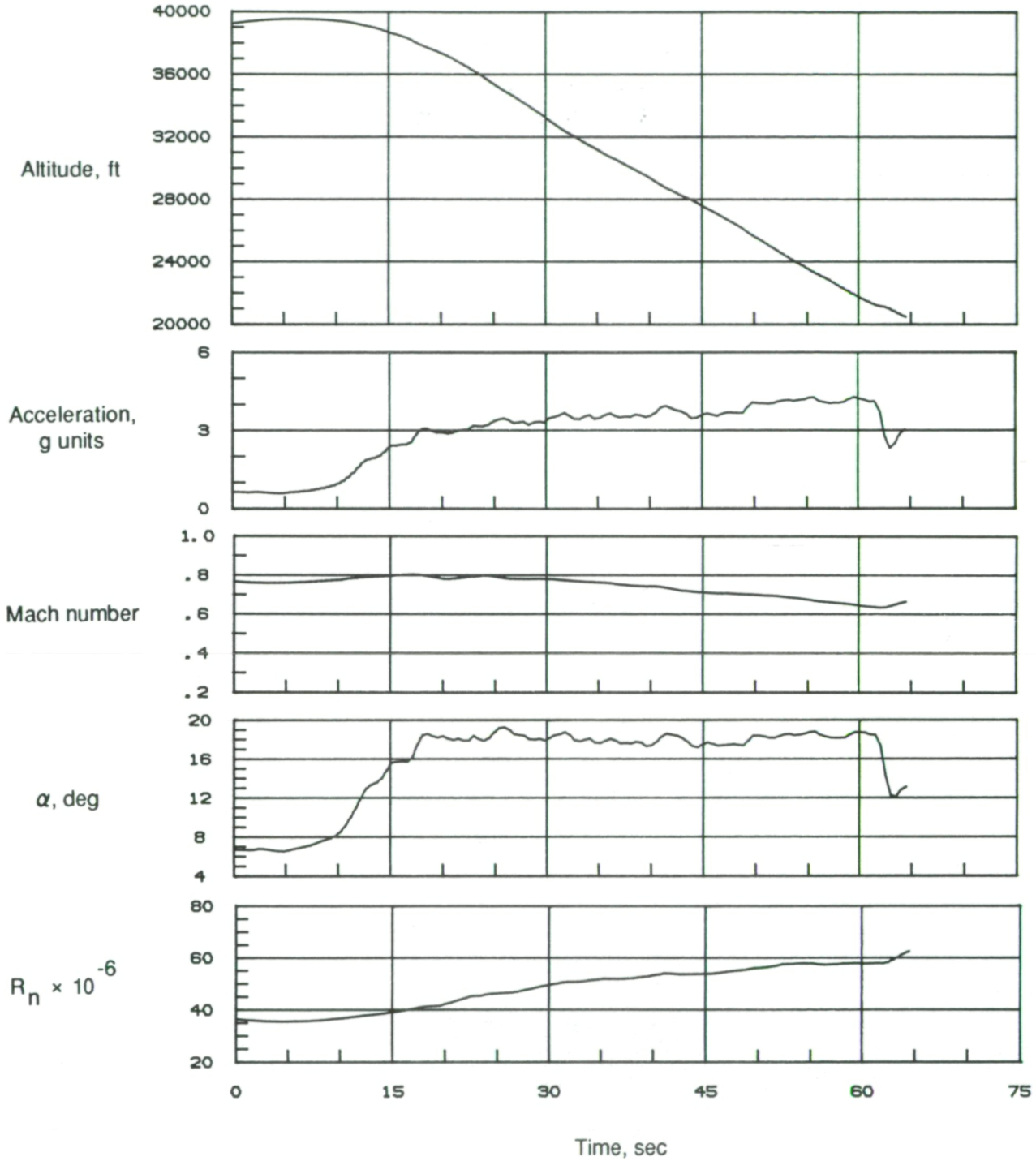

Figure 15. Time history of selected flight parameters at high-g during left spiral maneuver (85-011/08). Probe-tip location 6; slit width, 0.041 in.

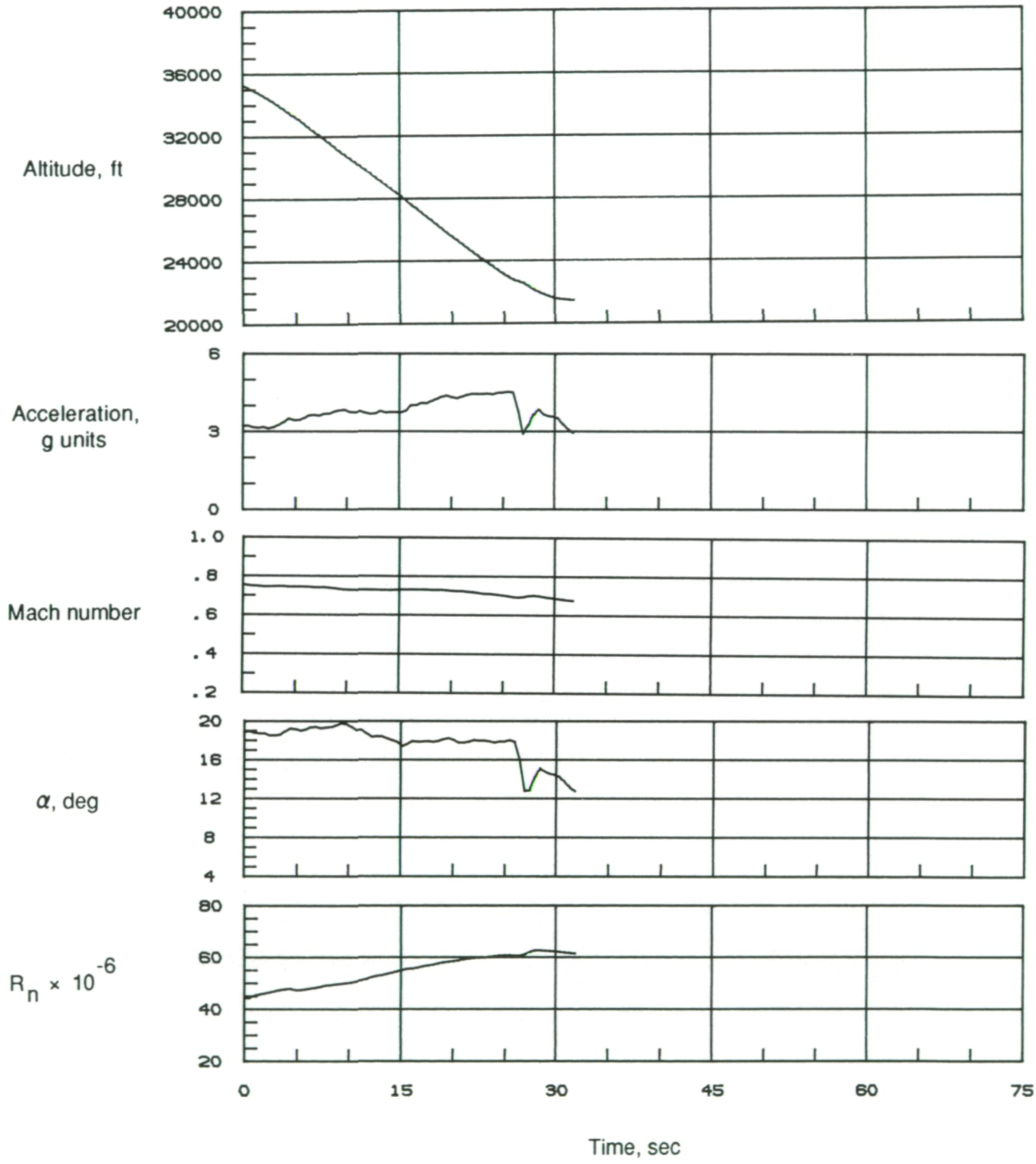

Figure 16. Time history of selected flight parameters at high-g during right spiral maneuver (85-011/09). Probe-tip location 6; slit width, 0.041 in.

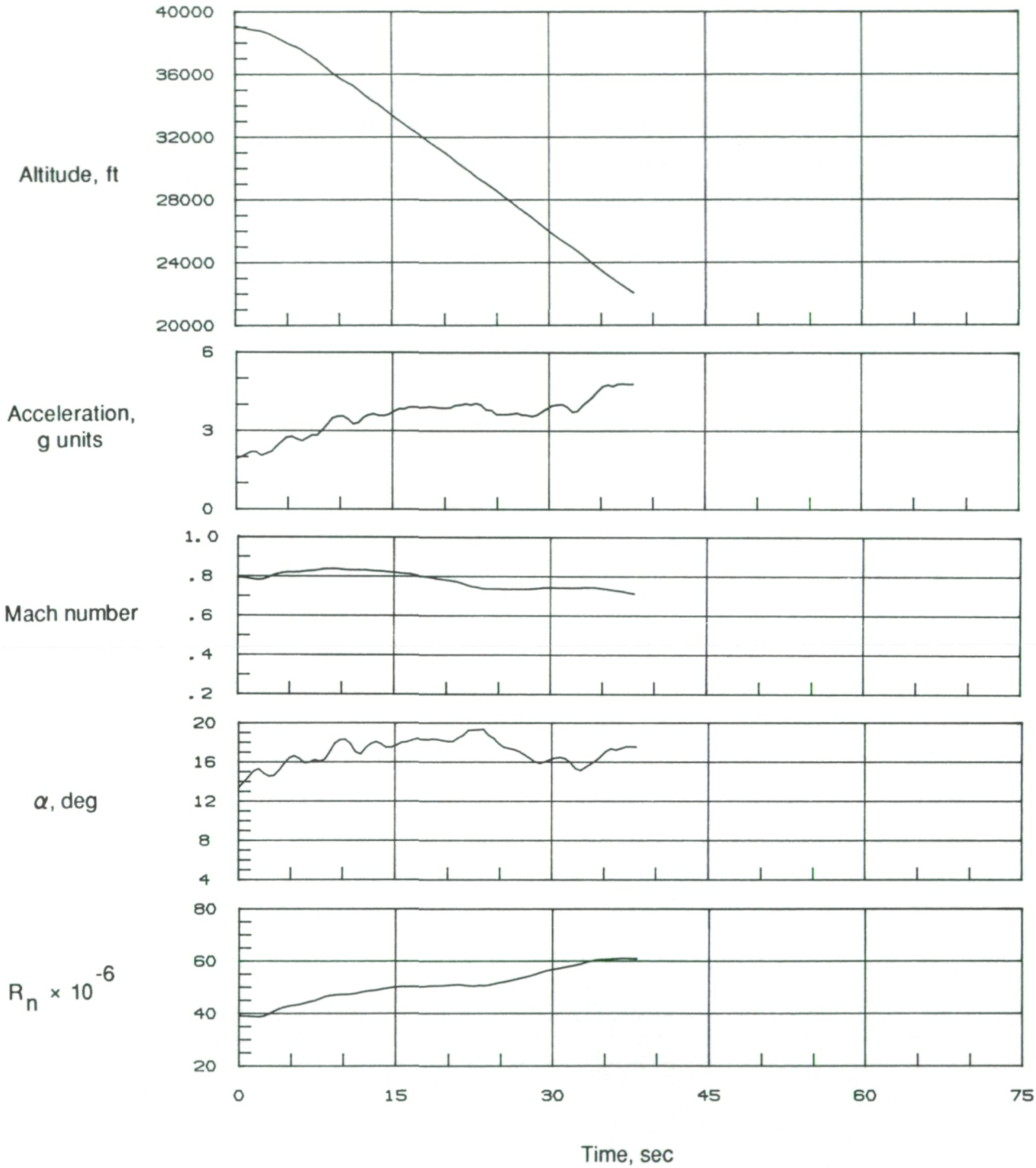

Figure 17. Time history of selected flight parameters at high-g during left spiral maneuver (85-012/09). Probe-tip location 6; slit width, 0.012 in.

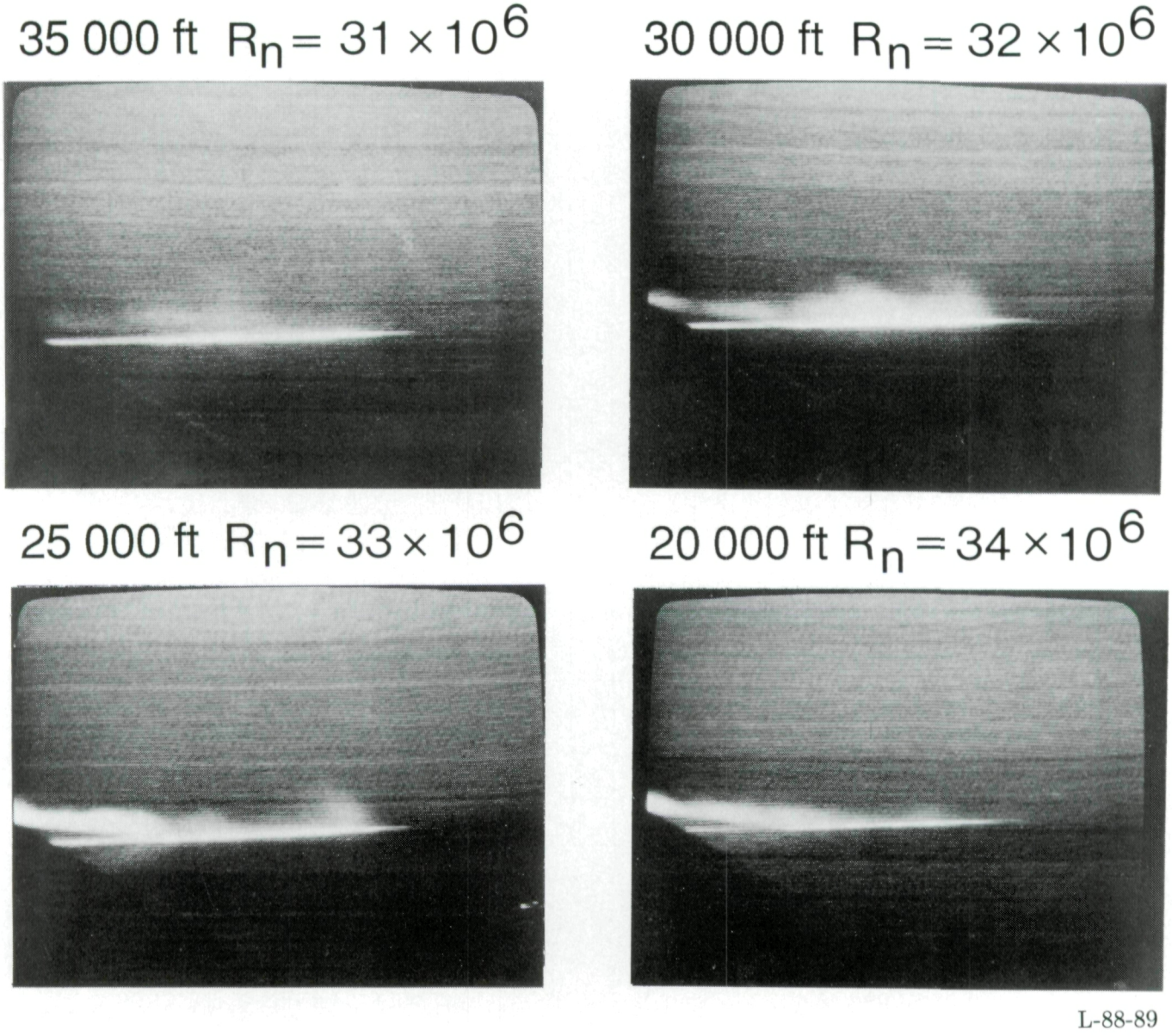

(a) $\alpha = 16°$.

Figure 18. Effect of Reynolds number on vortex system. $1g$ maneuver; $0.26 \leq M \leq 0.50$; probe-tip location 6; intermittent light-sheet operation; slit width, 0.041 in.

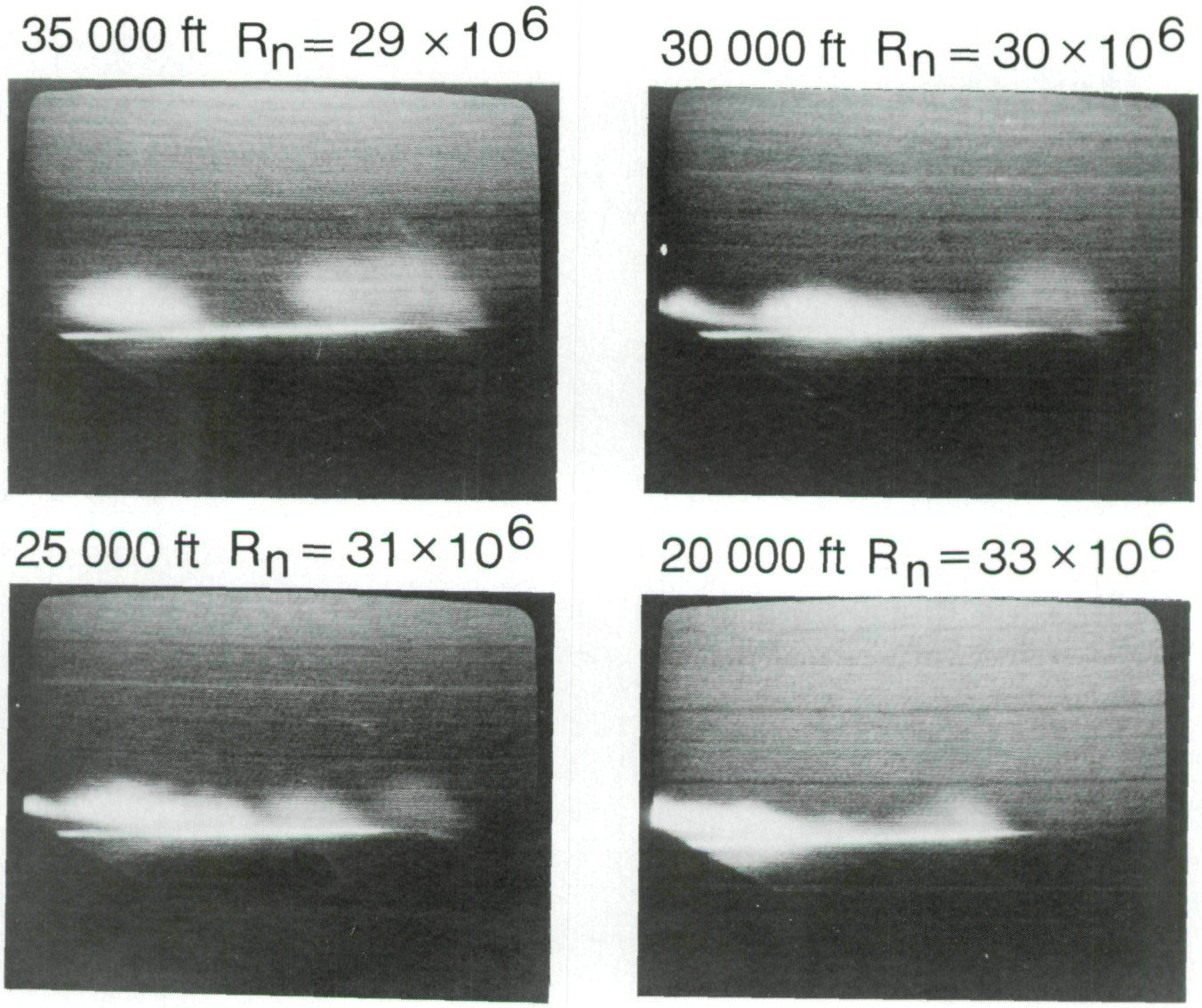

L-88-90

(b) $\alpha = 17°$.

Figure 18. Continued.

L-88-91

(c) $\alpha = 18°$.

Figure 18. Continued.

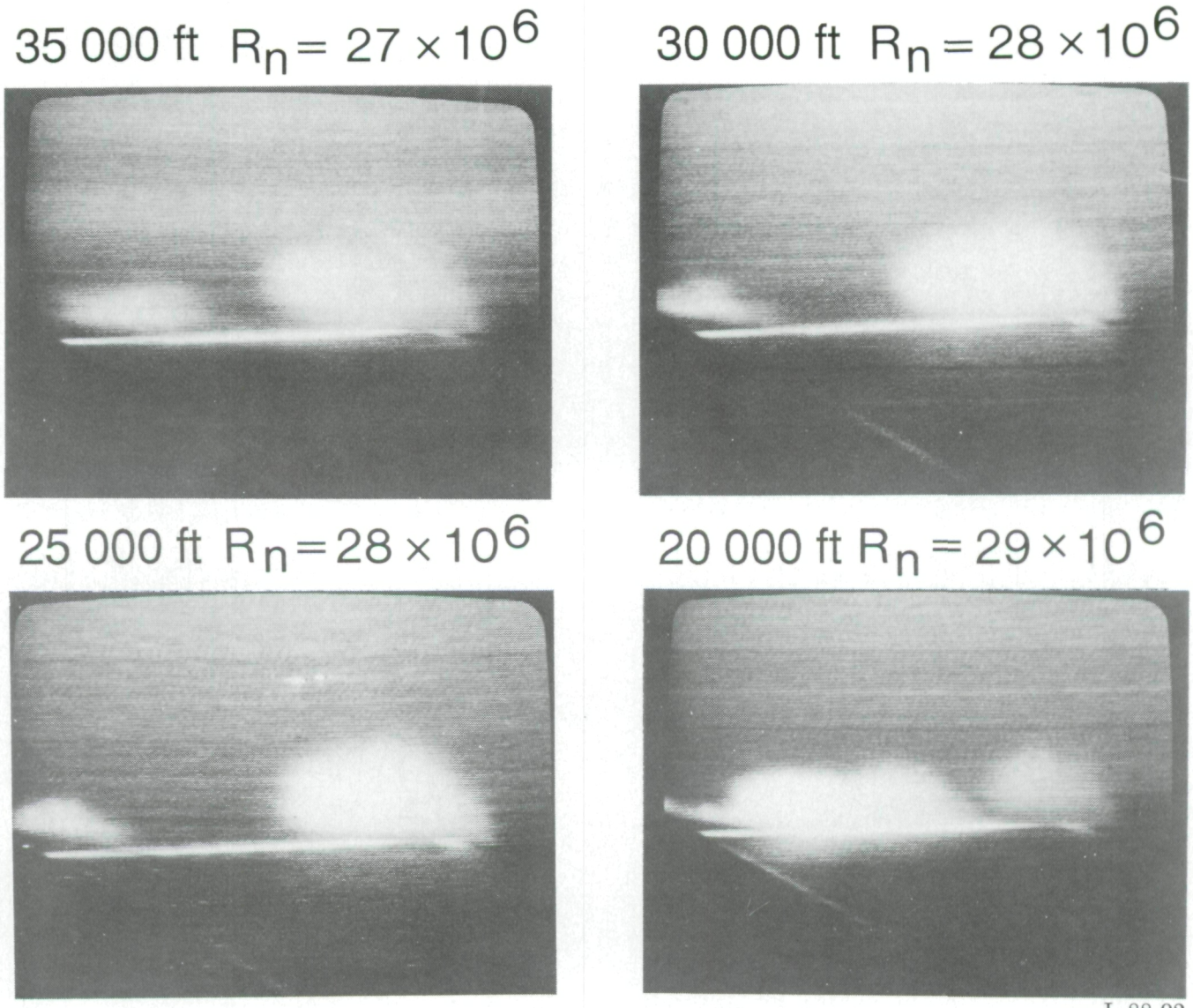

(d) $\alpha = 19°$.

Figure 18. Continued.

L-88-93

(e) $\alpha = 20°$.

Figure 18. Continued.

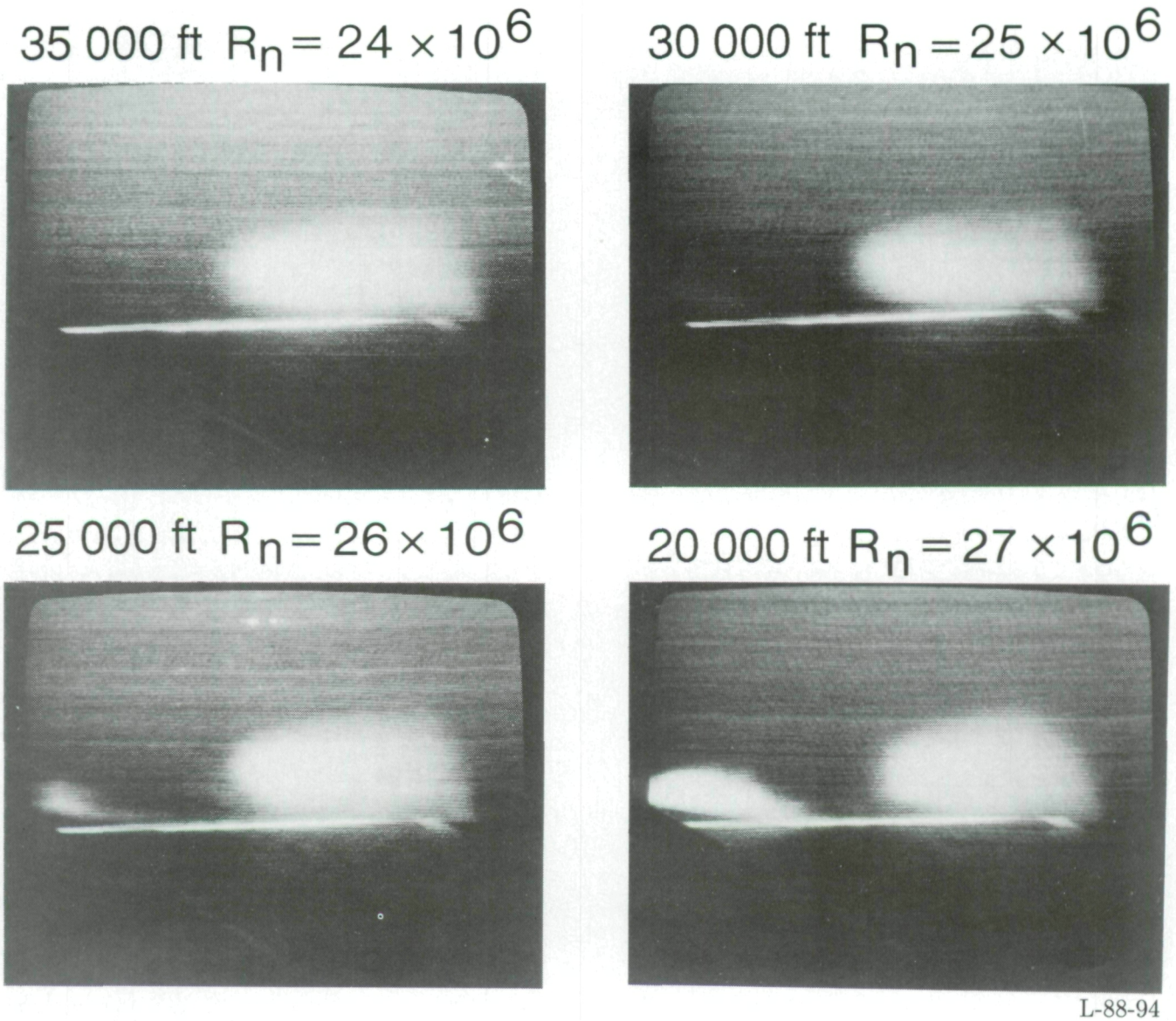

(f) $\alpha = 21°$.

Figure 18. Continued.

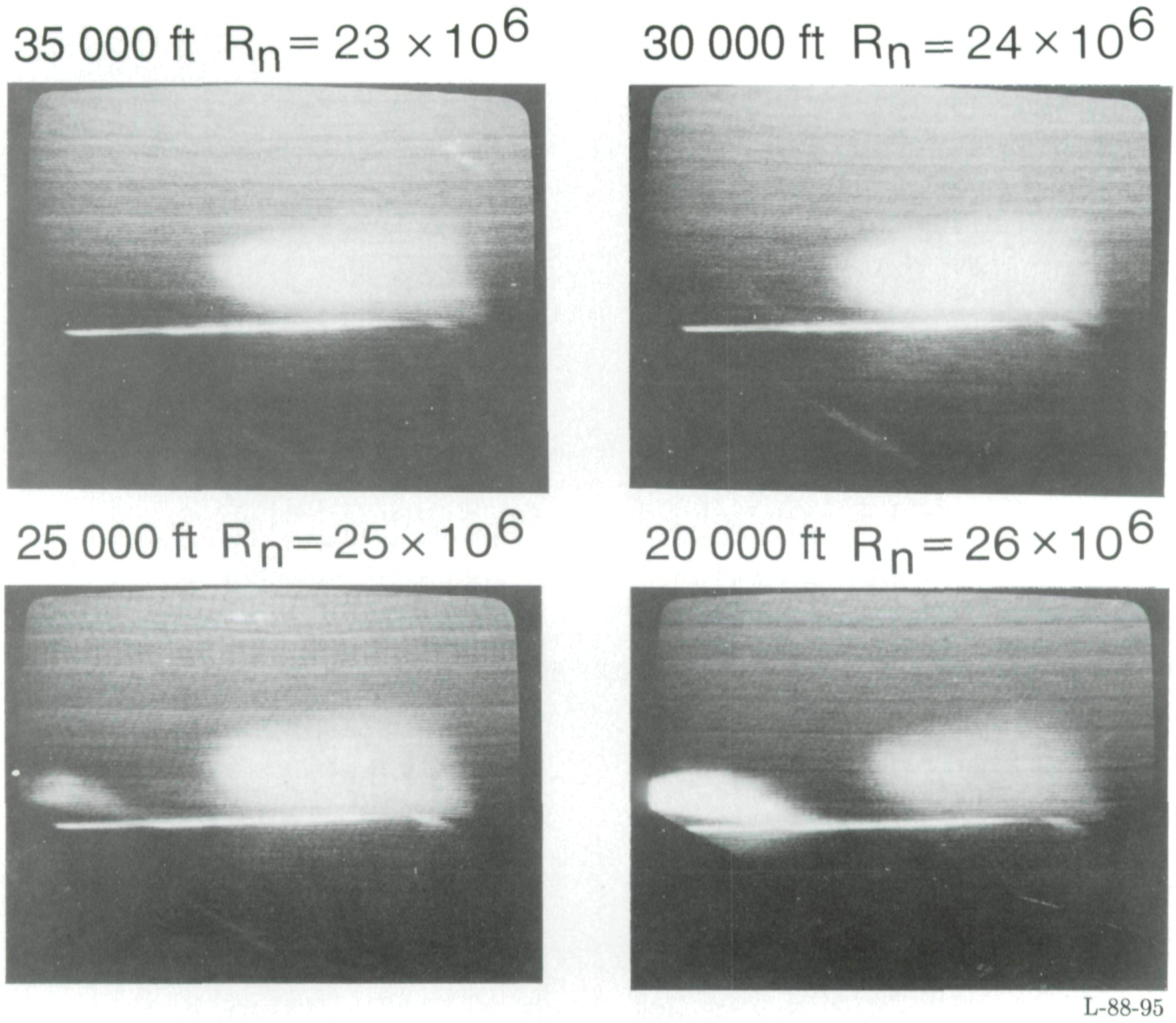

(g) $\alpha = 22°$.

Figure 18. Continued.

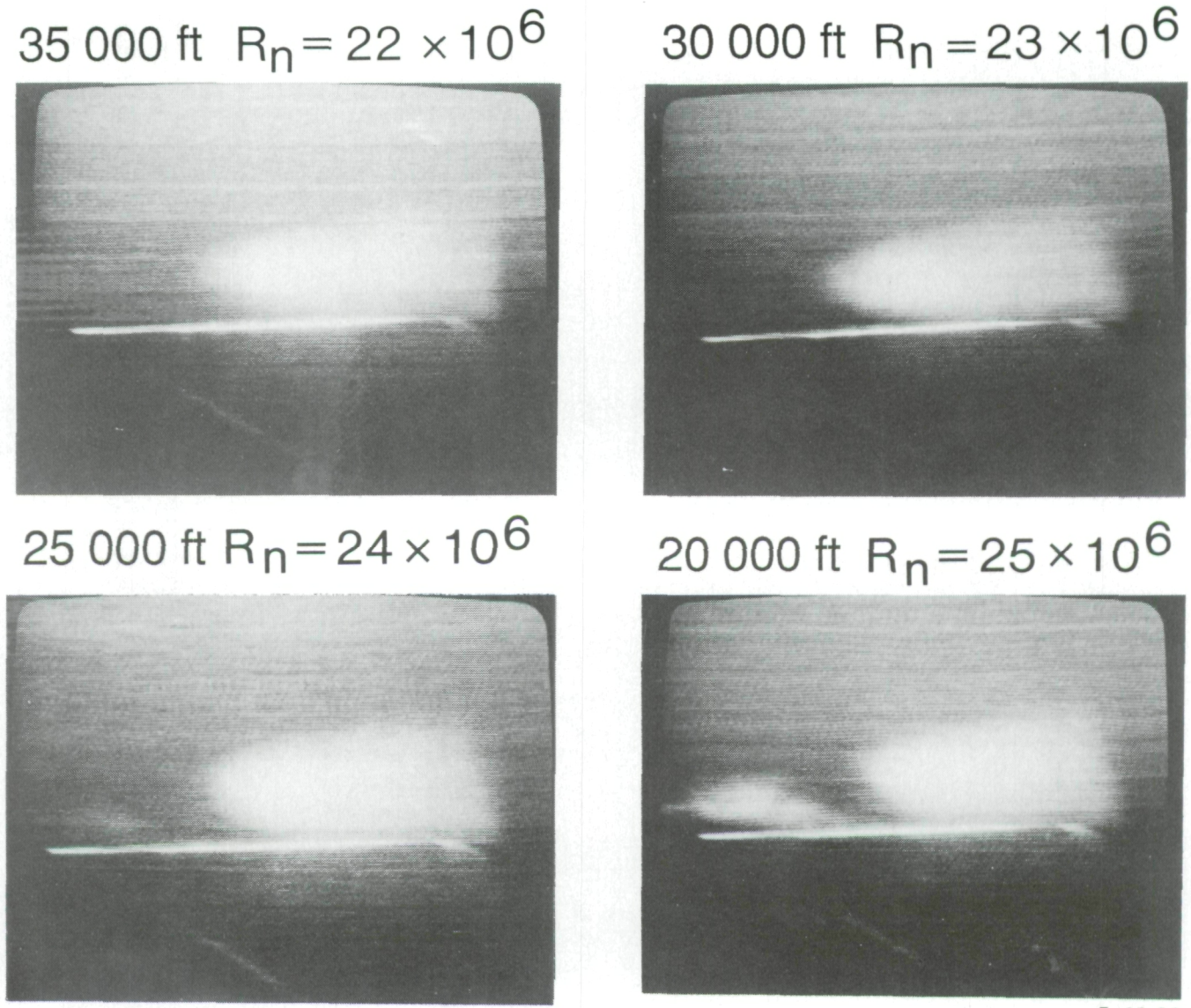

(h) $\alpha = 23°$.

Figure 18. Concluded.

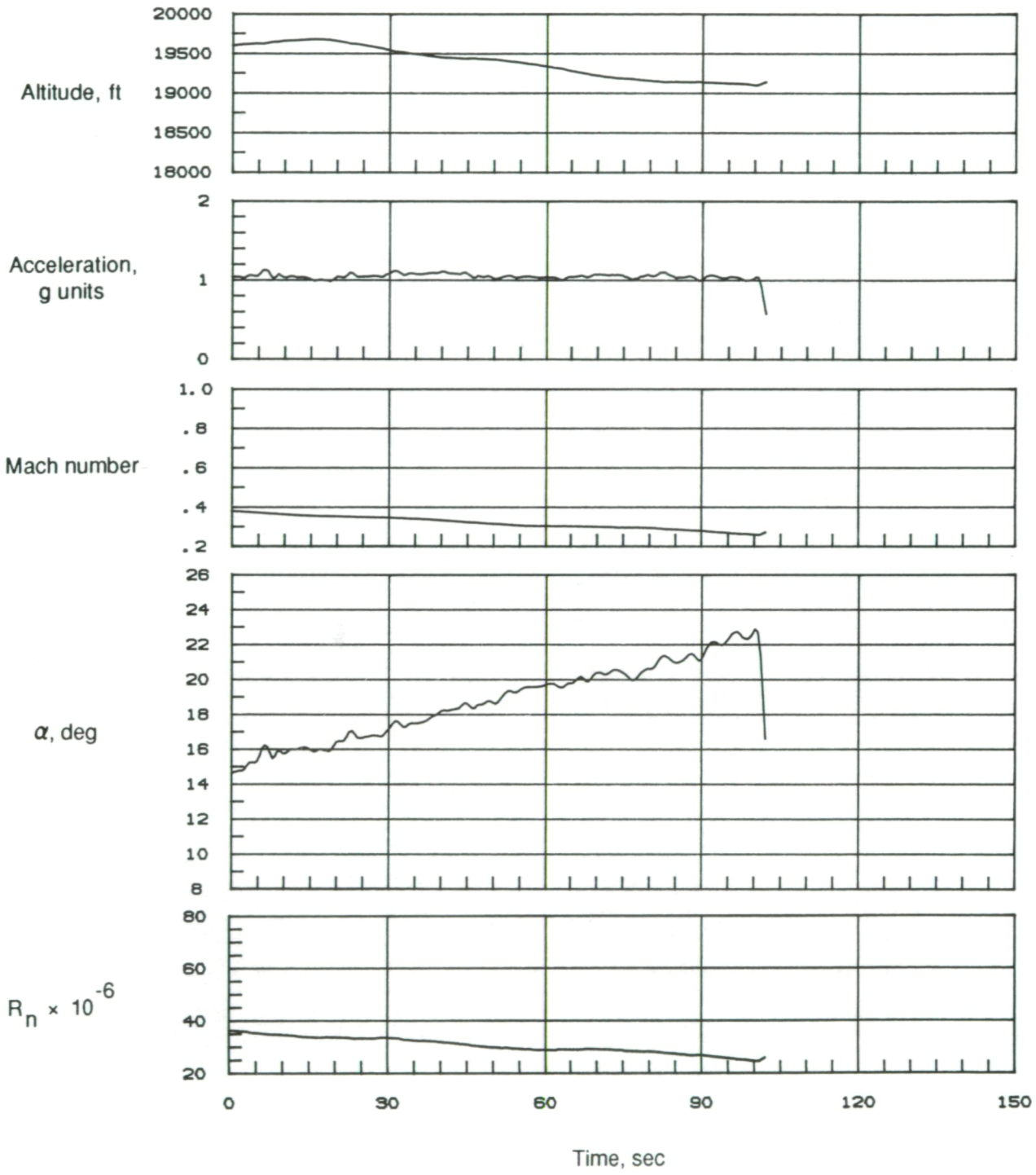

Figure 19. Time history of selected flight parameters for 1g maneuver at 20 000 ft (85-011/06). Probe-tip location 6; slit width, 0.041 in.

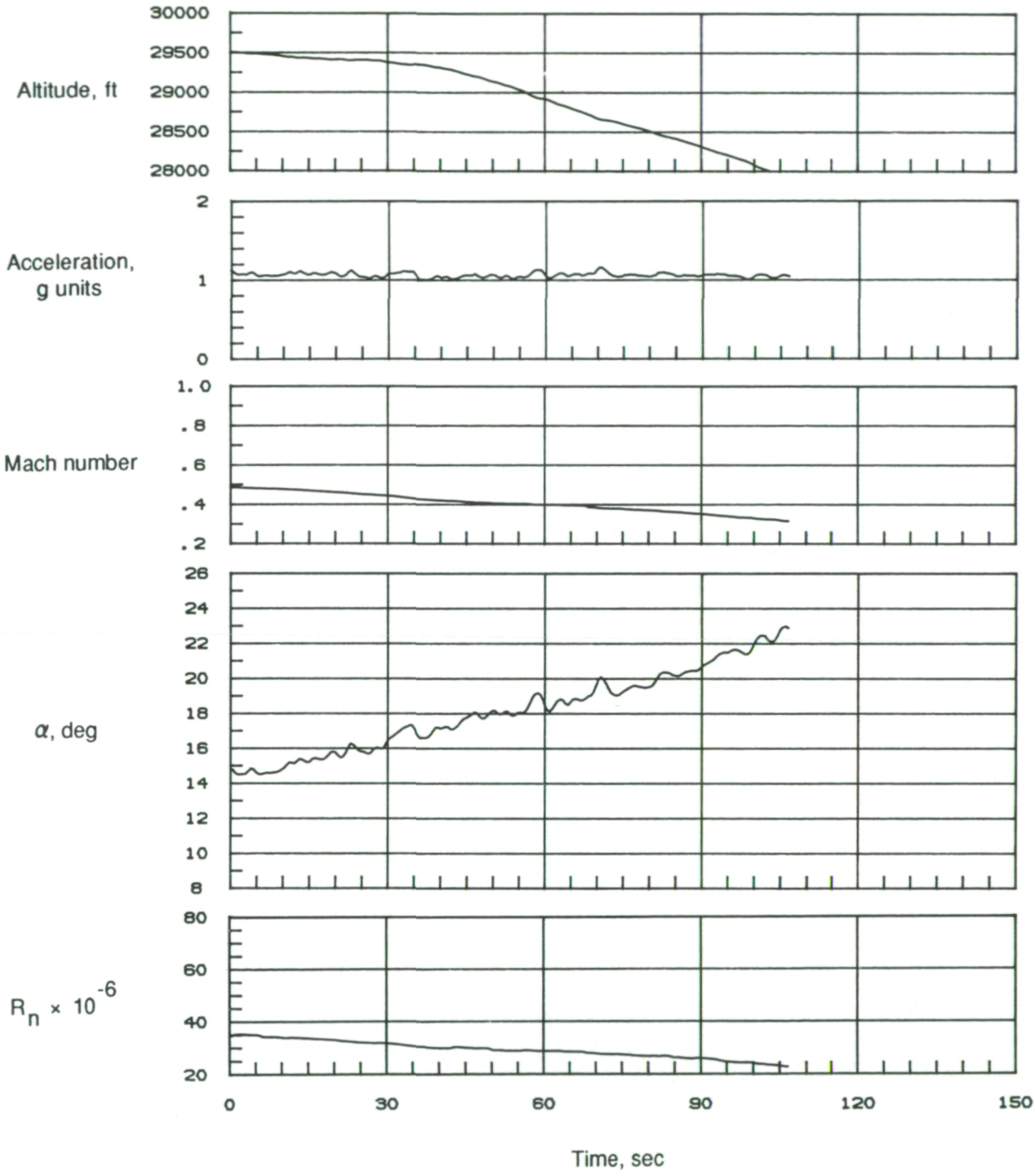

Figure 20. Time history of selected flight parameters for 1g maneuver at 30 000 ft (85-011/04). Probe-tip location 6; slit width, 0.041 in.

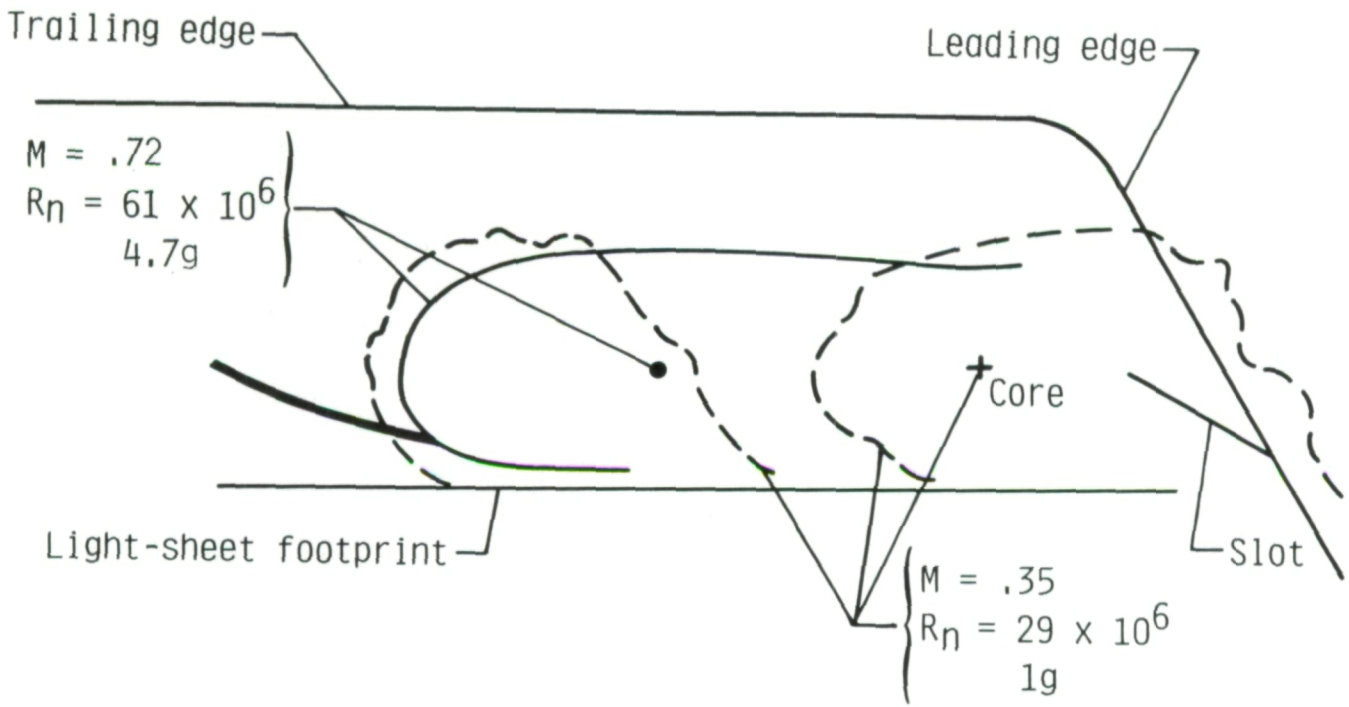

Figure 21. Effect of Mach number and load factor on vortex system. $\alpha \approx 18°$; altitude, 25 000 ft; probe-tip location 6; slit width, 0.012 in; intermittent light-sheet operation.

Figure 22. Vapor-screen images without and with digital enhancement. $M = 0.4$; $R_n = 30 \times 10^6$; altitude, 25 000 ft; 1g maneuver.

L-88-98

Figure 23. Flow visualization of vortex system above full-scale aircraft model in Langley 30- by 60-Foot Tunnel. $M = 0.1$; $R_n = 12 \times 10^6$; $\alpha = 20°$; elevons, 5° trailing edge up; continuous light-sheet operation.

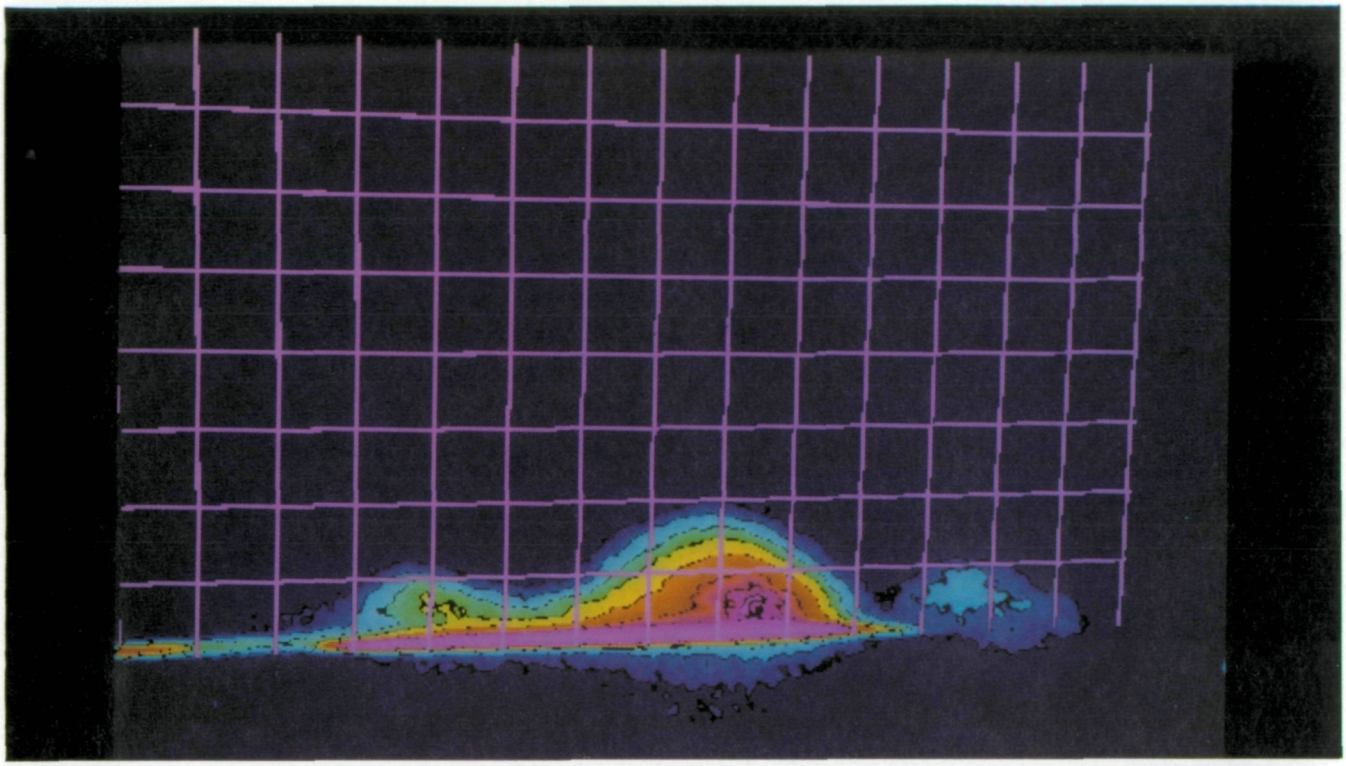

(a) $\alpha = 17°$.

L-87-1105

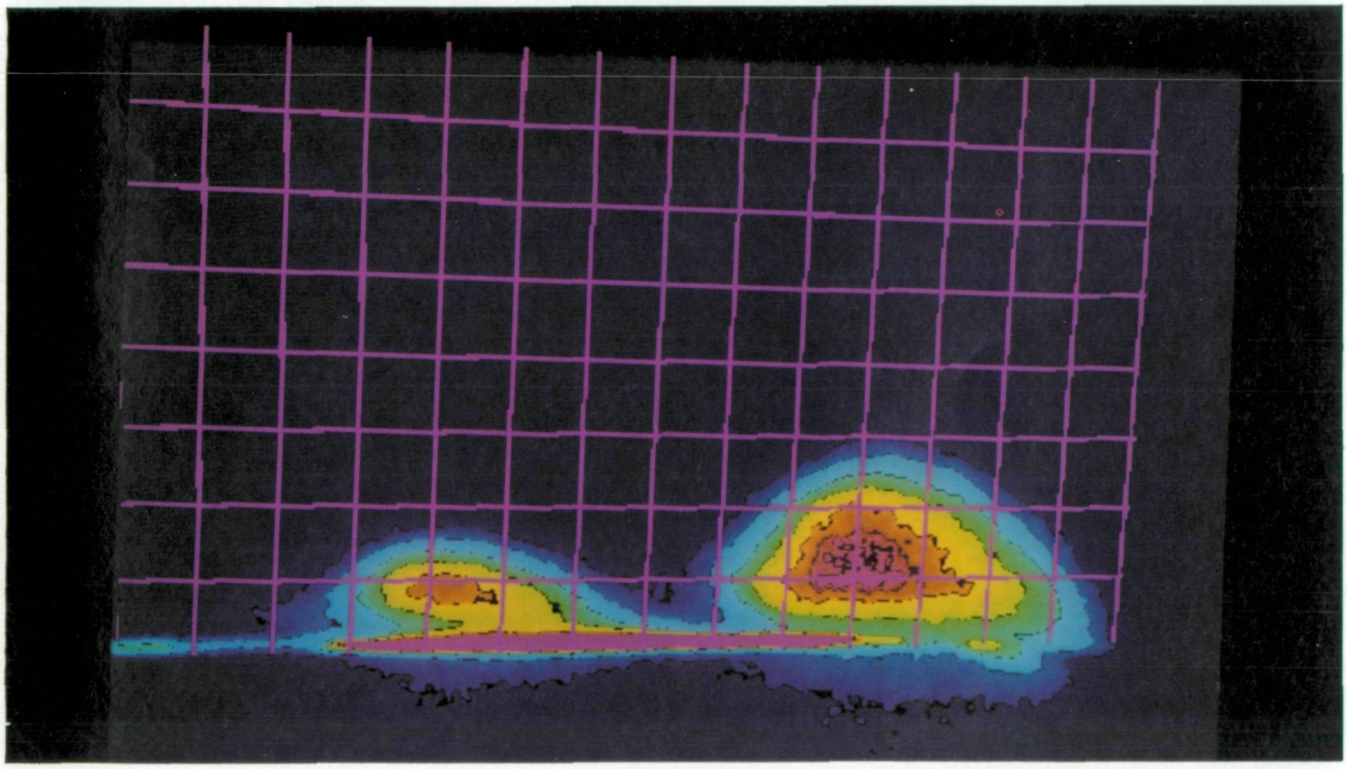

L-87-1095

(b) $\alpha = 18°$.

Figure 24. Vortex-system enhanced images for intermittent light-sheet operation. $1g$ maneuver; $0.30 \leq M \leq 0.40$; probe-tip location 1; altitude, 25 000 ft; slit width, 0.041 in.

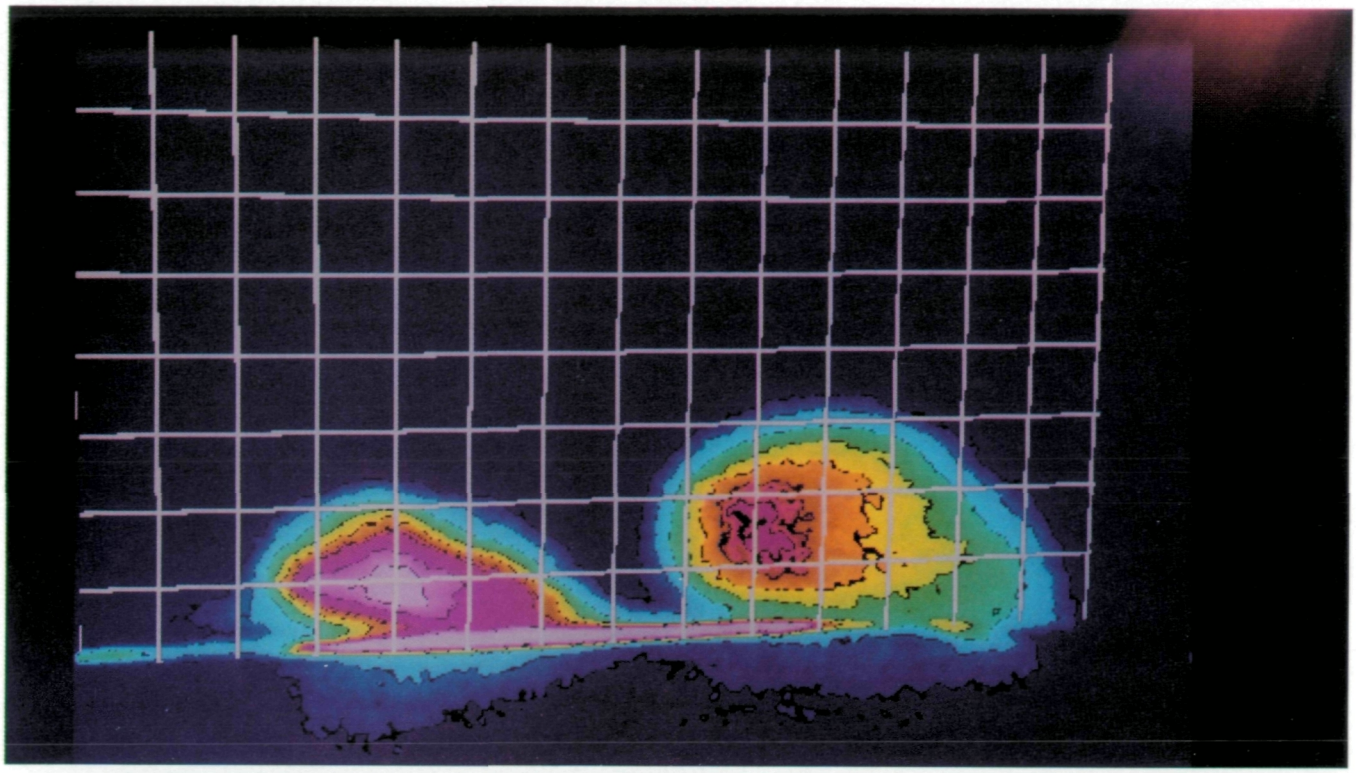

(c) $\alpha = 19°$.

L-87-1101

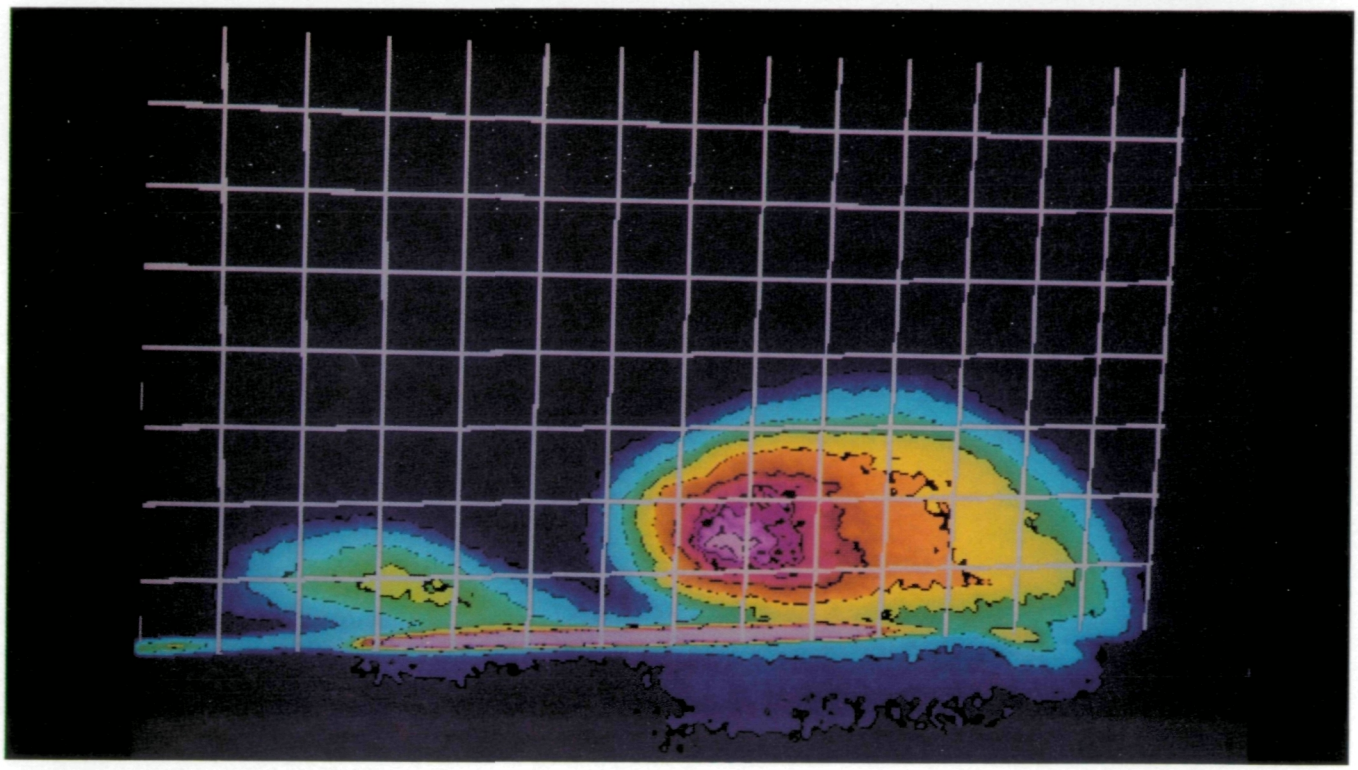

L-87-1093

(d) $\alpha = 20°$.

Figure 24. Continued.

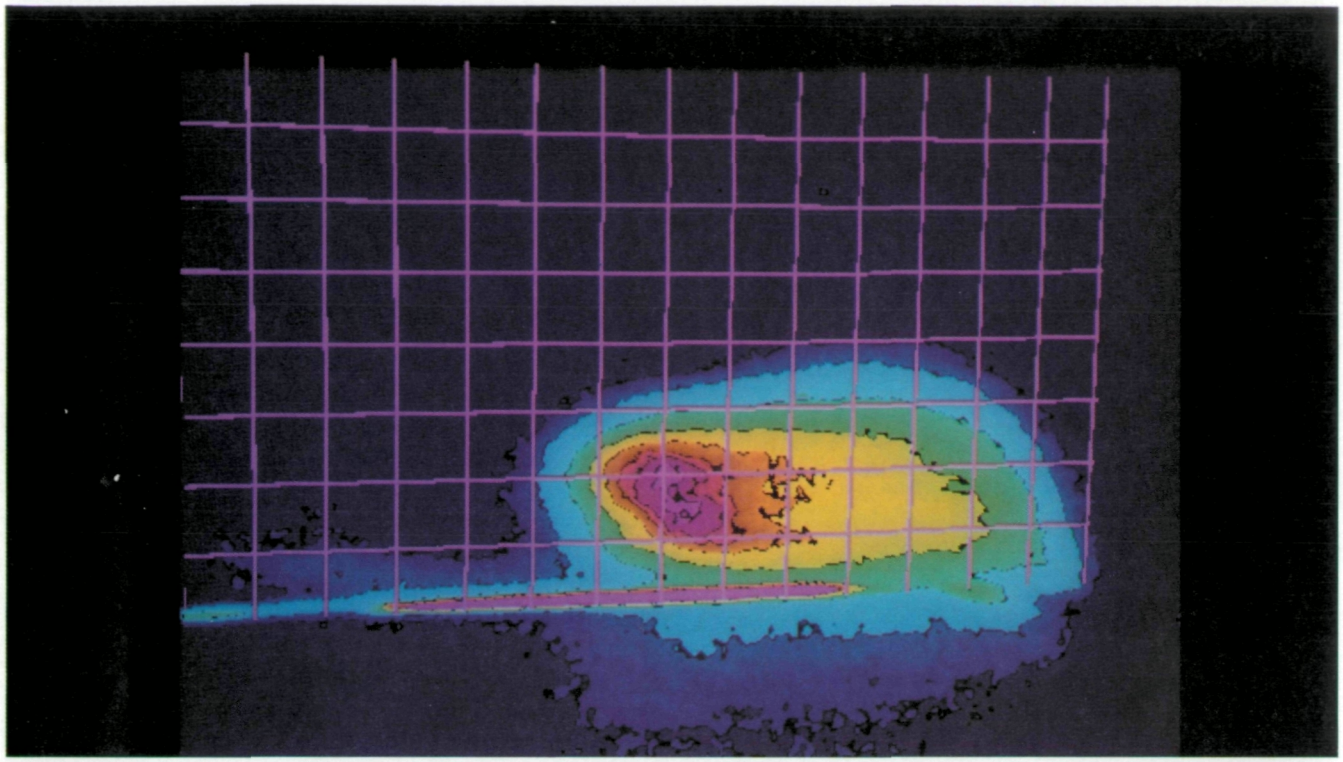

(e) $\alpha = 21°$.

L-87-1103

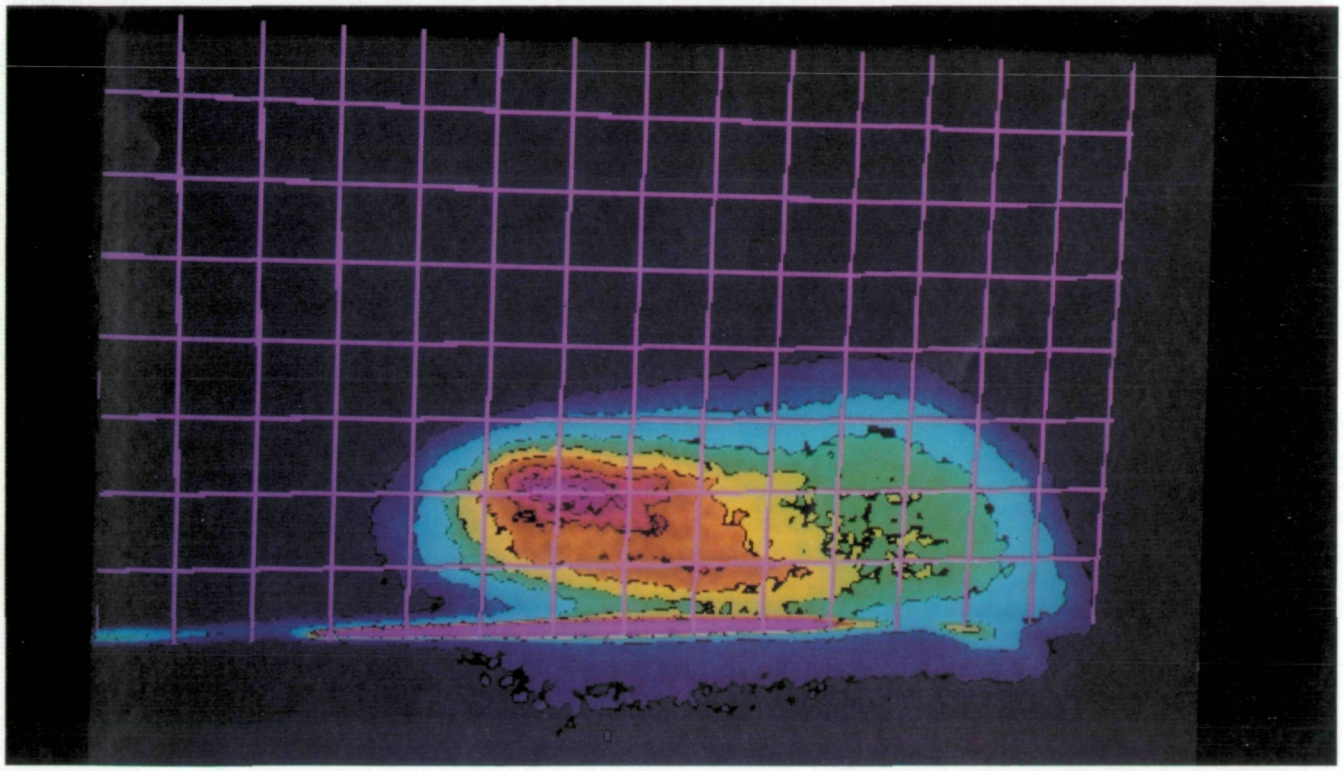

L-87-1104

(f) $\alpha = 22°$.

Figure 24. Continued.

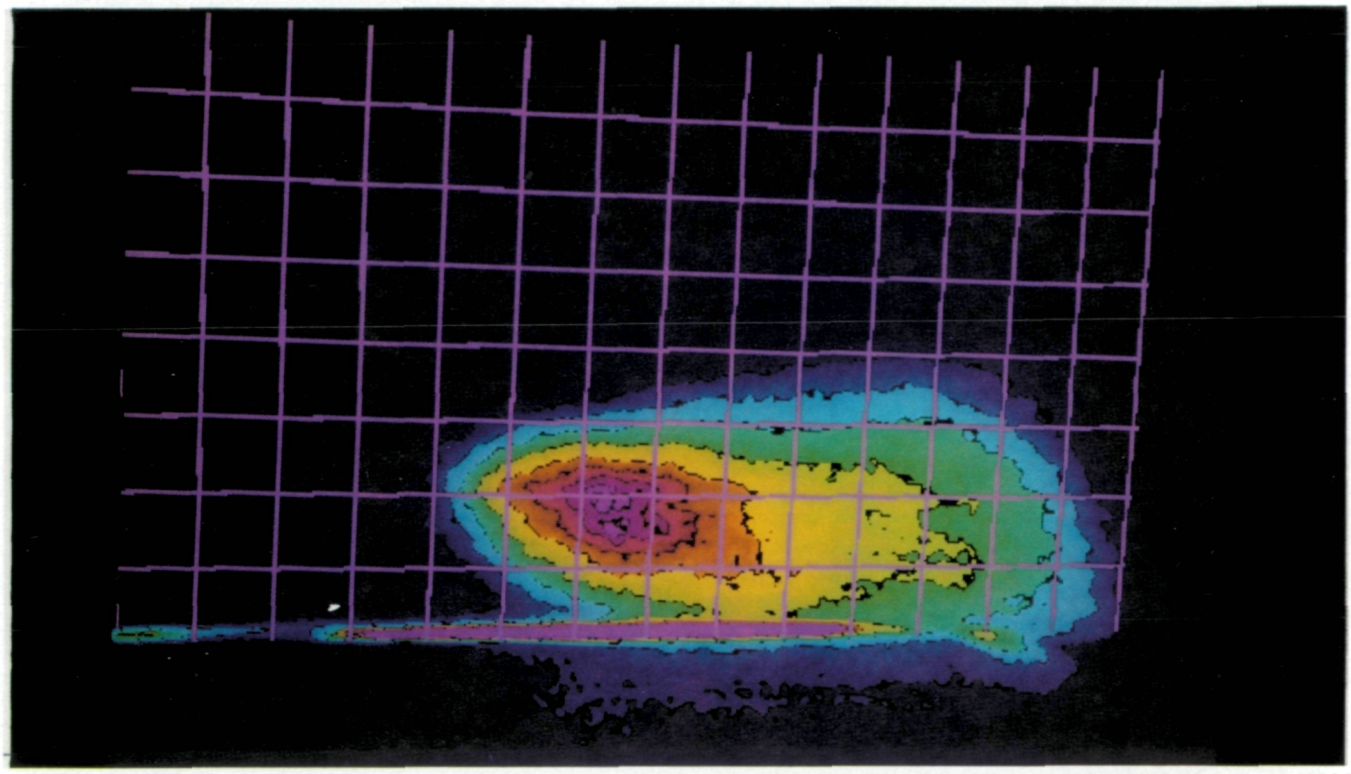

L-87-1089

(g) $\alpha = 23°$.

Figure 24. Concluded.

ORIGINAL PAGE
COLOR PHOTOGRAPH

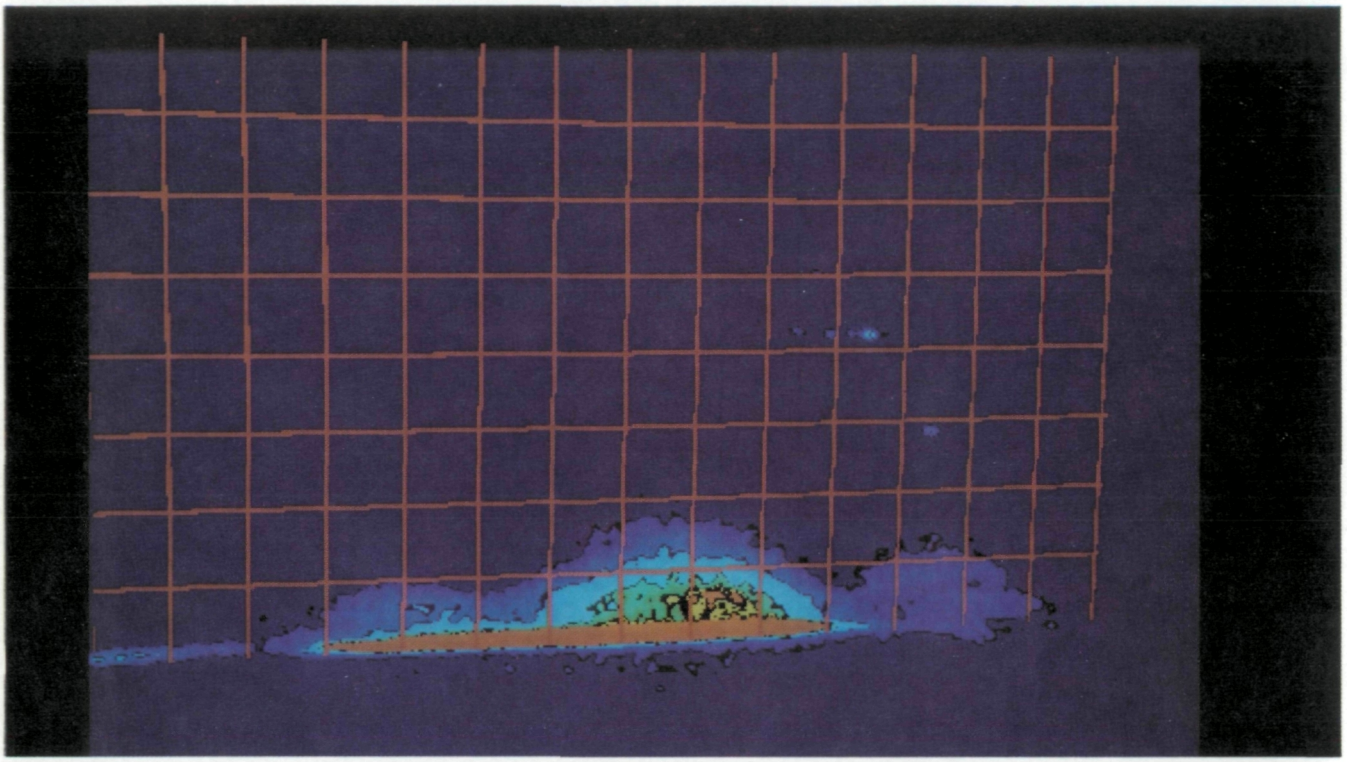

(a) $\alpha = 17°$. L-87-1102

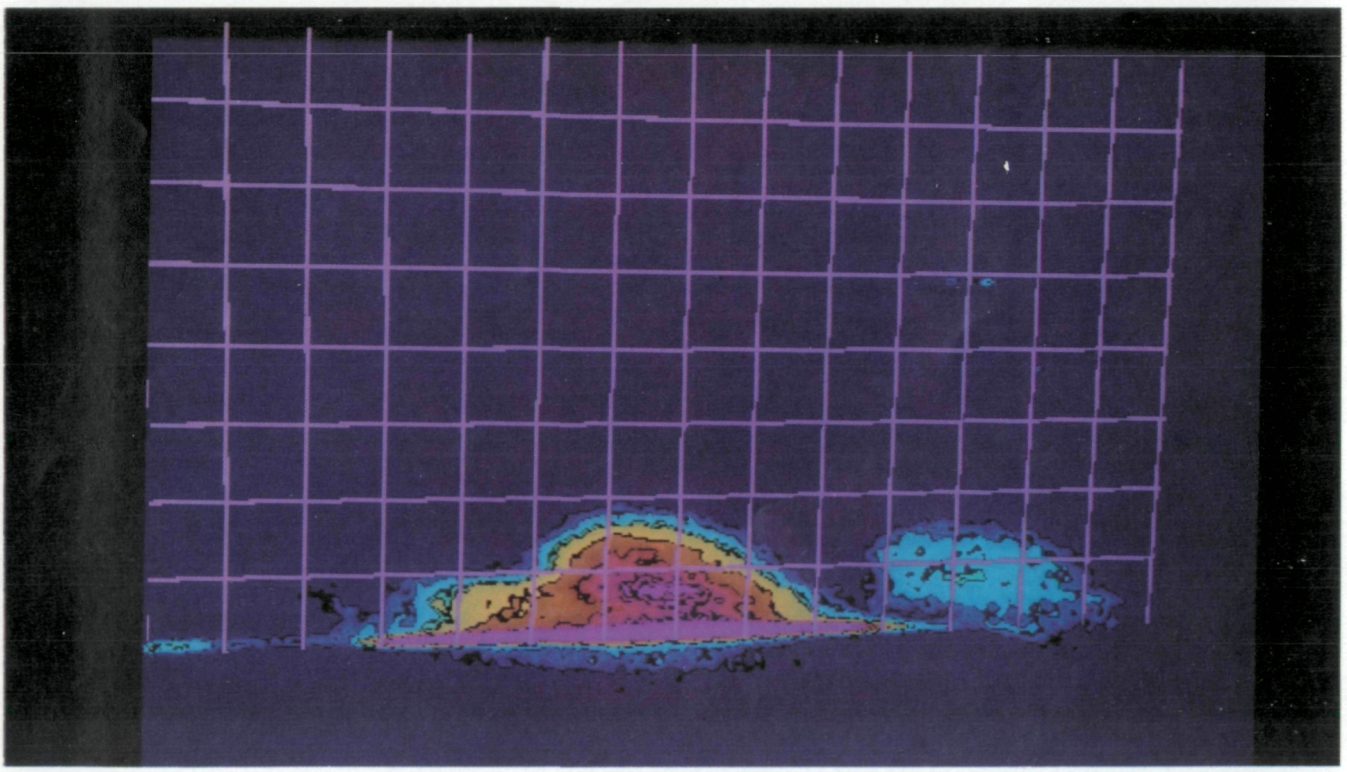

L-87-1100

(b) $\alpha = 18°$.

Figure 25. Vortex-system enhanced images for continuous light-sheet operation. $1g$ maneuver; $0.30 \leq M \leq 0.40$; probe-tip location 1; altitude, 25 000 ft; slit width, 0.041 in.

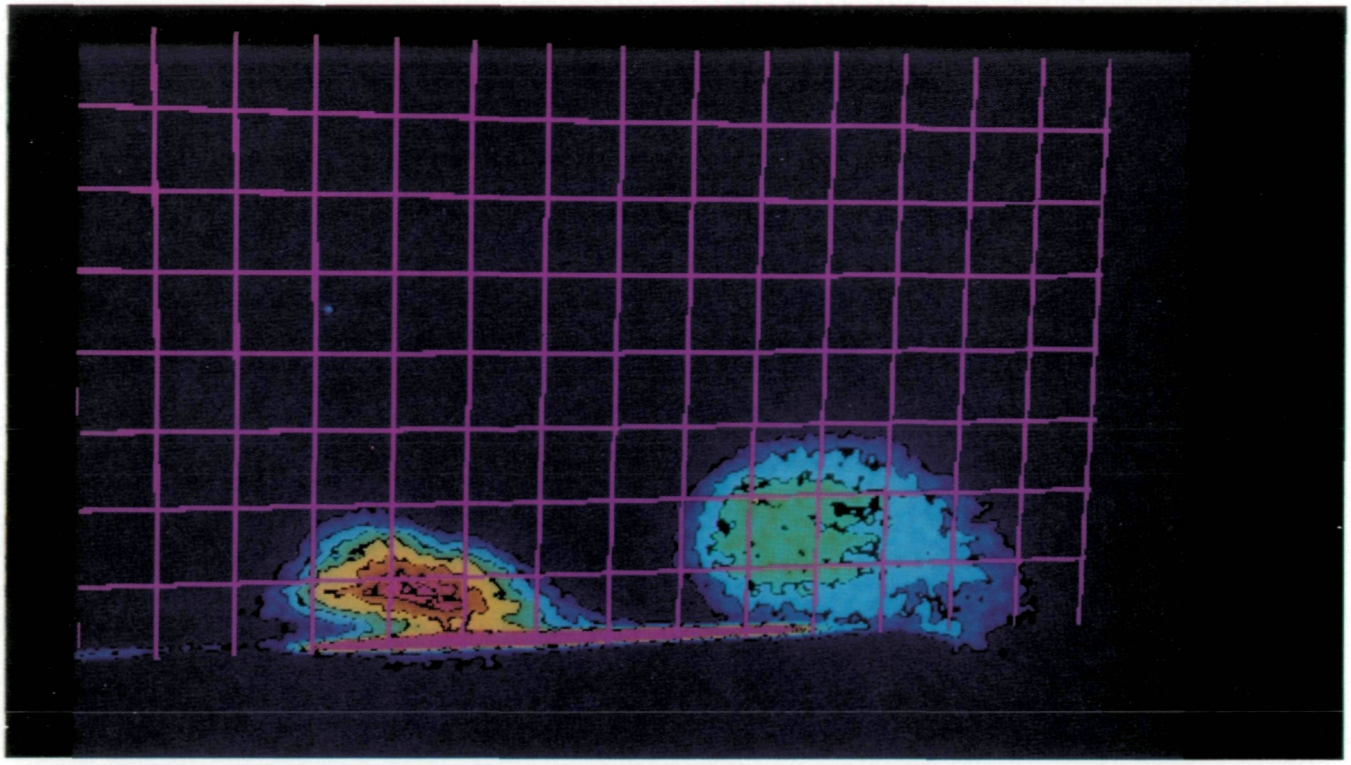

L-87-1094

(c) $\alpha = 19°$.

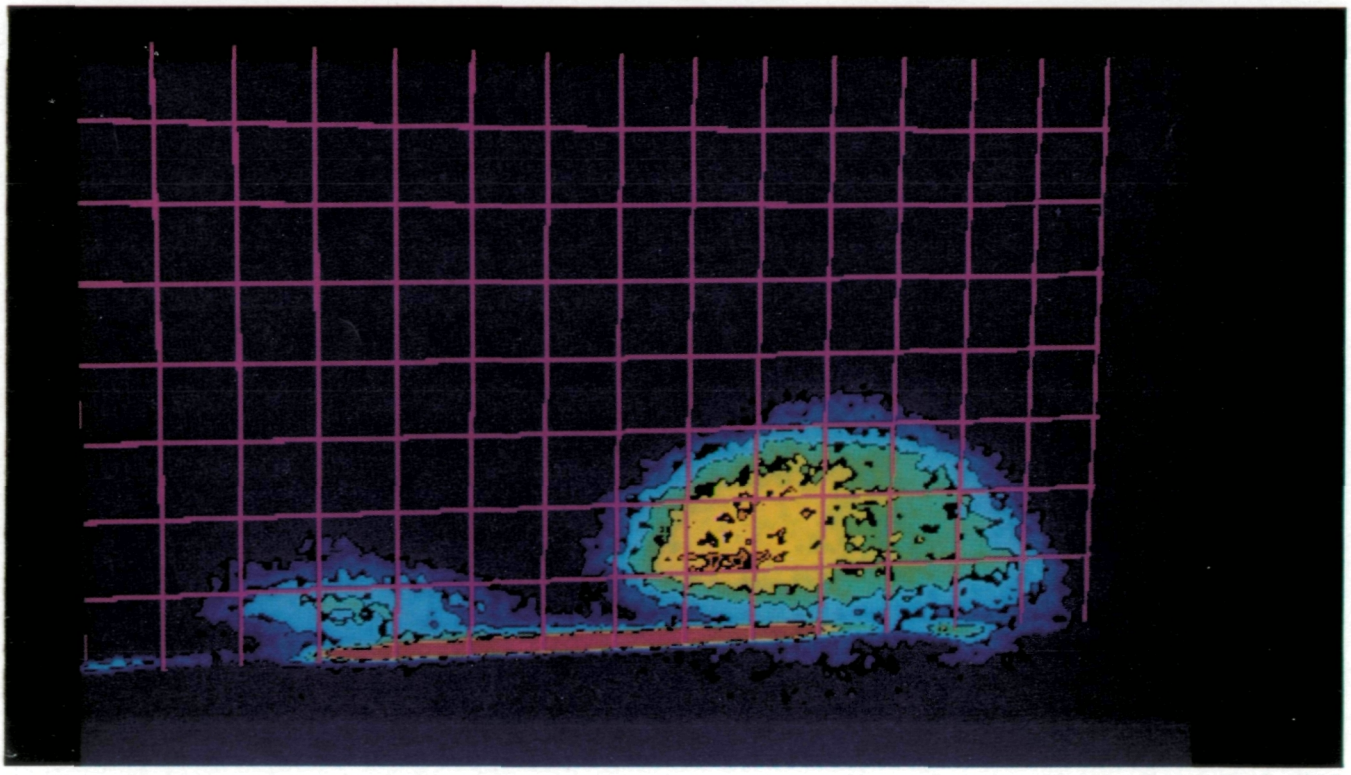

L-87-1099

(d) $\alpha = 20°$.

Figure 25. Continued.

ORIGINAL PAGE
COLOR PHOTOGRAPH

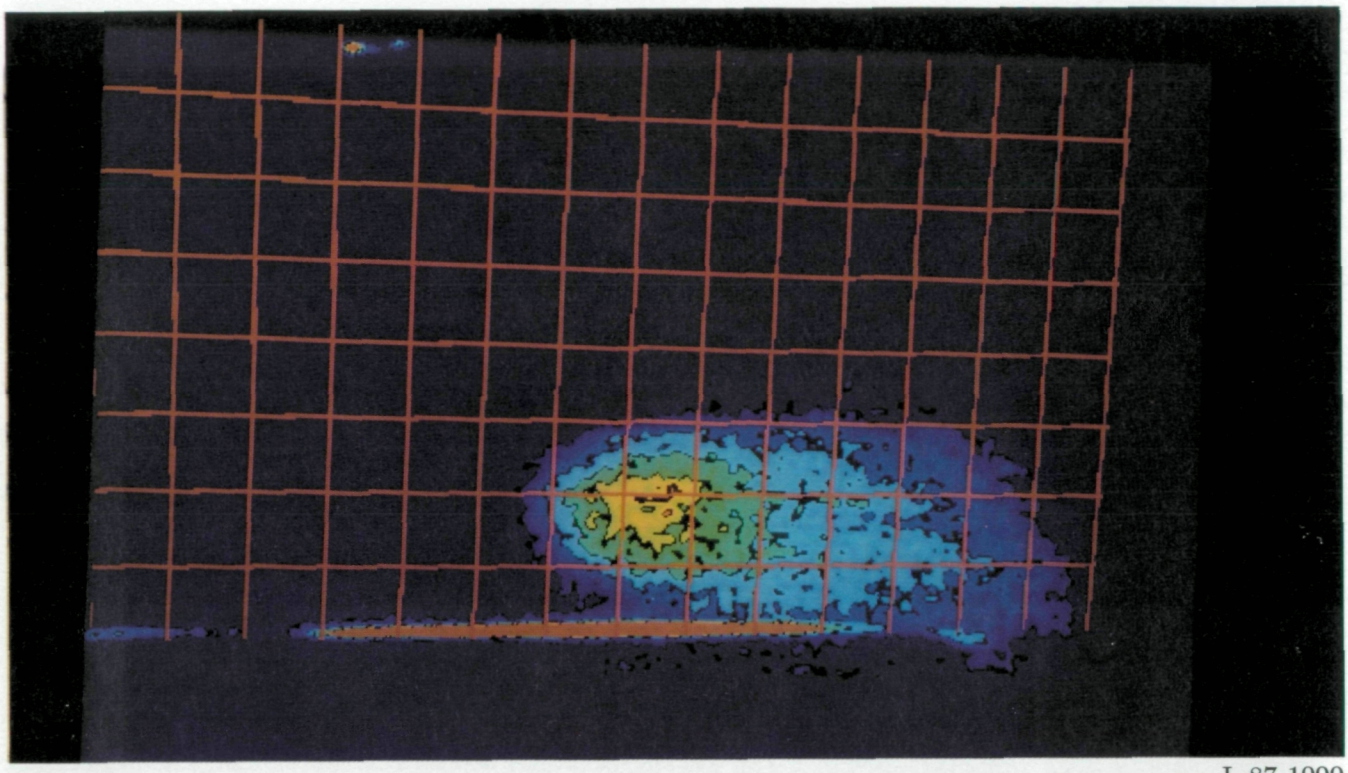

L-87-1090

(e) $\alpha = 21°$.

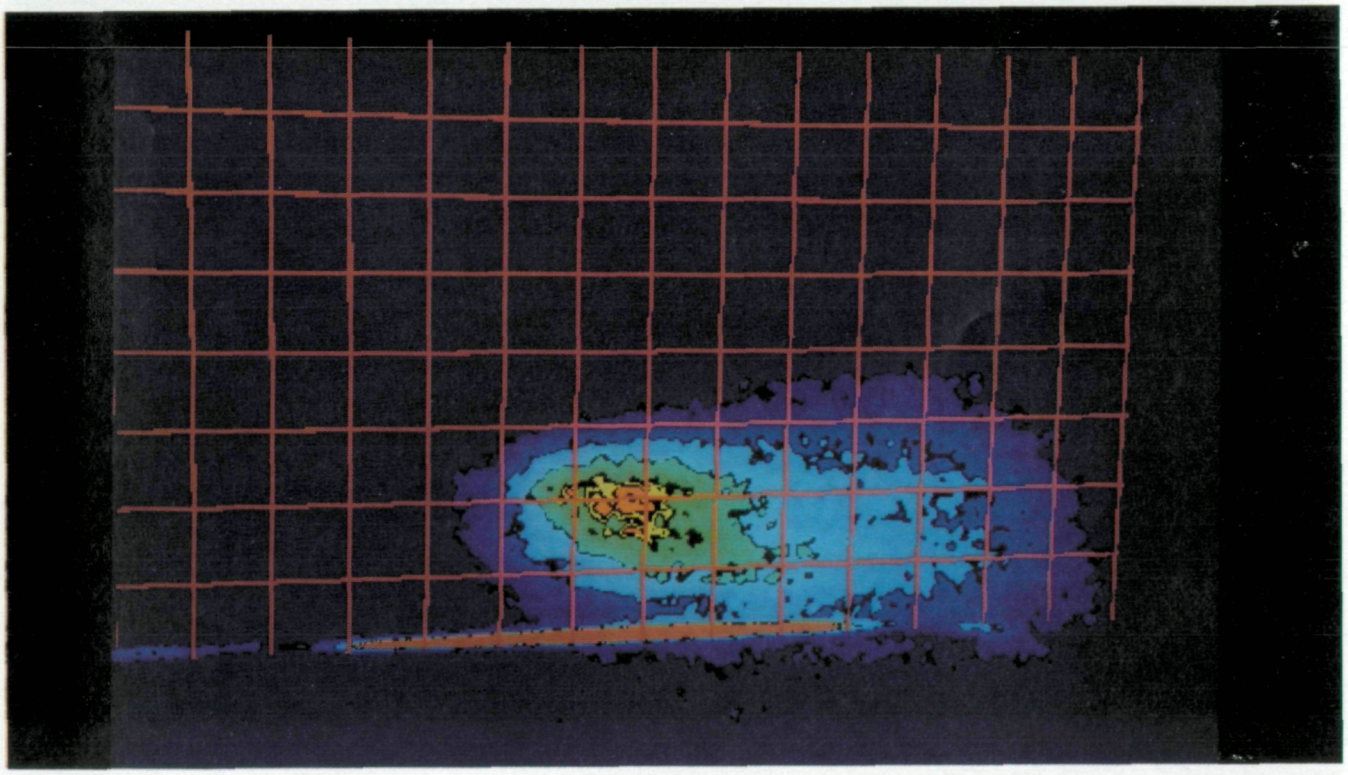

L-87-1106

(f) $\alpha = 22°$.

Figure 25. Continued.

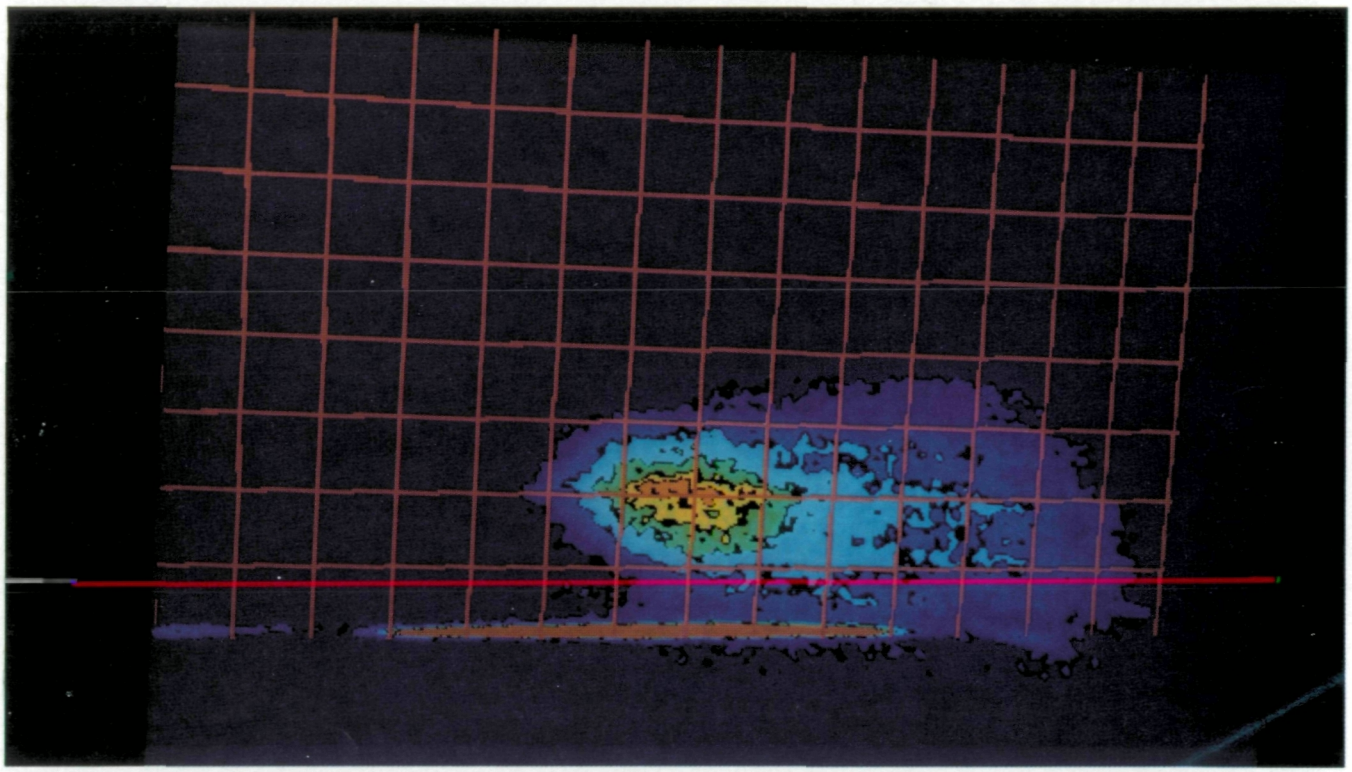

L-87-1091

(g) $\alpha = 23°$.

Figure 25. Concluded.

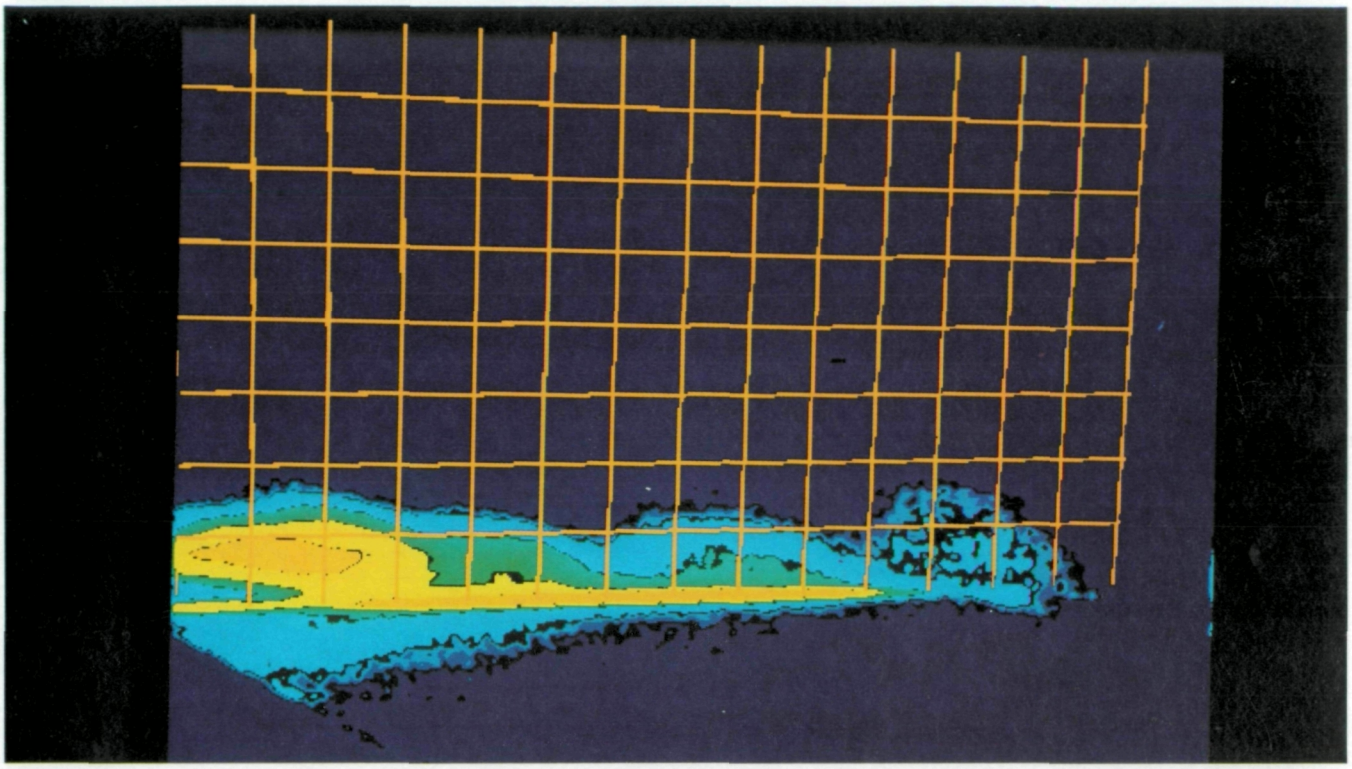

(a) $\alpha = 17°$. L-87-4069

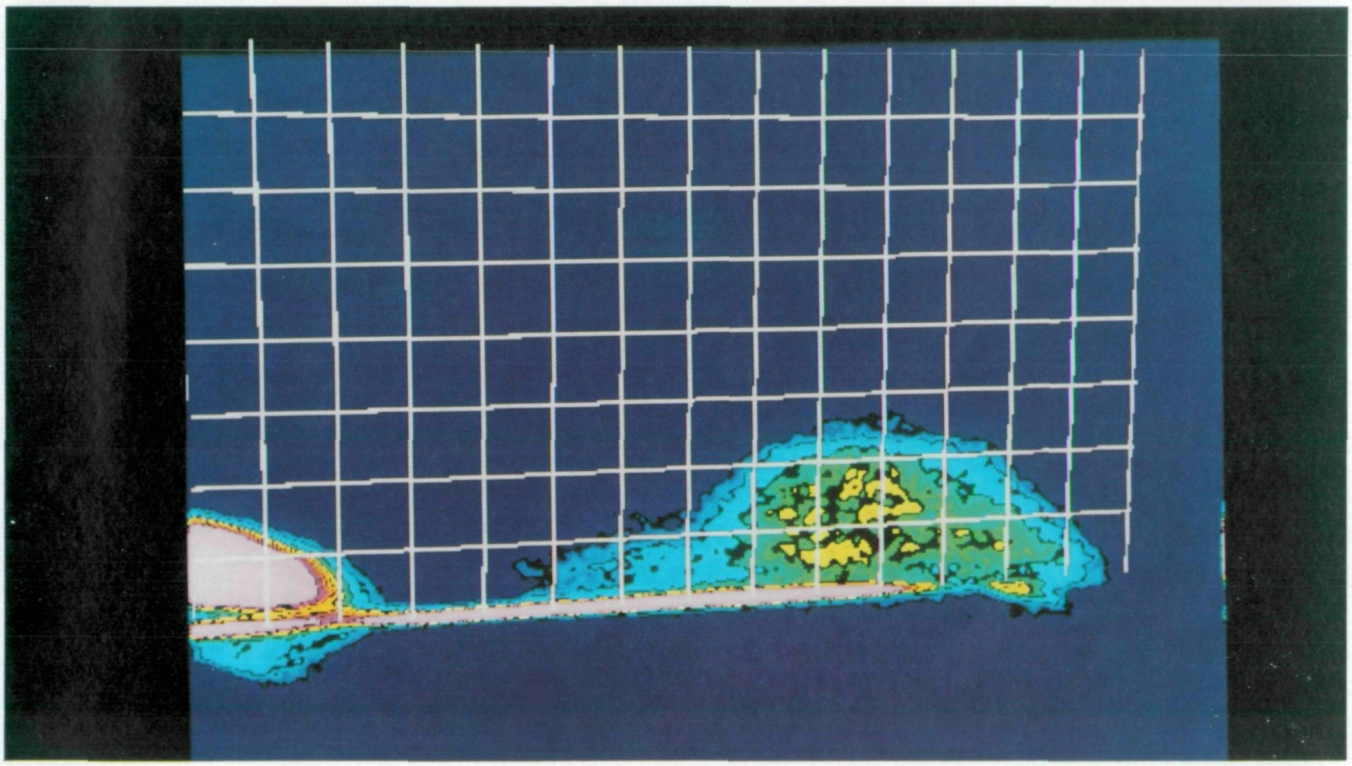

L-87-3884

(b) $\alpha = 18°$.

Figure 26. Vortex-system enhanced images for slit width of 0.041 in. and altitude of 25 000 ft. $1g$ maneuver; $0.30 \leq M \leq 0.40$; probe-tip location 6; intermittent light-sheet operation.

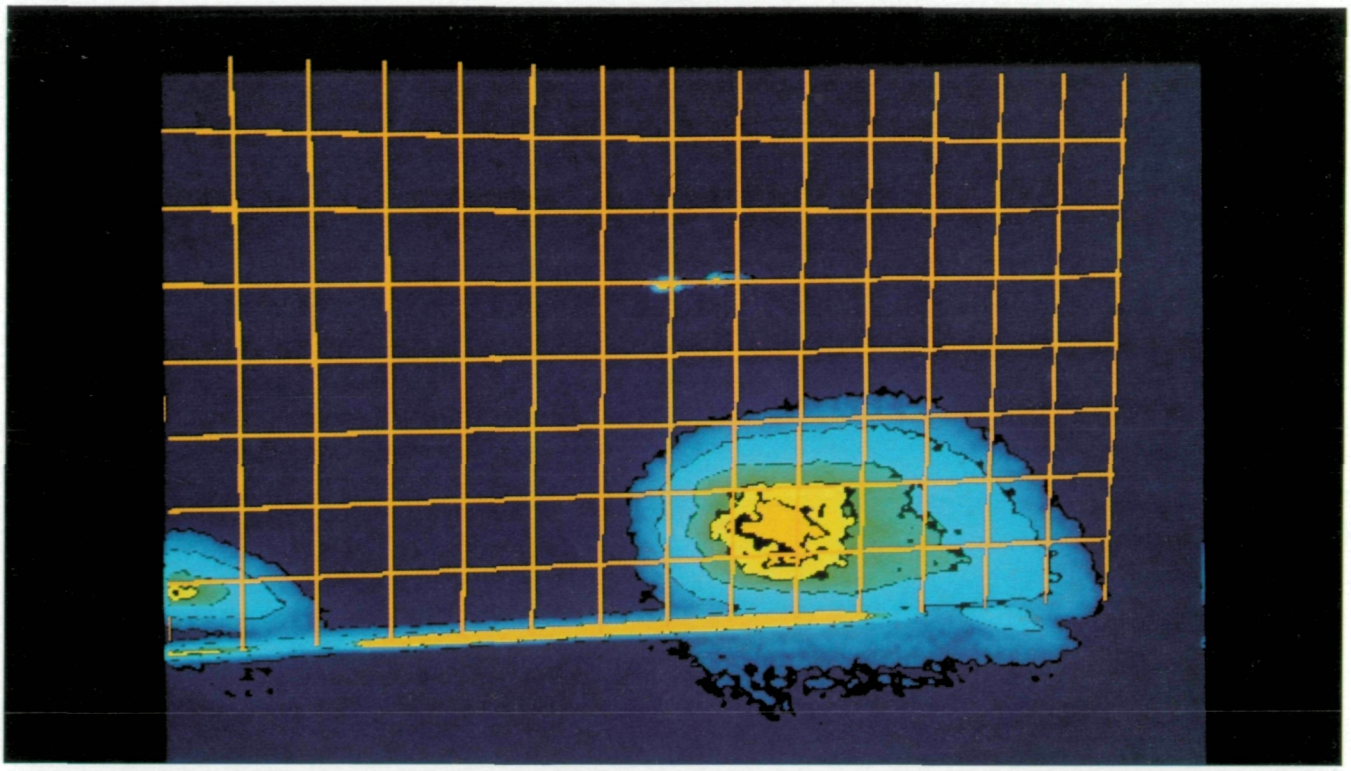

(c) $\alpha = 19°$.

L-87-4065

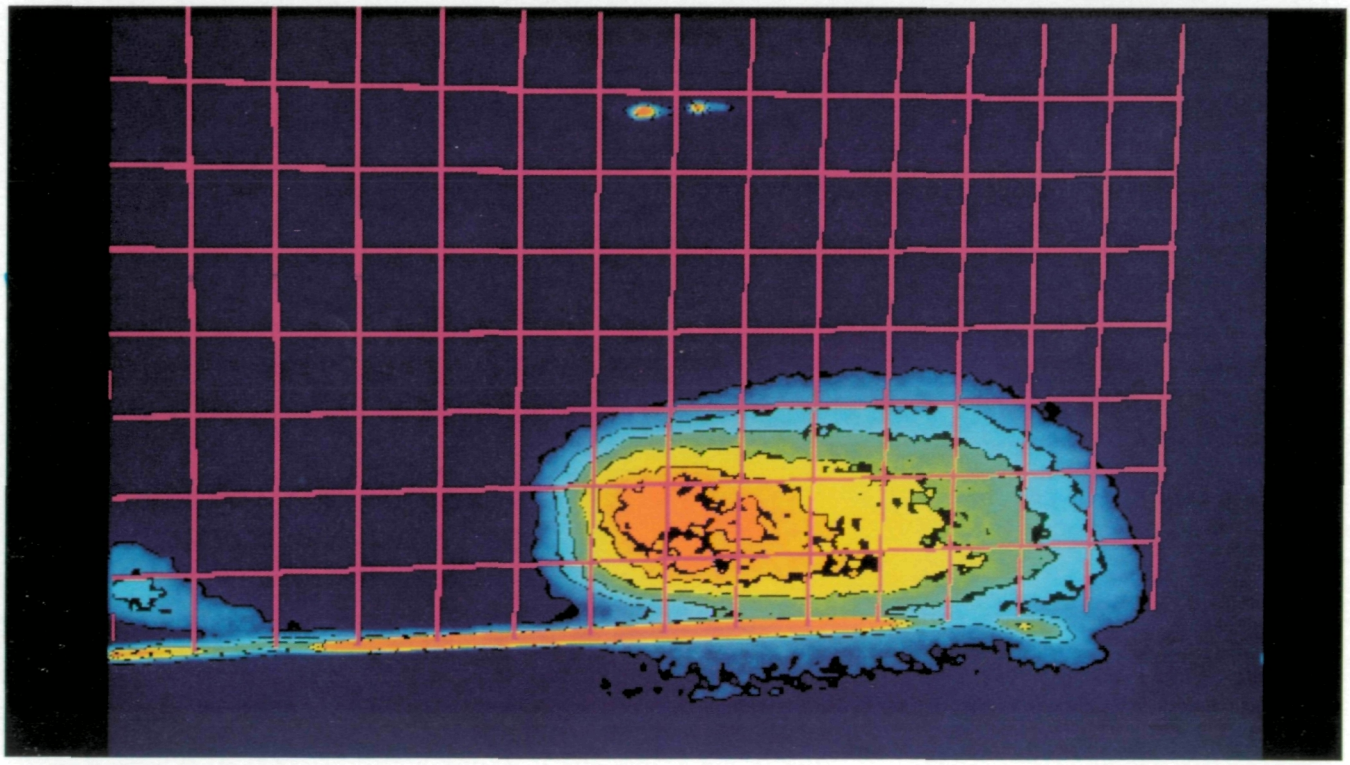

L-87-4073

(d) $\alpha = 20°$.

Figure 26. Continued.

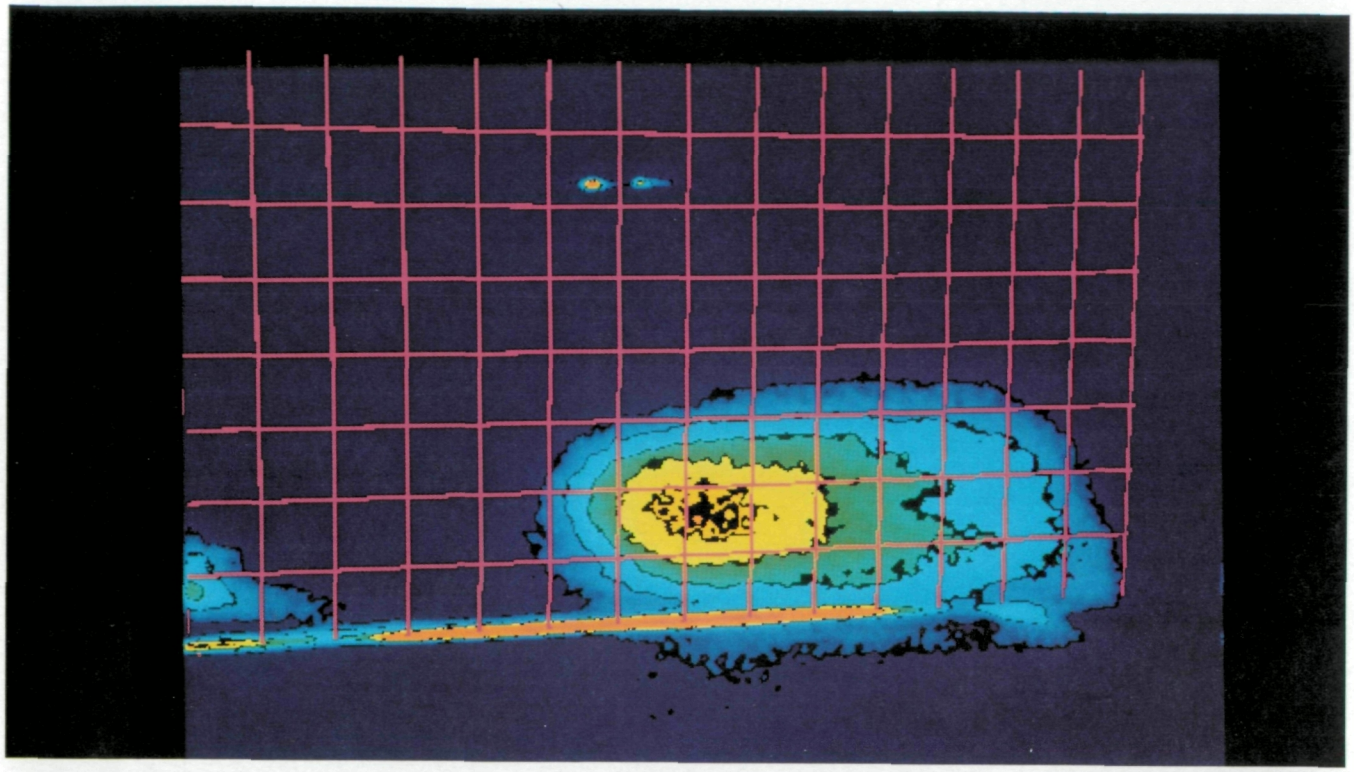

(e) $\alpha = 21°$.

L-87-4074

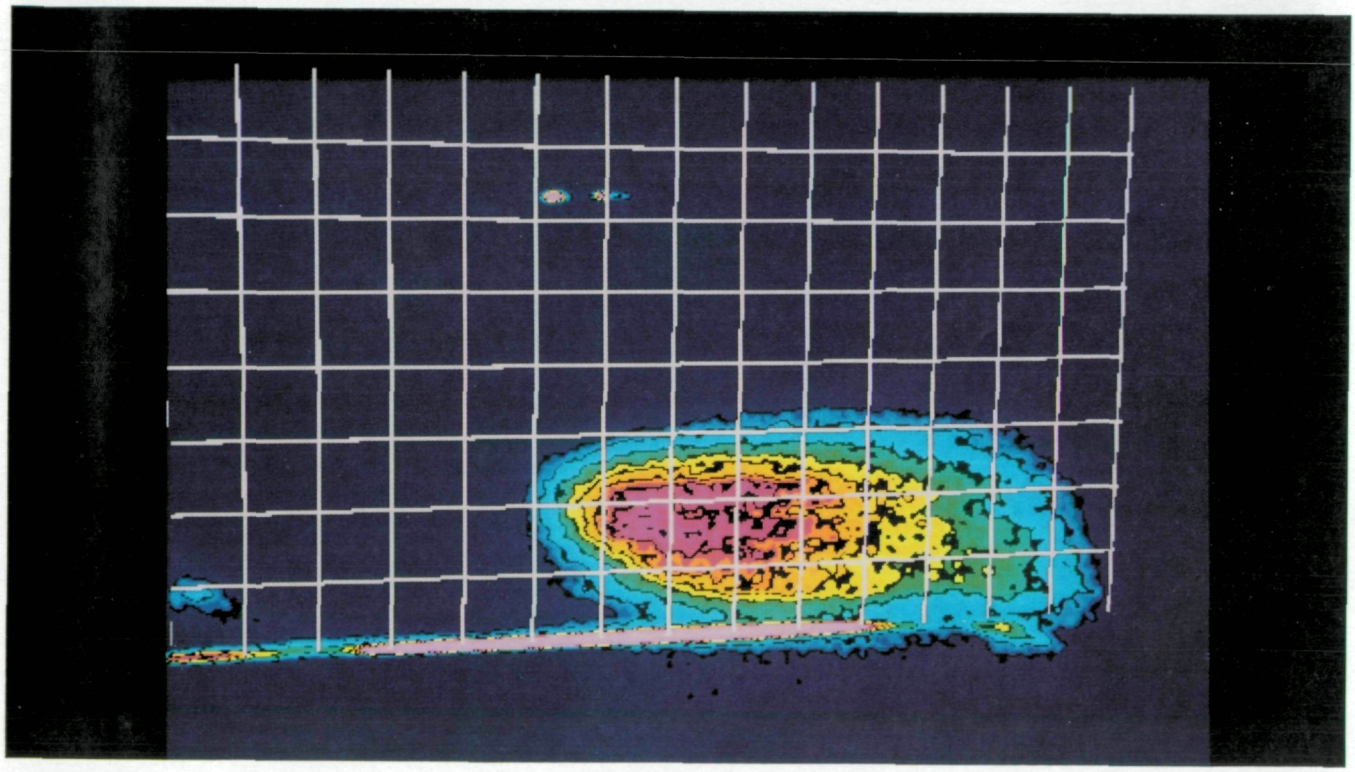

L-87-4076

(f) $\alpha = 22°$.

Figure 26. Continued.

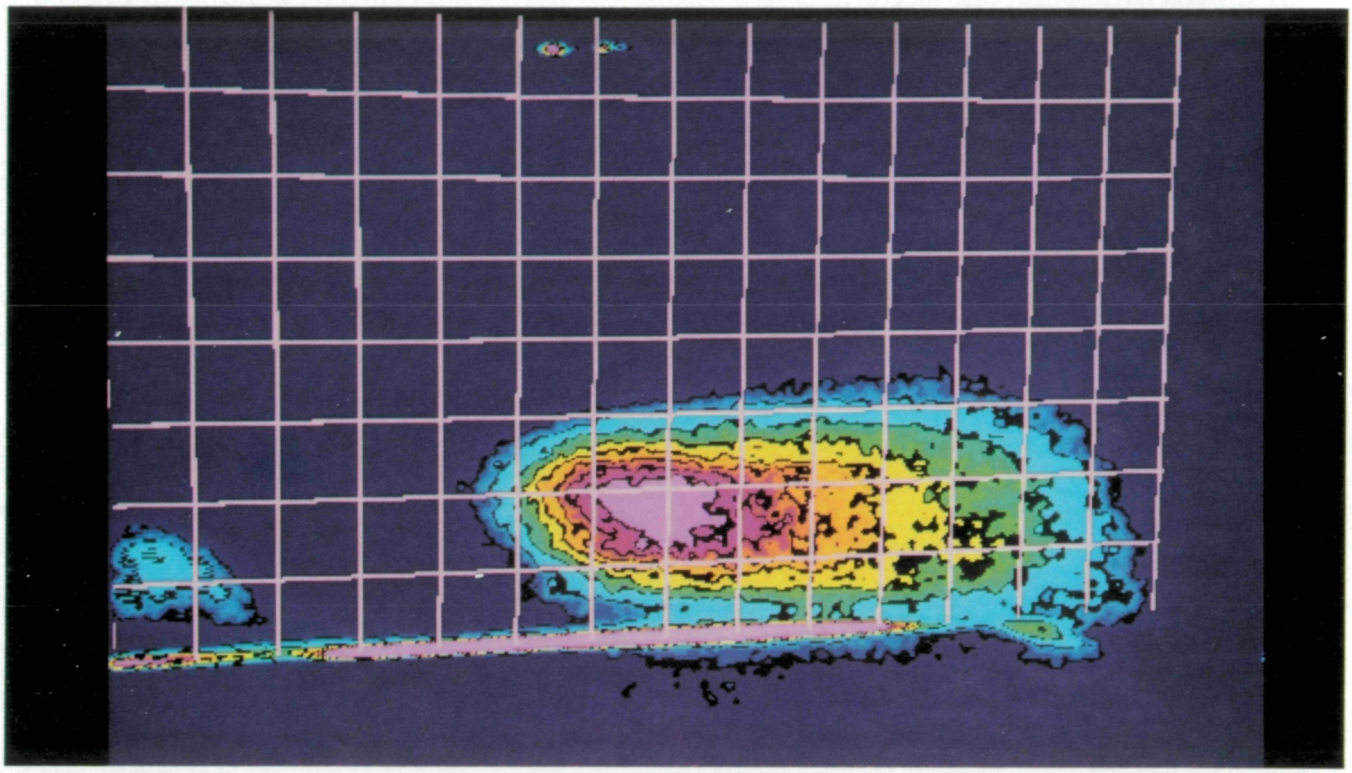

L-87-4075

(g) $\alpha = 23°$.

Figure 26. Concluded.

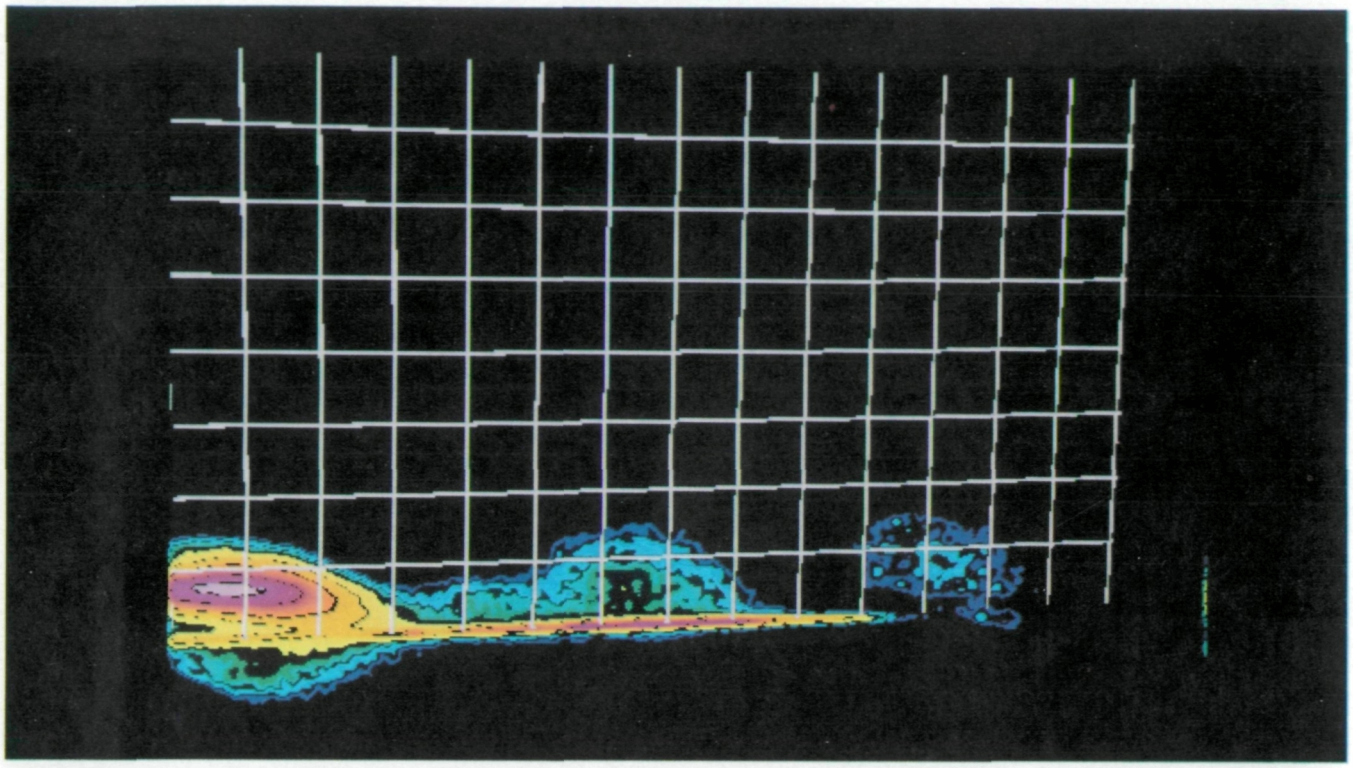

(a) $\alpha = 17°$.

L-87-2853

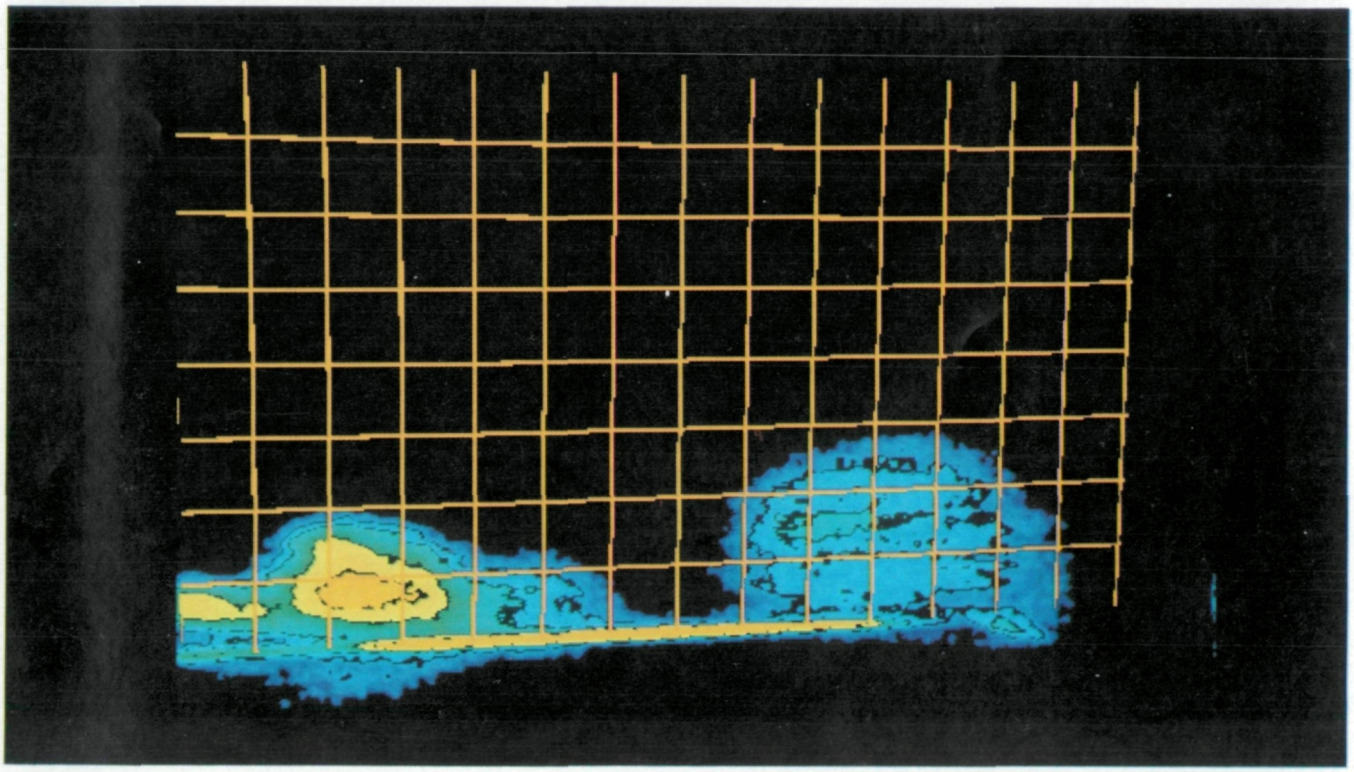

L-87-4064

(b) $\alpha = 18°$.

Figure 27. Vortex-system enhanced images for slit width of 0.012 in. and altitude of 25 000 ft. $1g$ maneuver; $0.30 \leq M \leq 0.40$; probe-tip location 6; intermittent light-sheet operation.

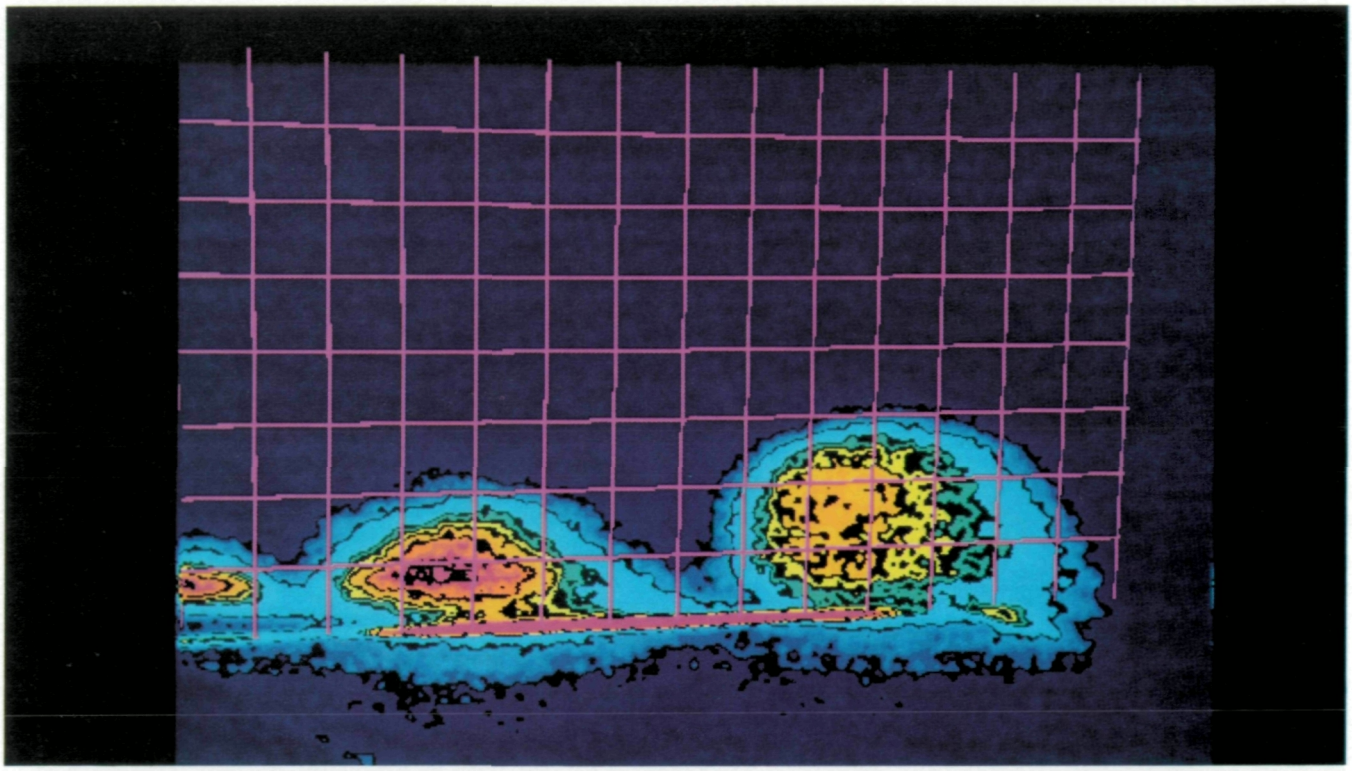

(c) $\alpha = 19°$.

L-87-2838

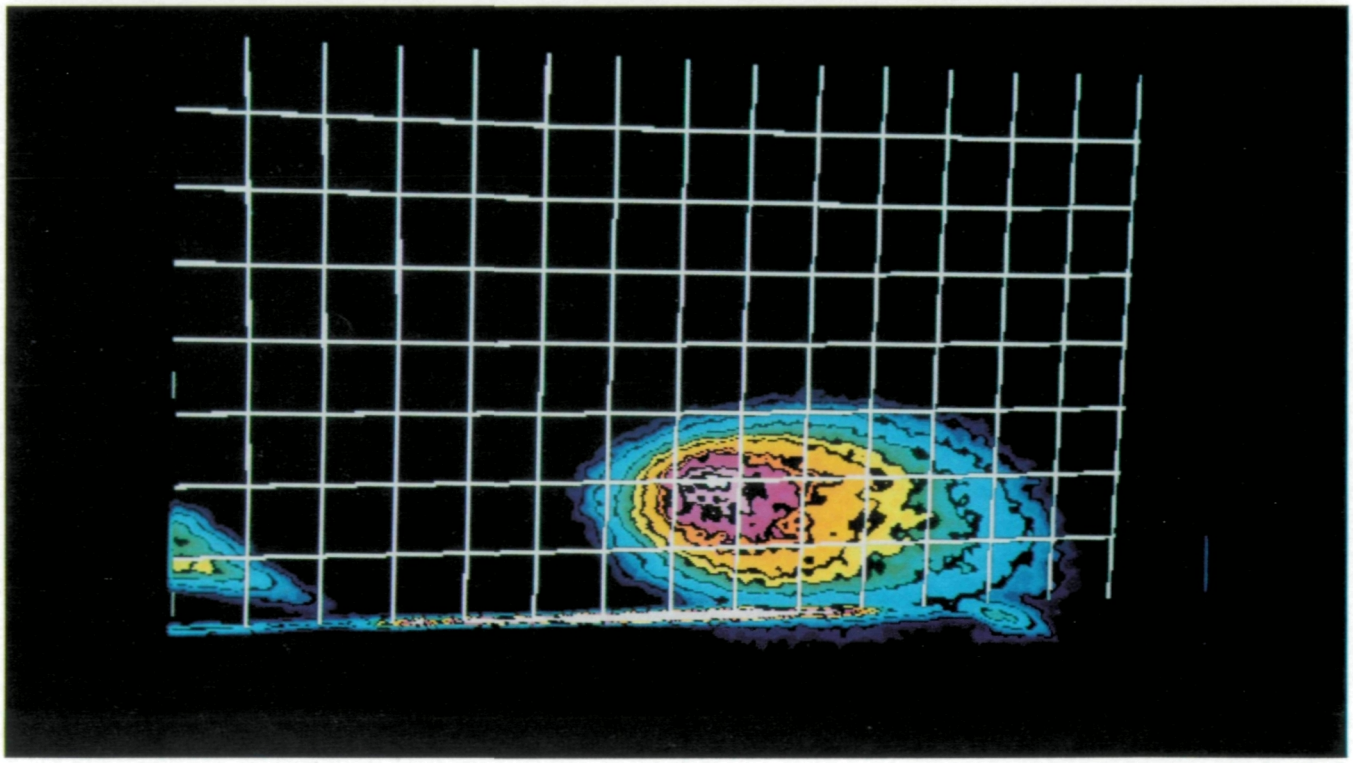

L-87-2847

(d) $\alpha = 20°$.

Figure 27. Continued.

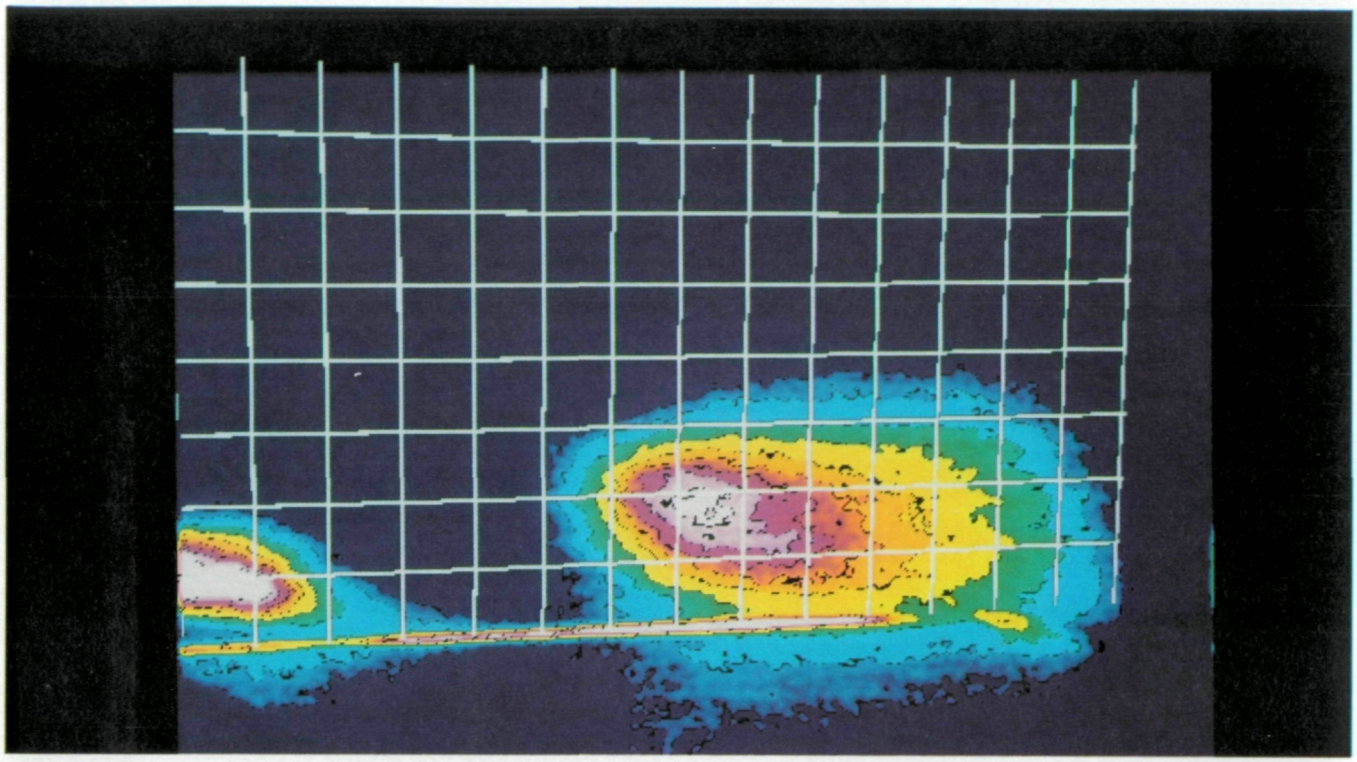

L-87-2852

(e) $\alpha = 21°$.

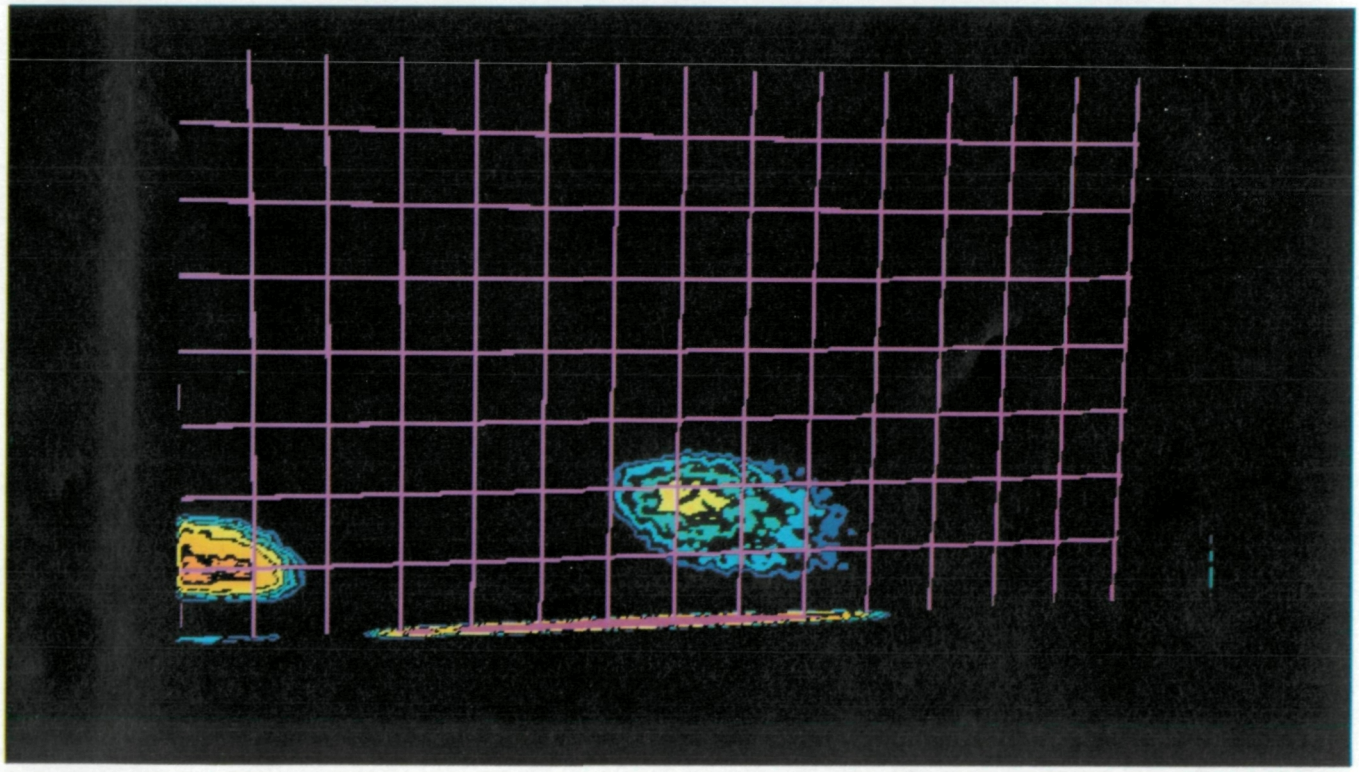

L-87-2843

(f) $\alpha = 22°$.

Figure 27. Continued.

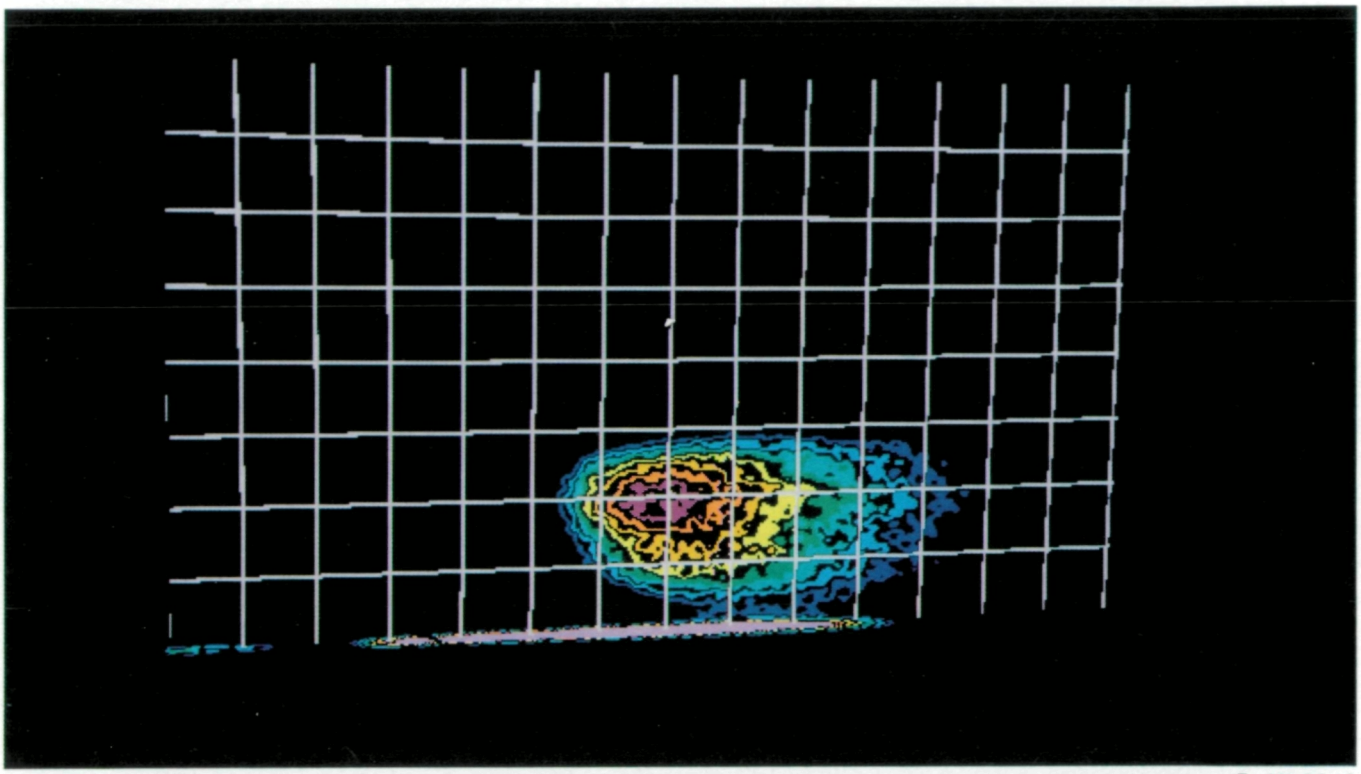

L-87-2842

(g) $\alpha = 23°$.

Figure 27. Concluded.

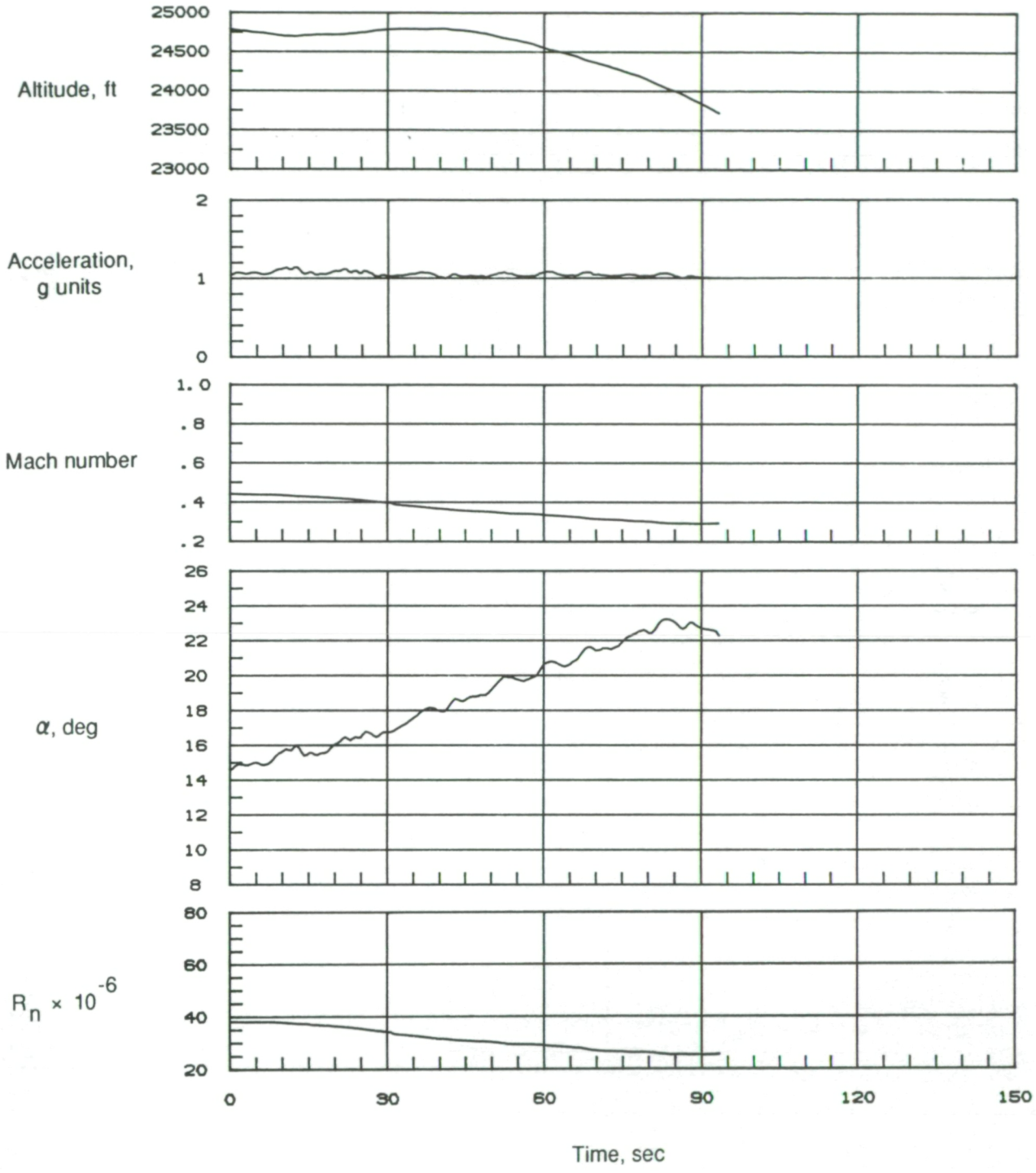

Figure 28. Time history of selected flight parameters for 1g maneuver at 25 000 ft (85-009/06a). Probe-tip location 1; slit width, 0.041 in.

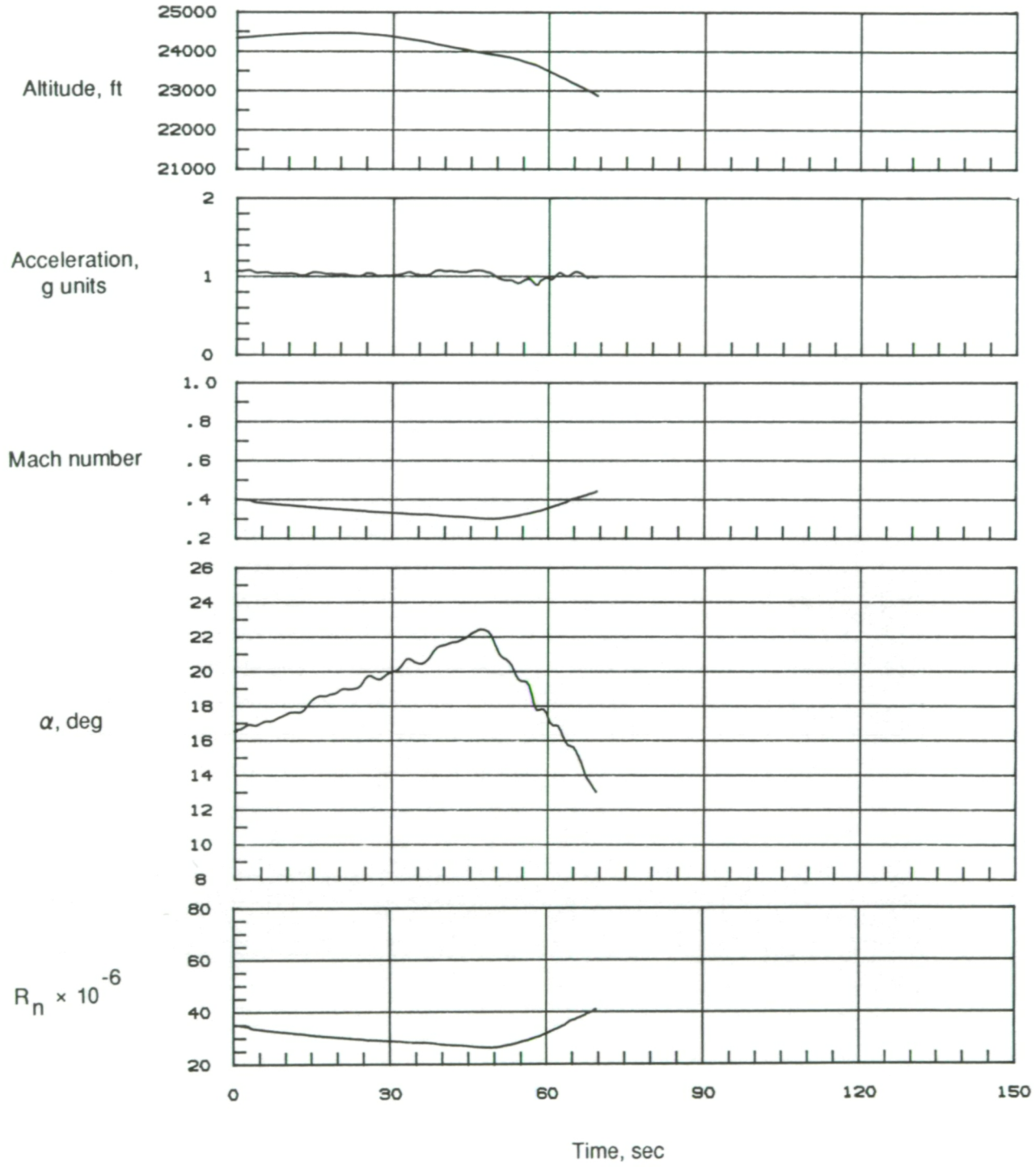

Figure 29. Time history of selected flight parameters for 1g maneuver at 25 000 ft (85-009/09). Probe-tip location 1; slit width, 0.041 in.

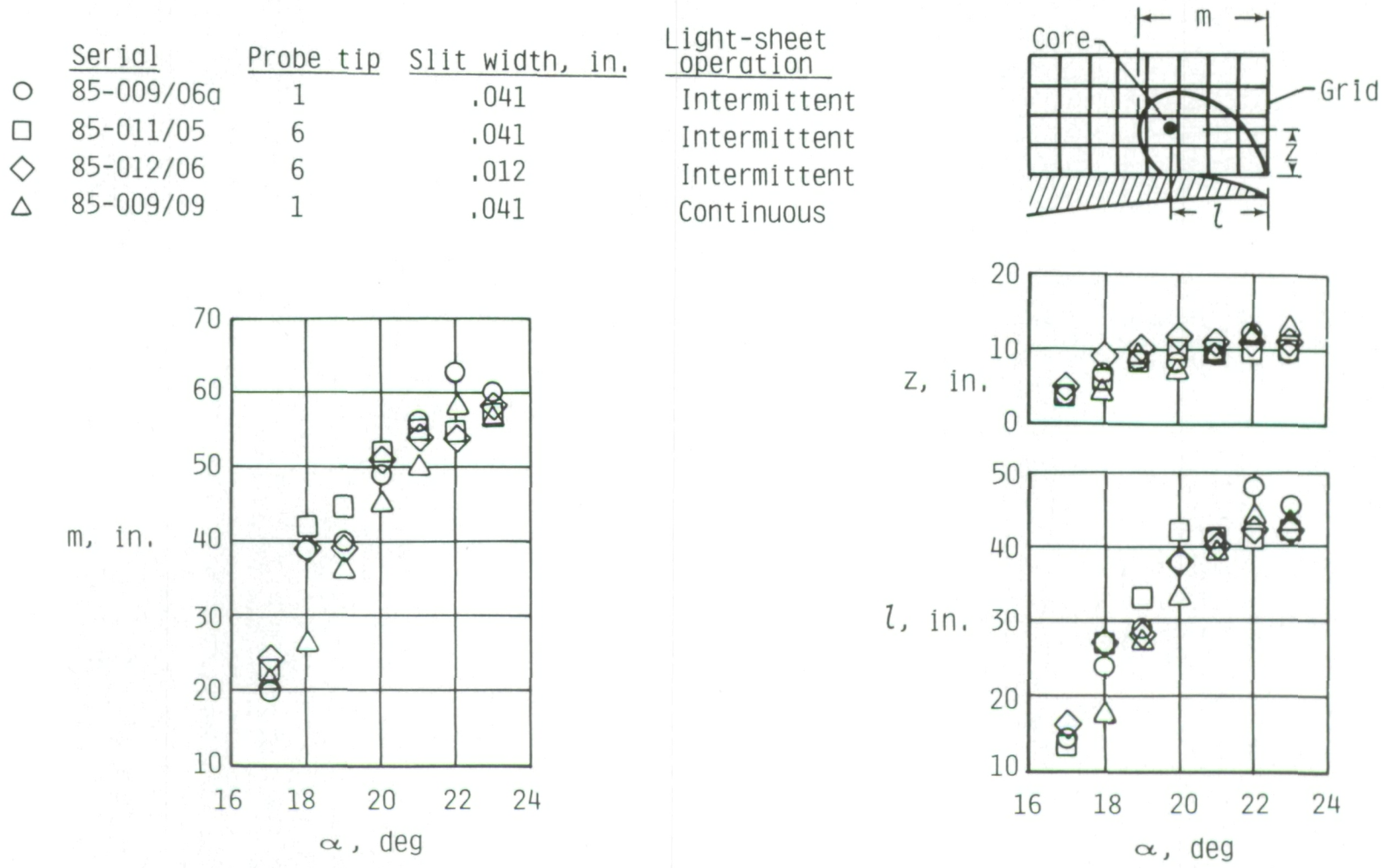

Figure 30. Effect of probe-tip location, slit width, and light-sheet operation on vortex-system image characteristics. $0.30 \leq M \leq 0.40$; $1g$ maneuver; altitude, 25 000 ft.

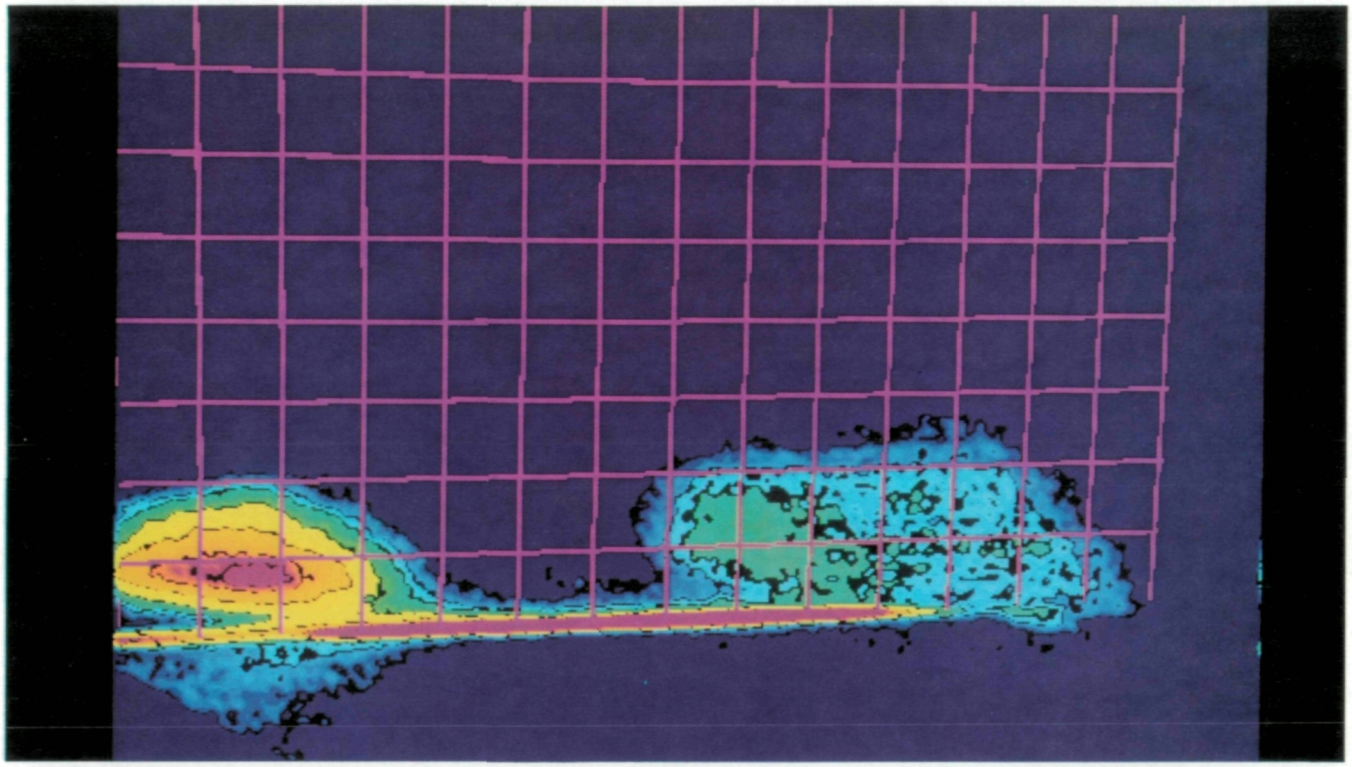

L-87-3891

(a) $\alpha = 17°$.

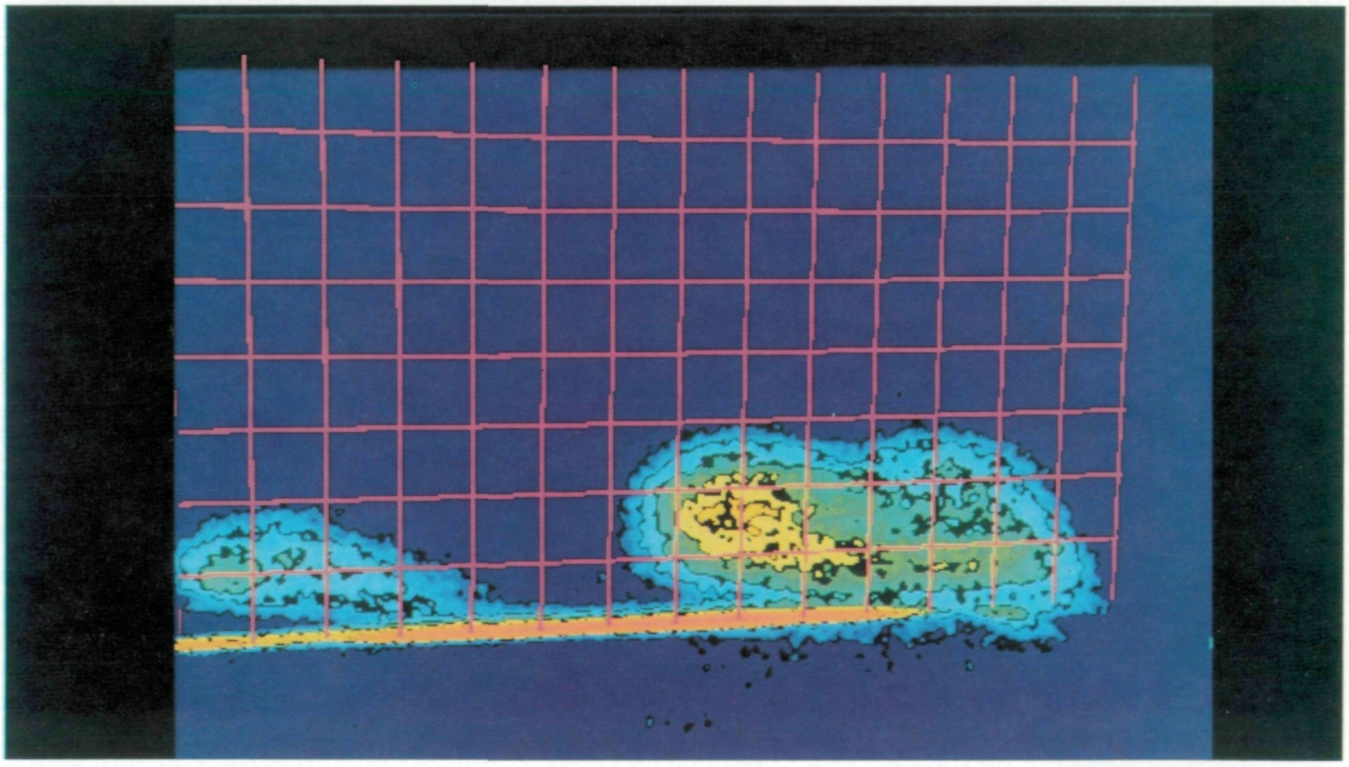

L-87-3892

(b) $\alpha = 18°$.

Figure 31. Vortex-system enhanced images for slit width of 0.041 in. and altitude of 35 000 ft. $1g$ maneuver; $0.35 \leq M \leq 0.50$; probe-tip location 6; intermittent light-sheet operation.

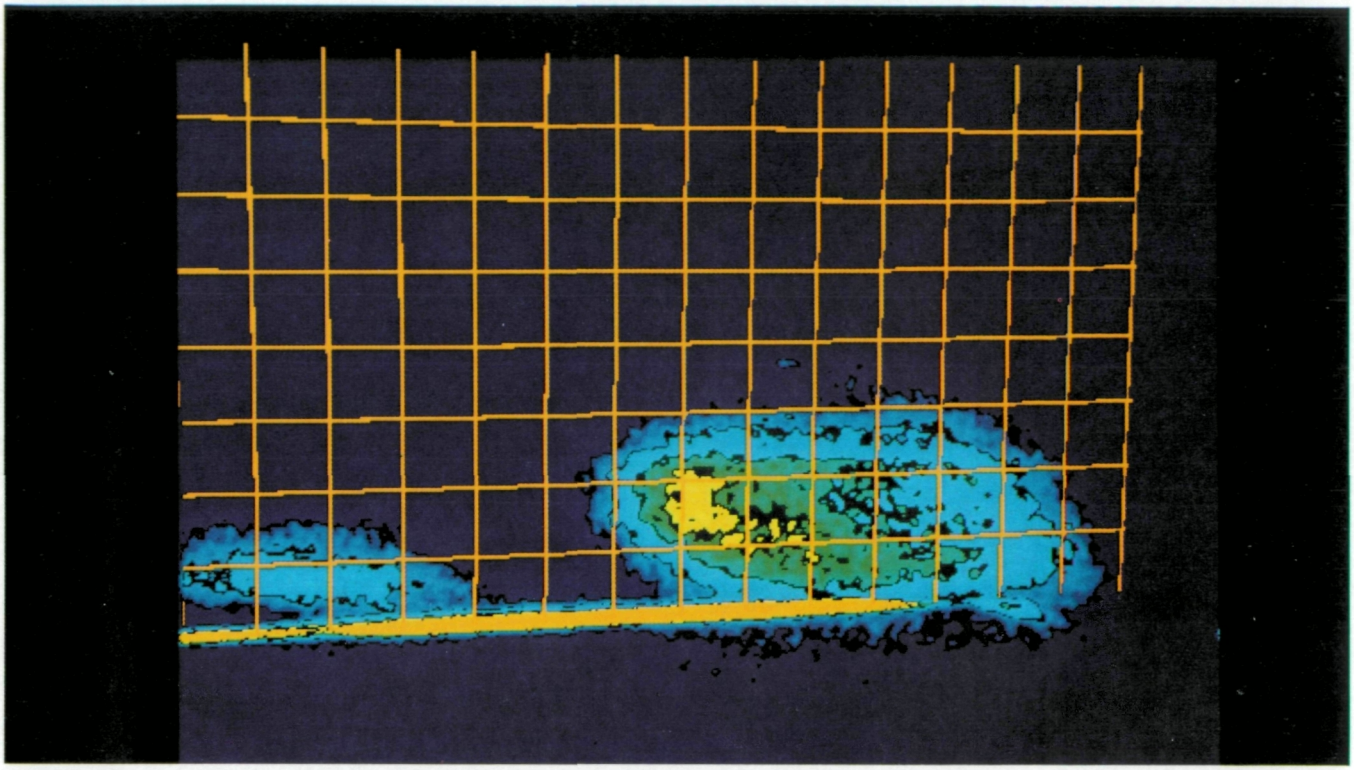

(c) $\alpha = 19°$.

L-87-4070

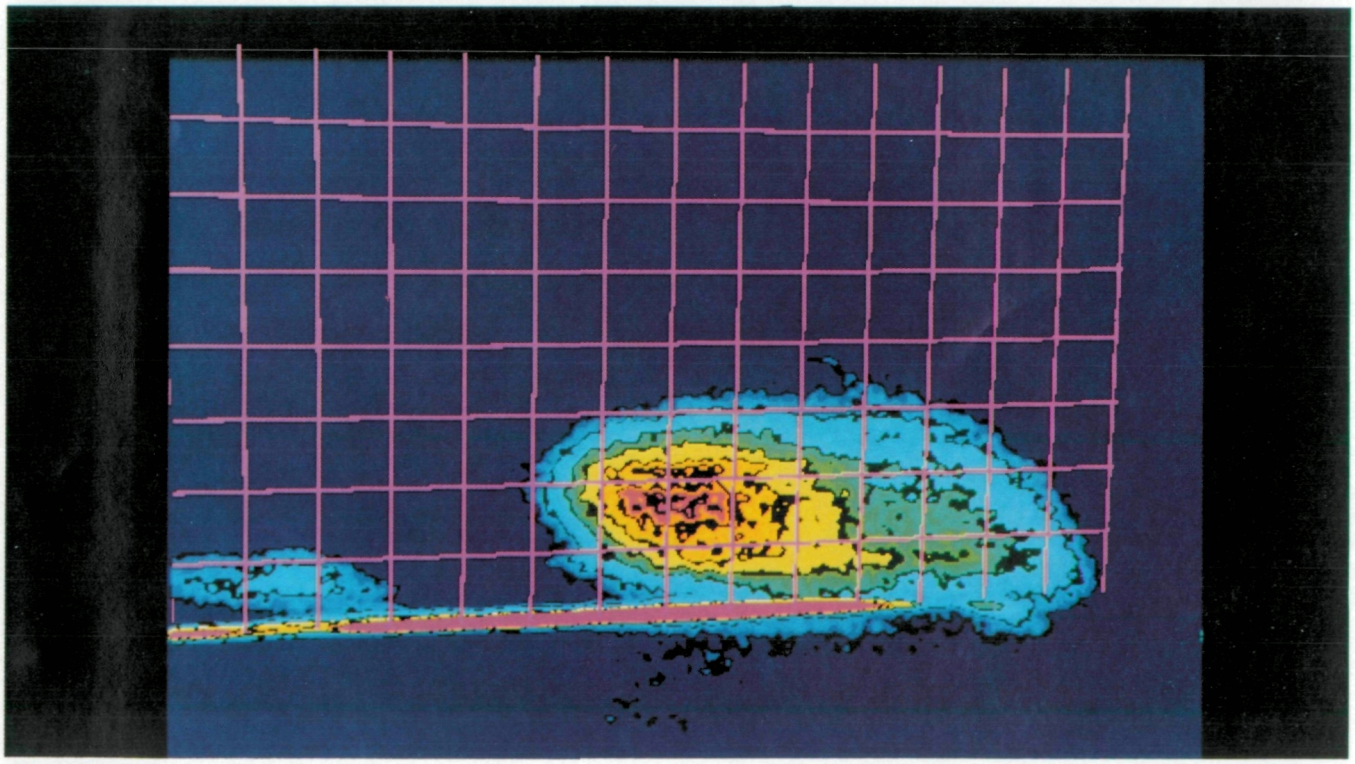

L-87-3886

(d) $\alpha = 20°$.

Figure 31. Continued.

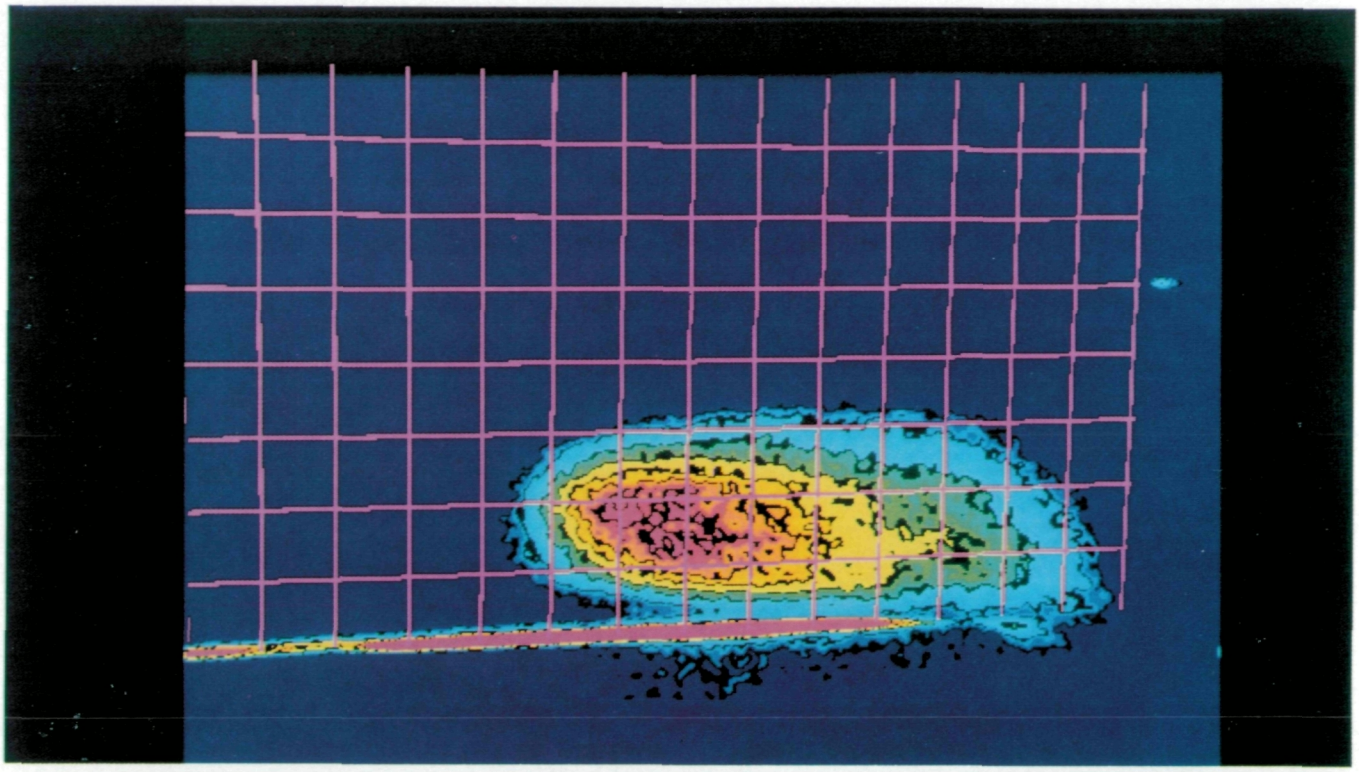

L-87-3887

(e) $\alpha = 21°$.

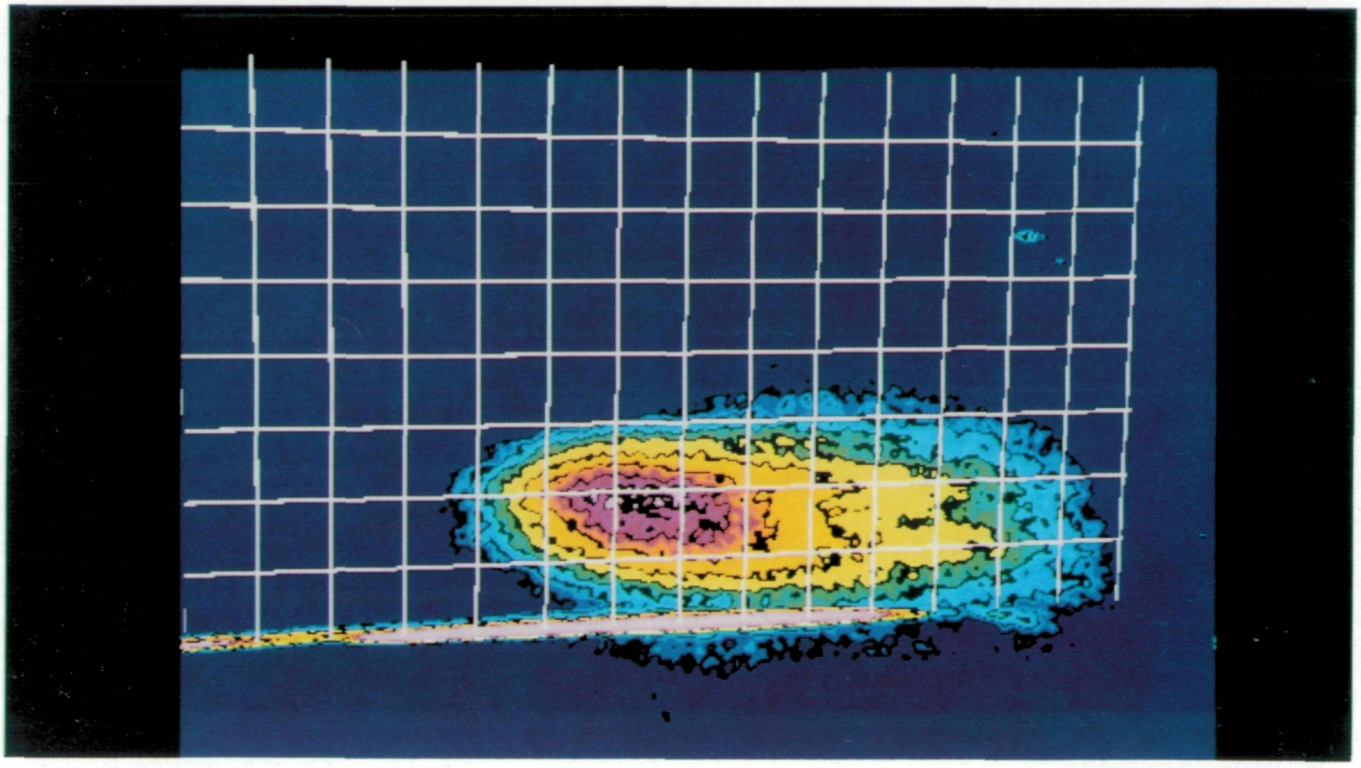

L-87-3888

(f) $\alpha = 22°$.

Figure 31. Continued.

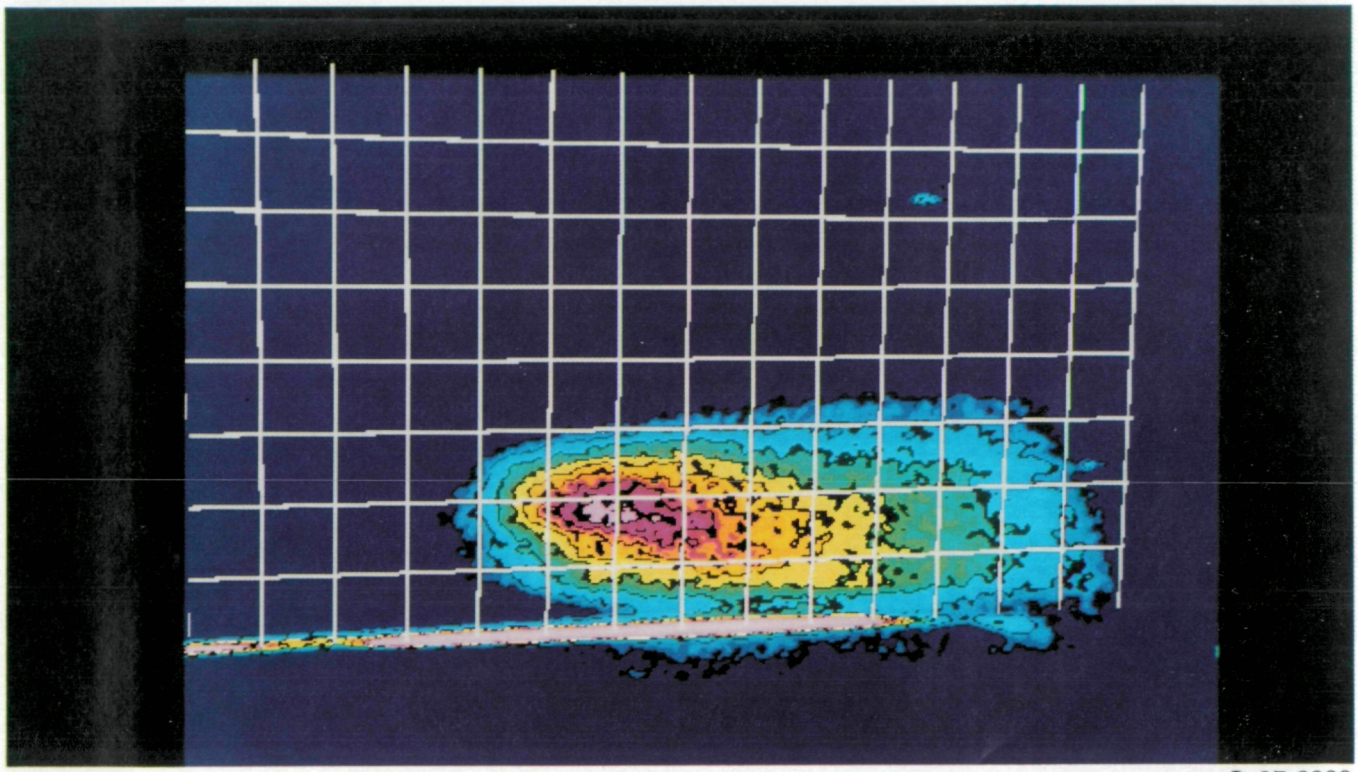

L-87-3889

(g) $\alpha = 23°$.

Figure 31. Concluded.

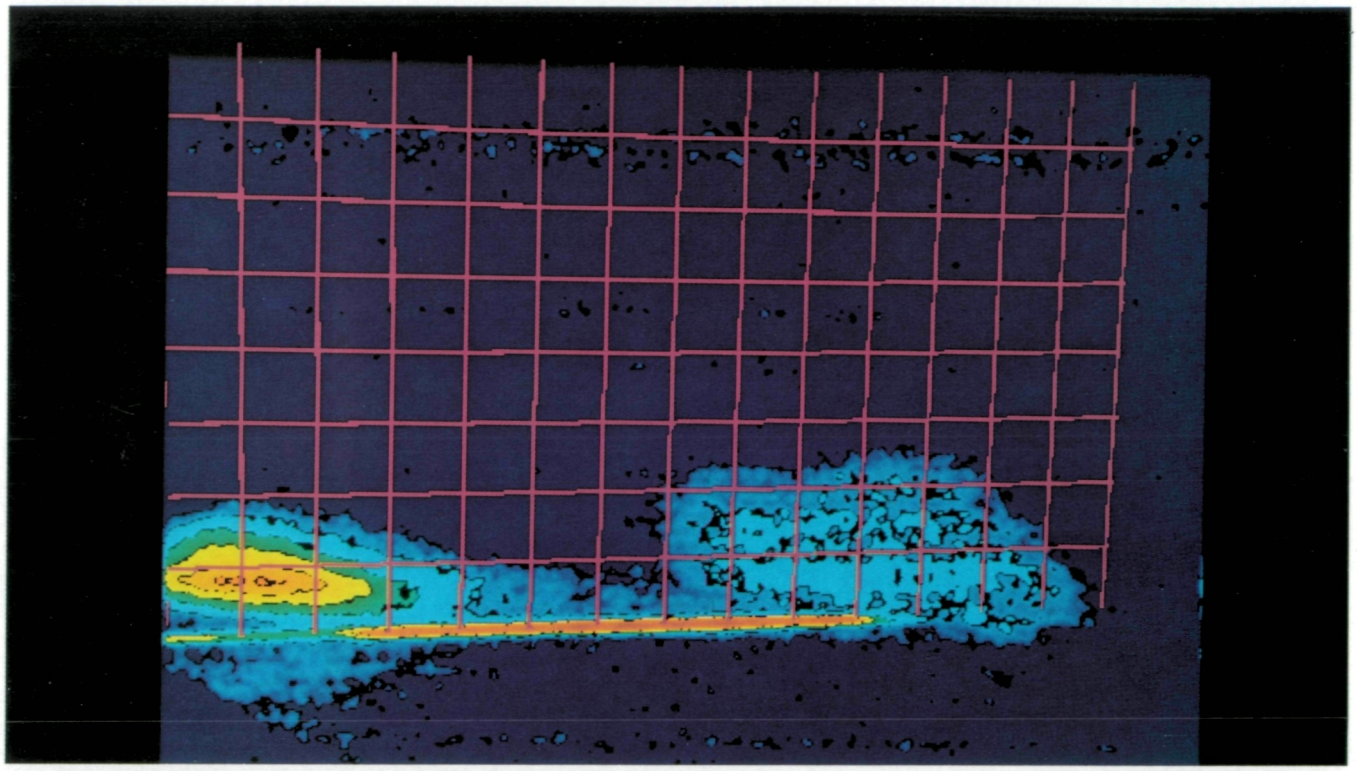

L-87-2845

(a) $\alpha = 17°$.

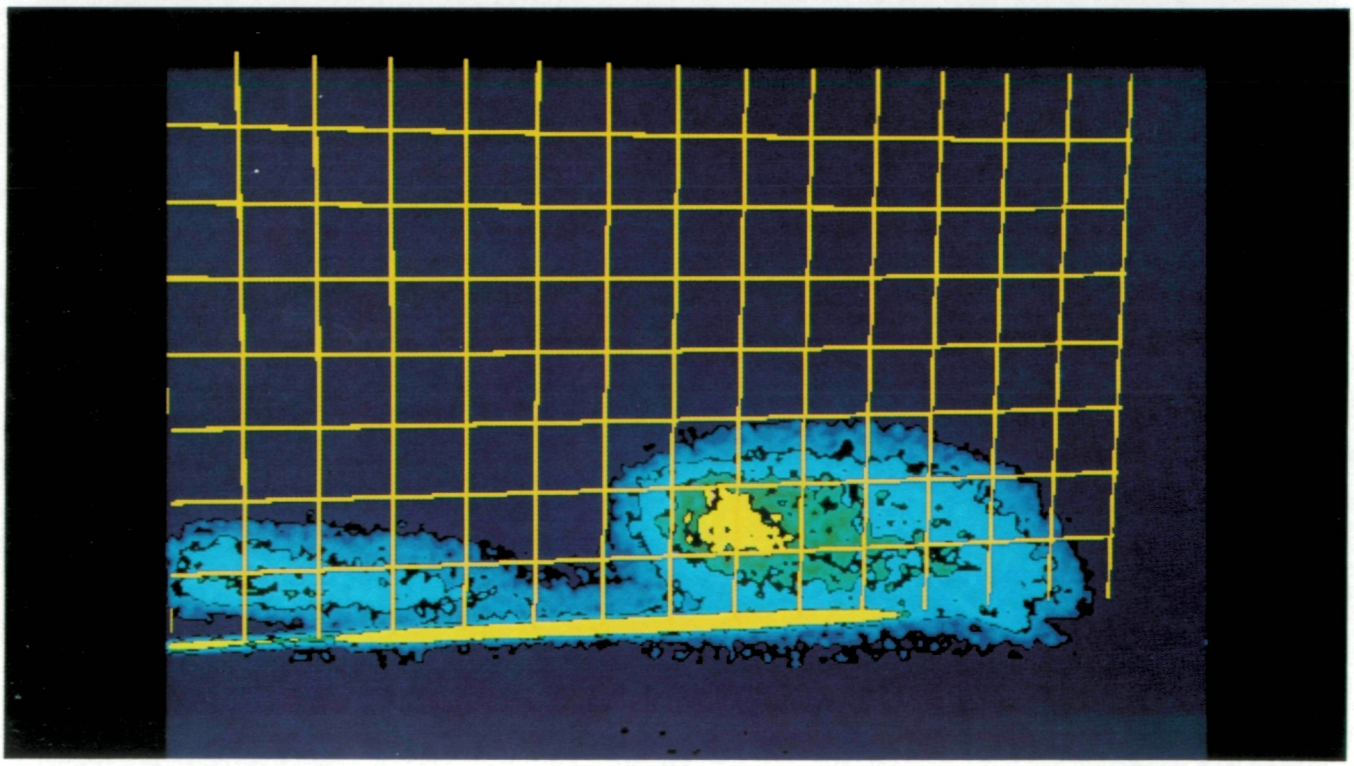

L-87-4066

(b) $\alpha = 18°$.

Figure 32. Vortex-system enhanced images for slit width of 0.012 in. and altitude of 35 000 ft. $1g$ maneuver; $0.30 \leq M \leq 0.48$; probe-tip location 6; intermittent light-sheet operation.

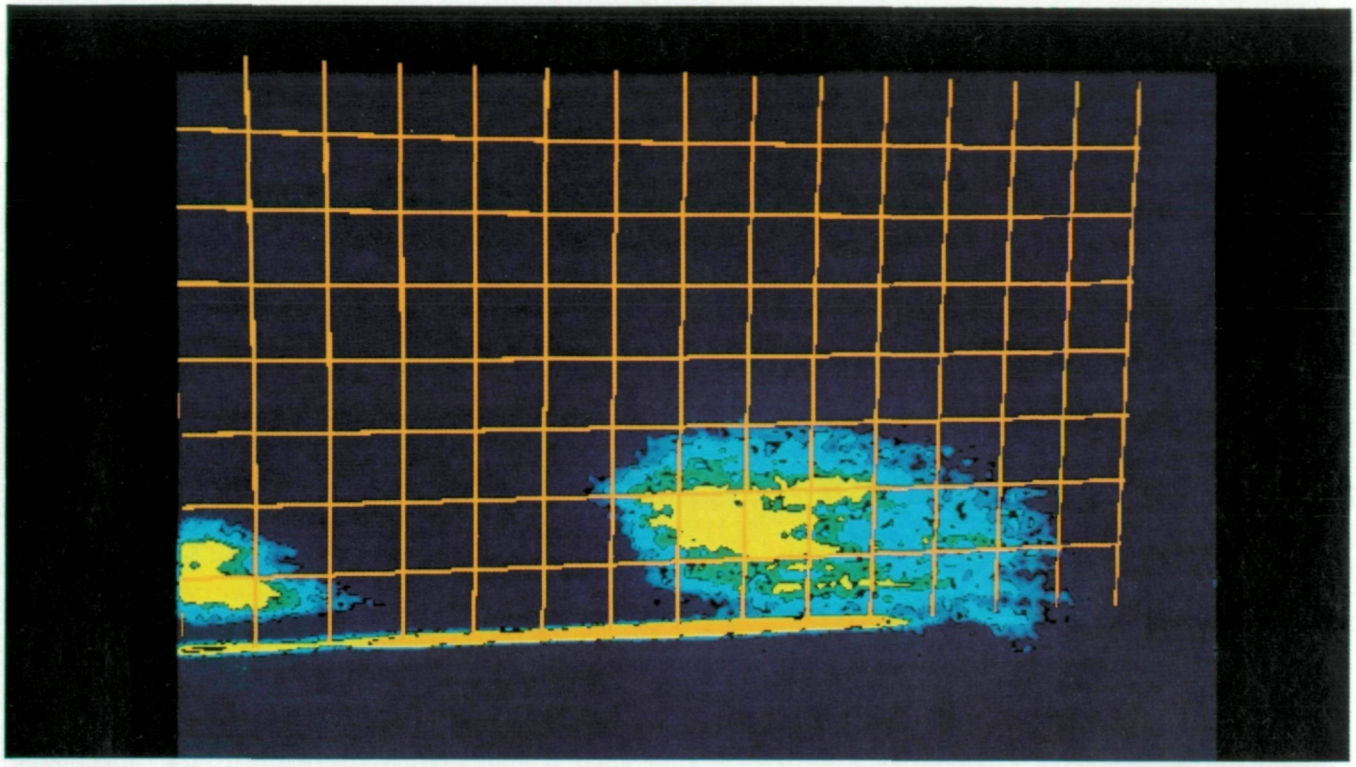

L-87-2848

(c) $\alpha = 19°$.

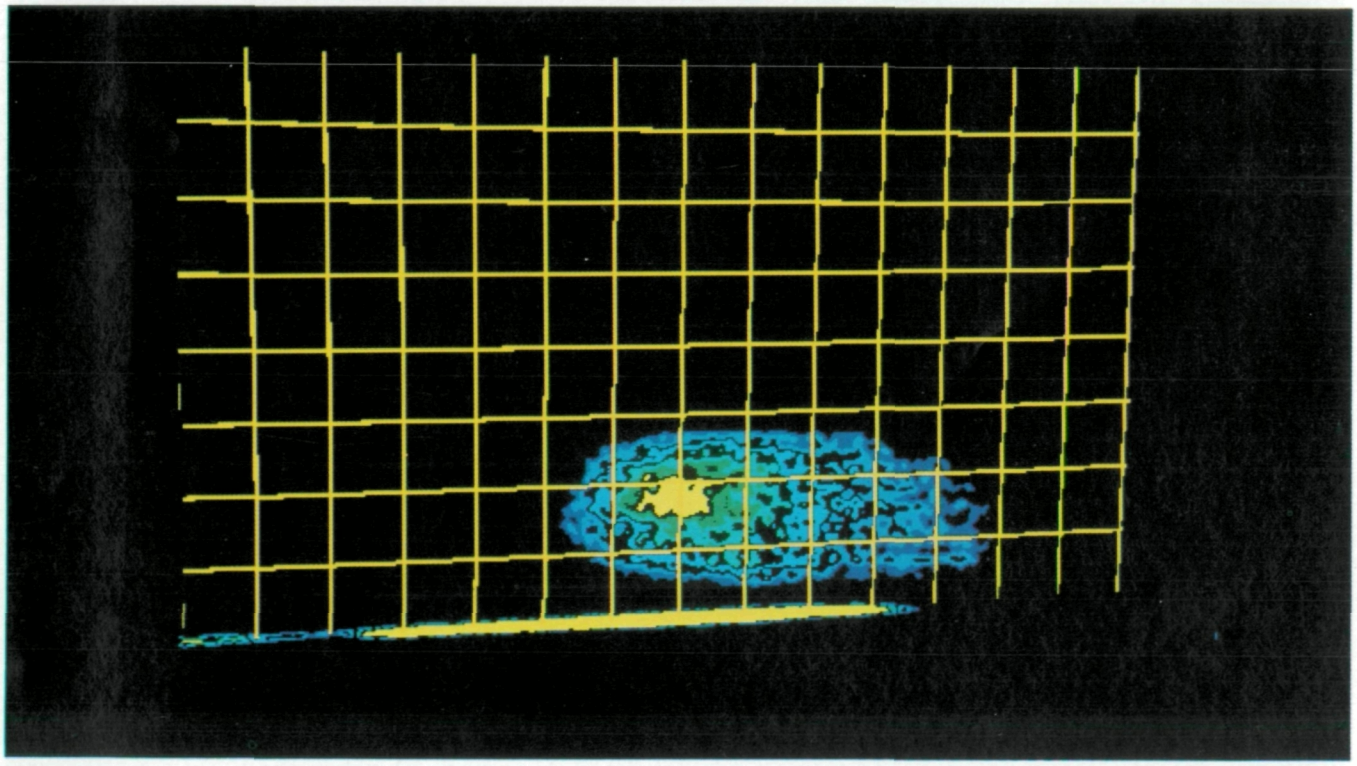

L-87-4067

(d) $\alpha = 20°$.

Figure 32. Continued.

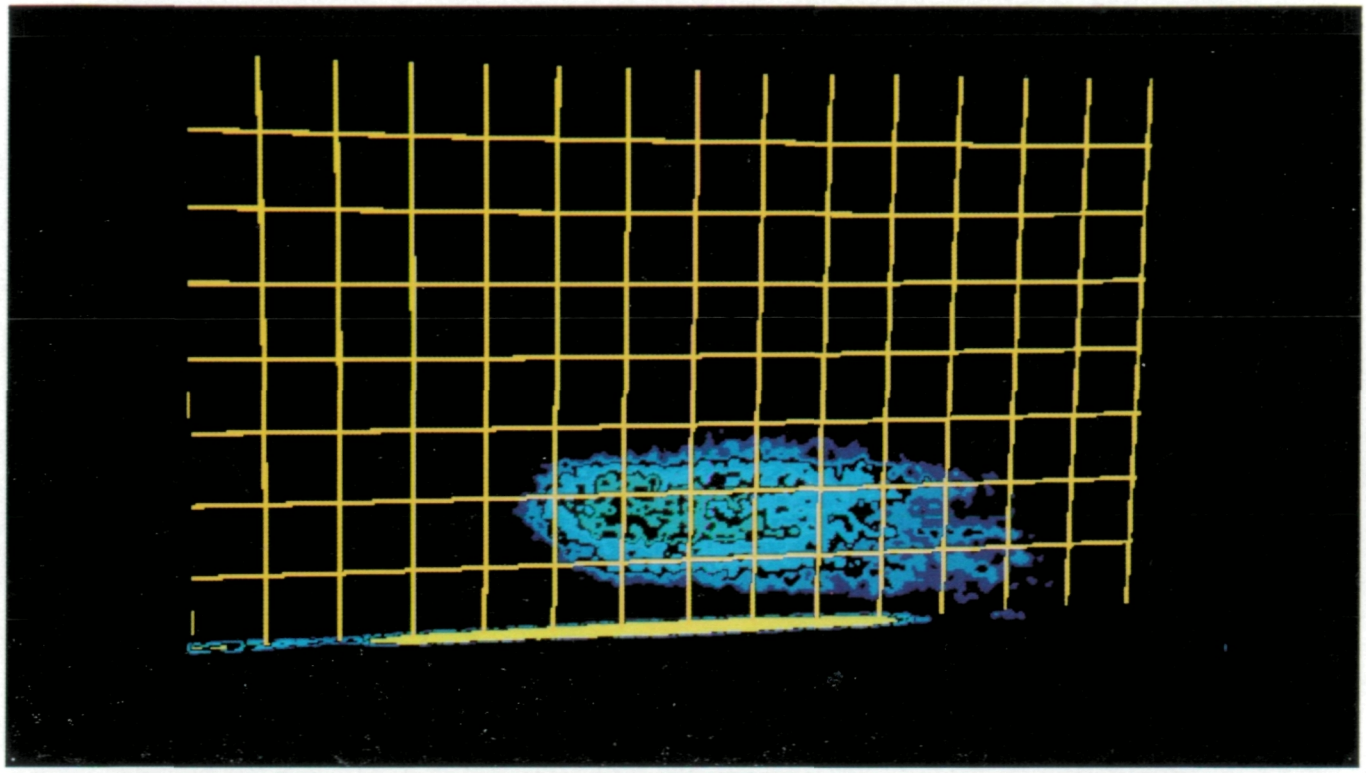

L-87-2841

(e) $\alpha = 21°$.

Figure 32. Concluded.

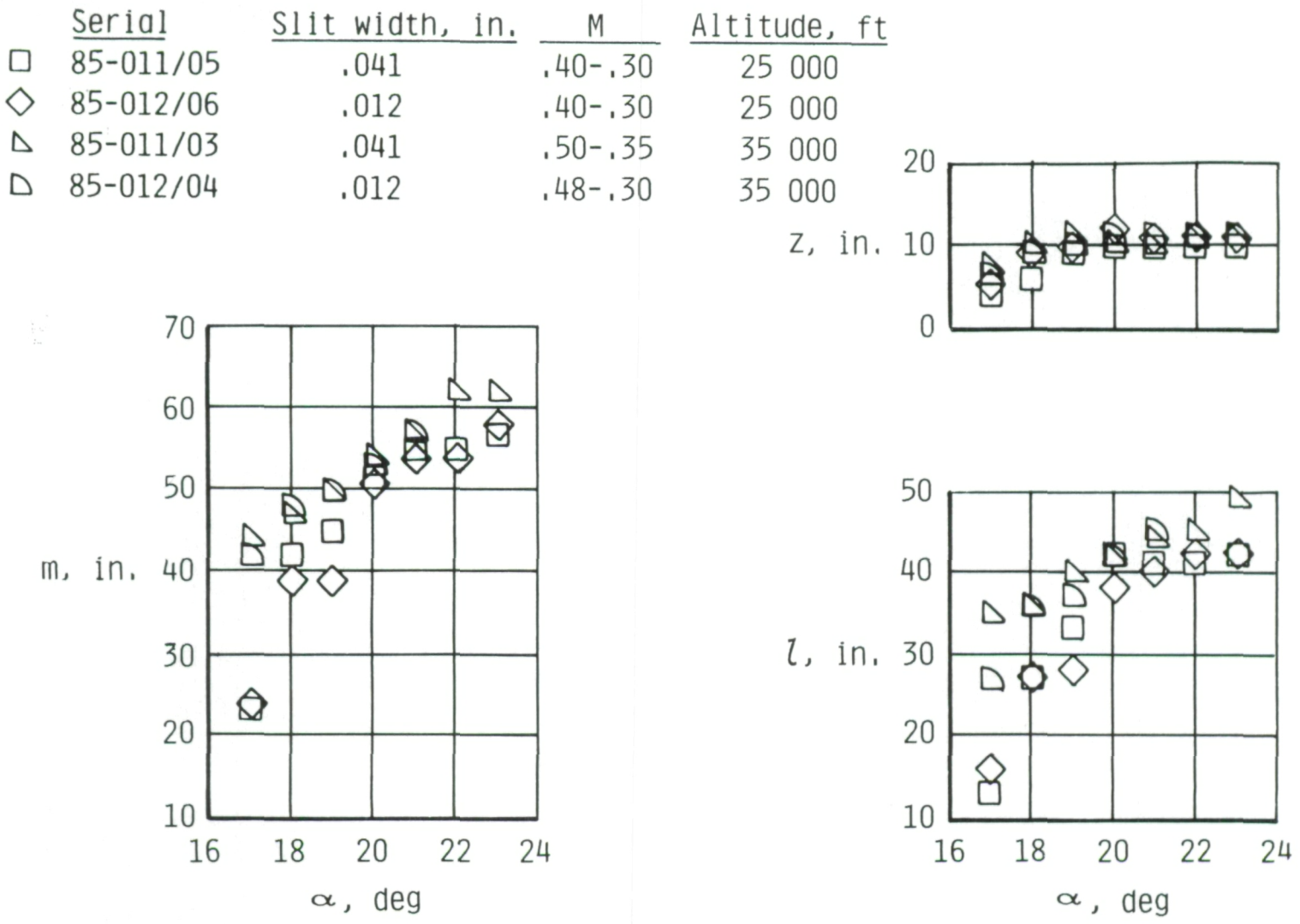

Figure 33. Effect of altitude and slit width on measured vortex-system image characteristics. 1g maneuver; probe-tip location 6; intermittent light-sheet operation.

NASA
National Aeronautics and Space Administration

Report Documentation Page

1. Report No.	2. Government Accession No.	3. Recipient's Catalog No.
NASA TP-2818		

4. Title and Subtitle	5. Report Date
Sensitivity of F-106B Leading-Edge-Vortex Images to Flight and Vapor-Screen Parameters	June 1988
	6. Performing Organization Code
7. Author(s)	8. Performing Organization Report No.
John E. Lamar and Thomas D. Johnson, Jr.	L-16395
9. Performing Organization Name and Address	10. Work Unit No.
NASA Langley Research Center Hampton, VA 23665-5225	505-61-71-03
	11. Contract or Grant No.
12. Sponsoring Agency Name and Address	13. Type of Report and Period Covered
National Aeronautics and Space Administration Washington, DC 20546-0001	Technical Paper
	14. Sponsoring Agency Code

15. Supplementary Notes

John E. Lamar: Langley Research Center, Hampton, Virginia.
Thomas D. Johnson, Jr.: Planning Research Corporation, Hampton, Virginia.

16. Abstract

A flight test was undertaken at NASA Langley Research Center with vapor-screen and image-enhancement techniques to obtain qualitative and quantitative information about near-field vortex flows above the wings of fighter aircraft. In particular, the effects of Reynolds and Mach numbers on the vortex system over an angle-of-attack range were sought. The relevance of these flows stems from their present and future use at many points in the flight envelope, especially during transonic maneuvers. The aircraft used in this flight program was the F-106B because it was available and had sufficient wing sweep (60°) to generate a significant leading-edge vortex system. The sensitivity of the visual results to vapor-screen hardware and to onset flow changes is discussed.

17. Key Words (Suggested by Authors(s))	18. Distribution Statement
Flight test Vortex flows Multiple vortices Vapor screen F-106B Image enhancement	Unclassified—Unlimited Subject Category 02

19. Security Classif.(of this report)	20. Security Classif.(of this page)	21. No. of Pages	22. Price
Unclassified	Unclassified	78	A05

NASA-Langley, 1988
For sale by the National Technical Information Service, Springfield, Virginia 22161-2171

National Aeronautics and
Space Administration
Code NTT-4

Washington, D.C.
20546-0001